Methods of Optimization for KCE-based Aptamer Selection

Stephanie de Jong

A THESIS SUBMITTED TO

THE FACULTY OF GRADUATE STUDIES

IN PARTIAL FULFILMENT OF THE REQUIREMENTS

FOR THE DEGREE OF

MASTER OF SCIENCE

GRADUATE PROGRAM IN CHEMISTRY

YORK UNIVERSITY

TORONTO, ONTARIO

June, 2013

Abstract

The success of KCE-based aptamer selection relies on three distinct steps of pre-selection optimization: (i) preventing protein adsorption to the inner walls of the capillary, (ii) maximizing the protein-DNA separation, and (iii) determining an appropriate aptamer-collection window. To perform the first step of optimization, we have developed a simple pressure-based approach which can qualitatively characterize protein adsorption on capillary walls in CE[1]. Conceptually, a short plug containing the protein solution is injected into the capillary and carried towards the detection point by applying a low pressure. A dual on-column detector is mimicked by repeating the experiment using the same capillary but a shortened distance to the detection window. The temporal propagation pattern of the protein, at each detection distance, is recorded and the degree of adsorption then analyzed by comparing peak areas and symmetry. This process can be repeated using different buffer additives[2], dynamic or permanent coatings until optimal conditions are established. The remaining two steps of pre-selection optimization can be solved by fluorescently labelling the target protein so that its compatibility with KCE separation is maintained[3]. By labeling the protein with Chromeo P503, we demonstrate that target detection in CE is markedly improved without significantly affecting the proteins electrophoretic mobility or ability to bind DNA. Thus, Chromeo-labelling can facilitate the accurate identification of both the protein and protein-aptamer complex, which is necessary for maximizing protein-DNA separation and selecting the aptamer collection window.

Target-specific considerations must also be optimized prior to commencement of KCE-SELEX. Exonuclease targets, such as Exonuclease I (*E.coli*), recognize the DNA library as a substrate to be degraded. As a result, the enzyme must be inactivated while still maintaining its native three-dimensional structure during aptamer collection. In addition, non-specific, or

unwanted binding at the active site must be avoided, as collection of non-aptamers would limit the progress of KCE-SELEX. For Exo1, a divalent metal chelating agent was found to effectively suppress library degradation through experimental optimization. In addition, a small oligonucleotide-based competitive inhibitor was found to bind to the active site with high affinity. This effectively eliminates any unwanted binding of the DNA library at the substrate binding site. The Exo1-inhibitor complex can then serve as a target for aptamer development towards an allosteric site of the protein.

Acknowledgements

It is with sincere gratitude that I acknowledge all the support and guidance that my Master's Thesis supervisor, Professor Sergey Krylov, has given me throughout the course of this project. I would like to thank Prof. Krylov for always being a great mentor, and for inspiring me to reach my potential through his continuous encouragement. I'd also like to extend my appreciation to Dr. Svetlana Krylova, for first noticing my interest in scientific research when I was an undergraduate, and for her encouragement and motivation throughout my graduate study. Prof. Krylov and Dr. Krylova are both wonderful role models and teachers who have allowed me to gain self-confidence and helped me further develop as a young scientist.

I would also like to thank the members of my research committee Professor Derek Wilson and Professor Philip Johnson. A special thanks to Prof. Wilson, for mentoring me as an undergraduate, I am forever grateful for all the skills I have learned from you and the members of your lab. Prof. Wilson and Prof. Johnson are both excellent teachers, and I am grateful for all the advice they have given me throughout my graduate study. I would also like to thank my external examiner, Prof. Scheid, for finding time in his busy schedule to review and comment on this report.

I'd like to thank, Dr. Michael Musheev and Anna Karkhanina, for transferring their knowledge and laboratory skills to me when I first began this project and for the useful advice they had both provided me. I truly appreciate all the support and discussions that I have had with all members of the Krylov lab, none of this work would be possible without your help. I would also like to express my gratitude to Nicolas Epelbaum, for all the experimental work he had conducted as a summer student for the semi-permanent coating project.

I would like to thank my parents John and Iris de Jong for their patients and understanding, my sister, Kristine de Jong, for her moral support and friendship, and last but not least, my fiancé, Carlos Orbegozo for always believing in me and fully encouraging me along the way.

Table of Contents

List of Figures

[Figure 11] Effect of Chromeo labeling on protein mobility in CE. Unlabeled proteins were detected by UV absorbance at 214 nm using 50 μM fluorescein as a migration standard (blue traces). Chromeo-labeled proteins were prepared at the same concentrations that were used for UV absorbance detection. Fluorescence of labeled proteins was excited by a 488 nm solid-state laser and detected through a 610 nm filter (red traces). Fluorescence of the migration standard, 10 nM fluorescein, and the DNA library were excited using the same 488 nm laser and detected through a 520 nm filter (black traces).

[Figure 12] Influence of Chromeo-labeling on aptamer binding and affinity for thrombin (upper panel) and AlkB protein (lower panel). NECEEM binding assays were performed by using equilibrium mixtures containing labeled aptamer and either labeled (red lines) or unlabeled (black lines) protein. The concentrations of thrombin and its aptamer were 0.5 and 0.1 μM, respectively. The concentrations of AlkB protein and its aptamer were 80 and 30 nM, respectively. Only DNA is detected when fluorescence is measured at 520 nm.

[Figure 13] Peak identification of the thrombin-aptamer complex through the combined use of Chromeo-labeled thrombin and Alexa488 labeled aptamer. Back traces depict fluorescence at 520 nm while the red traces represent fluorescence at 610 nm. Upper panels show NECEEM electropherograms obtained with the native thrombin; lower panels show NECEEM electropherograms obtained with the Chromeo-labeled thrombin. The left panels show the measured signals, while the right panels show the same data with the red electropherograms rescaled to have the heights of the left peaks identical for the black and red electropherograms. The concentrations of thrombin and aptamer were 0.5 and 0.1 μM, respectively.

[Figure 14] Negligible effect of amino-containing buffer components on fluorescence signal from Chromeo-labeled Exo1 protein. The top trace shows the electropherogram obtained from the Chromeo-labeled Exo1, which was stored in buffer containing 10 mM Tris-HCl. The middle trace is a control illustrating how this Tris buffer reacts with the Chromeo dye. The bottom trace is a second control which illustrates the peak obtained from the Chromeo dye alone.

[Figure 15] Electropherograms illustrating the improvement in CE detection of BSA by labeling protein with Chromeo P503. The top panel shows the data obtained using fluorescence detection while the lower panel illustrates the data obtained using UV absorbance detection. The respective concentrations are indicated in the right corners.

[Figure 16] Electropherograms illustrating the improvement in CE detection of HSA by labeling protein with Chromeo P503. The top panel shows the data obtained using fluorescence detection while the lower panel illustrates the data obtained using UV absorbance detection. The respective concentrations are indicated in the right corners.

[Figure 17] Electropherograms illustrating the improvement in CE detection of AGP by labeling protein with Chromeo P503. The top panel shows the data obtained using fluorescence detection while the lower panel illustrates the data obtained using UV absorbance detection. The respective concentrations are indicated in the right corners.

[Figure 18] Electropherograms illustrating the improvement in CE detection of myoglobin by labeling protein with Chromeo P503. The top panel shows the data obtained using fluorescence detection while the lower panel illustrates the data obtained using UV absorbance detection. The respective concentrations are indicated in the right corners.

[Figure 19]. Electropherograms illustrating the improvement in CE detection of α-lactalbumin by labeling protein with Chromeo P503. The top panel shows the data obtained using fluorescence detection while the lower panel illustrates the data obtained using UV absorbance detection. The respective concentrations are indicated in the right corners.

[Figure 20] UV absorbance data demonstrating how protein adsorption influences the EOF in an untreated fused-silica capillary. CE separation was performed at 300 V/cm using 50 mM Tris acetate (pH 8.2) run buffer. In each trace, 0.2% DMSO was used as a neutral EOF marker. Trace 1 presents DMSO migration in the absence of any protein. The calculated EOF values are shown on the right of each electropherogram. Traces 2-4 present results where protein samples of varying adsorptive properties are introduced into the capillary. AGP was selected as an example of a nonadsorptive protein (2), conalbumin as a moderately adsorptive representative (3), and cytochrome *c* as a highly adsorptive protein (4). All proteins were diluted to the same final concentration of 4 mg/mL and injected into the uncoated capillary together with DMSO. For cytochrome *c*, no protein peak is visible due to irreversible adsorption at the inner capillary surface and the limited detection capabilities of UV absorbance.

[Figure 21] Pressure-driven migration profiles of the 100 nM thrombin-binding aptamer by applying either a low or high forward pressure. Sample plug schematics were created using COMSOL Multiphysics modeling. The resulting parabolic pressure profiles were generated for pressures of 0.5 (A) and 5 (B) psi. Experimental electropherograms (C,D) are shown below the corresponding schematic representations. Tris acetate (50 mM, pH 8.2) was used as the run buffer, and the fluorescent emission was detected at 520 nm.

[Figure 22] (A) Schematic representation of extensive protein adsorption which may occur within the capillary and how a reduction in sample concentration can be analyzed by using the two-detector pressure-driven approach. Panels B and C show the experimental migration pattern obtained from the 40 and 10 cm propagations of 274 μM Chromeo-labeled lysozyme, respectively. Protein fluorescence was detected at 610 nm using a 50 mM Tris acetate (pH 8.2) run buffer.

[Figure 23] NECEEM electropherograms produced using the thrombin-aptamer binding system in an uncoated capillary (top panel) and PVA-coated capillary (lower panel). The equilibrium mixtures consisted of 455 nM thrombin and 91 nM aptamer and separated using normal polarity in the uncoated capillary and reverse polarity with the PVA coating. The areas corresponding to free aptamer (A_1), aptamer dissociated from the complex (A_3), and intact complex (A_2) are identified in the electropherogram produced using the PVA-coated capillary. The uncoated capillary could not be analyzed as the areas are poorly defined.

[Figure 24] Temporal propagation patterns of 9.8 μM Chromeo-labeled α_1-acid glycoprotein after 10-cm and 40-cm pressure-driven propagations using an uncoated capillary, a capillary coated with CElixir dynamic modifier, a capillary with a permanently adsorbed PVA coating and a capillary covalently bonded with LPA.

[Figure 25] Temporal propagation patterns of 5.3 μM Chromeo-labeled conalbumin after 10-cm and 40-cm pressure-driven propagations using an uncoated capillary, a capillary coated with CElixir dynamic modifier, a capillary with a permanently adsorbed PVA coating and a capillary covalently bonded with LPA.

[Figure 26] Temporal propagation patterns of 171 μM Chromeo-labeled cytochrome C after 10-cm and 40-cm pressure-driven propagations using an uncoated capillary, a capillary coated with CElixir dynamic modifier, a capillary with a permanently adsorbed PVA coating and a capillary covalently bonded with LPA.

[Figure 27] Temporal propagation patterns of 10.1 μM Chromeo-labeled thrombin after 10-cm and 40-cm pressure-driven propagations using an uncoated capillary, a capillary coated with CElixir dynamic modifier, a capillary with a permanently adsorbed PVA coating and a capillary covalently bonded with LPA.

[Figure 28] Temporal propagation patterns of 137 μM Chromeo-labeled lysozyme after 10-cm and 40-cm pressure-driven propagations using an uncoated capillary, a capillary coated with CElixir dynamic modifier, a capillary with a permanently adsorbed PVA coating and a capillary covalently bonded with LPA.

[Figure 29] Gel CE results illustrating Exo1 activity with various buffer additives. Panel A displays the DNA ladder containing 100 nM of the 20 nt sequence, 400 nM of the 37 nt sequence, 300 nM of the 56 nt sequence and 200 nM of the 80 nt sequence. Panel B shows the electropherogram obtained with a EM containing 100 nM Exo1 and 5 μM N40 DNA library incubated in a 50 mM Tris-acetate (pH 8.2), 100 mM NaCl, 5 mM $MgCl_2$ buffer for 15 minutes. The EM was co-injected with the DNA ladder in order to estimate the extent of DNA degradation. Panel C displays the electropherogram obtained with a EM containing 100 nM Exo1 and 5 μM N40 DNA library incubated in a 50 mM Tris-acetate (pH 8.2), 100 mM NaCl buffer incubated for 60 minutes and co-injected with the DNA ladder. Panel D shows the electropherogram obtained with a EM containing 100 mM Exo1and 5 μM N40 DNA library incubated in a 50 mM Tris-acetate (pH 8.2), 100 mM NaCl, 5 mM EDTA buffer incubated for 60 minutes and co-injected with the DNA ladder.

[Figure 30] NECEEM experiments performed to assess both Exo1-DNA affinity and exonuclease activity in the presence (b) and absence (a) of 5 mM EDTA. The black traces represent the NECEEM electropherograms of the equilibrium mixture. The blue lines show the DNA only control, and the red traces show the heat denatured protein-DNA mixtures. (a) EM containing 435 nM Exo1 and 100 nM of Alexa-488 labeled N40 DNA library in a 50 mM Tris-acetate (pH 8.2) incubation buffer supplemented with 50 mM KCl. (b) EM containing 435 nM Exo1 and 100 nM Alexa-488 labeled N40 DNA library in a 50 mM Tris-acetate (pH 8.2) incubation buffer supplemented with 50 mM KCl and 5 mM EDTA. In the presence of 5 mM EDTA the bulk K_d was estimated at 259 nM,

[Figure 31] Peak identification of the Exo1-N40 library complex through the combined use of Chromeo P503 labeled Exo1 and Alexa-488 labeled N40 DNA library. Black traces depict fluorescence at 520 nm while the red traces represent fluorescence through the 610 nm filtered channel. The left panel show the measured signal obtained through both channels, while the right panels show the same data with the red electropherograms rescaled so that the height of the rightmost peaks are equivalent for both the black and red electropherograms. The concentration of Exo1 and N40 library were 510 and 100 nM, respectively.

[Figure 32] NECEEM binding tests using Alexa-647 labeled 5nt, 10nt, and 15nt inhibitors as ligands towards Exo1. (A) 5nt DNA inhibitor in s 50 mM Tris-acetate (pH 8.2); 50 mM KCl run buffer. (B) 10nt DNA inhibitor in a 50 mM Tris-acetate (pH 8.2); 50 mM KCl run buffer. (C) 15nt DNA inhibitor in a 50 mM Tris-acetate (pH 8.2); 50 mM KCl un buffer. (D) 5nt DNA inhibitor in a 50 mM Tris-acetate (pH 8.2); 50 mM KCl; 5 mM EDTA run buffer. (E) 10nt DNA inhibitor in a 50 mM Tris-acetate (pH 8.2); 50 mM KCl; 5 mM EDTA run buffer. (F) 15nt DNA inhibitor in a 50 mM Tris-acetate (pH 8.2); 50 mM KCl; 5 mM EDTA run buffer. Black traces represent NECEEM electropherograms of the EM, blue traces illustrate the inhibitor controls, and red traces depict heat denatured equilibrium mixtures.

[Figure 33] Two substrate competition assays investigated through NECEEM. Exo1 was incubated with the Alexa-488 labeled N40 DNA library and either the 5 nt, 10 nt or 15 nt inhibitors, each labeled with the Alexa-647 fluorophore. Fluorescence emission at 520 nm and 655 nm were detected simultaneously using a two channel filtration system. Green traces correspond to Alexa-488 emission after separation through a 520 nm band-pass filter. Black traces correspond to Alexa-647 emission following the separation through a 655 nm band-pass filter. The top panels illustrate results of the competition assay after the 15 min incubation with both substrates. The middle panels illustrate the same equilibrium mixtures following complex denaturation through heat-induced Exo1 deactivation. The lower panels depict the controls where Exo1 was excluded from the EM. All experiments were performed in a 50 mM Tris-acetate (pH 8.2); 50 mM KCl; 5 mM EDTA incubation buffer and a 50 mM Tris-acetate (pH 8.2) run buffer (A) 96.7 nM Exo1, 100 nM N40 and 100 nM 5 nt inhibitor (B) 96.7 nM Exo1, 100 nM N40 and 100 nM 10 nt inhibitor (C) 96.7 nM Exo1, 100 nM N40 and 100 nM 15 nt inhibitor (D) 96.7 nM Exo1, 100 nM N40 and 300 nM 5 nt inhibitor (E) 96.7 nM Exo1, 100 nM N40 and 100 nM 5 nt inhibitor after heating at 95°C for 20 min (F) 96.7 nM Exo1, 100 nM N40 and 100 nM 10 nt inhibitor after heating at 95°C for 20 min. (G) 96.7 nM Exo1, 100 nM N40 and 100 nM 15 nt inhibitor after heating at 95°C for 20 min. (H) 96.7 nM Exo1, 100 nM N40 and 300 nM 15 nt inhibitor after heating at 95°C for 20 min. (I) 100 nM N40 and 100 nM 5 nt inhibitor (J) 100 nM N40 and 100 nM 10 nt inhibitor (K) 100 nM N40 and 100 nM 15 nt inhibitor (L) 100 nM N40 and 300 nM 15 nt inhibitor

[Figure 34] NECEEM binding tests using Alexa-647 labeled 15nt polyT DNA sequence as an Exo1 inhibitor. The concentration of Exo1 and the 15nt inhibitor were 131 nM and 50 nM, respectively. Black traces represent NECEEM electropherograms of the EM, blue traces illustrate the inhibitor controls, and red traces depict heat denatured equilibrium mixtures. The top figure is a magnified image illustrating the Exo1-inhibitor interaction, highlighting the decay. Under these conditions, K_d was estimated at 51 nM and k_{off} at 1.8 $*10^{-2}$ s^{-1}.

[Figure 35] NECEEM binding tests using Alexa-647 labeled 15nt polyT inhibitor after 5 min and 15 min incubation times, shown in the right and left panels, respectively.. The concentration of Exo1 and the 15nt inhibitor were 435 nM and 100 nM, respectively. Black traces represent NECEEM electropherograms of the EM, blue traces illustrate the inhibitor controls, and red traces depict heat denatured equilibrium mixtures.

[Figure 36] Temporal propagation patterns of 5.1 μM Chromeo-labeled Exo1 after 10-cm and 40-cm pressure-driven propagations using an uncoated capillary and 50 mM Tris acetate (pH 8.2) as the run buffer for the first 40 min of the experiment. After the 40 min time point, 100 mM NaOH was introduced to strip off any adsorbed protein.

[Figure 37]: Pressure-induced propagation patterns are shown up until the 6 min migration time mark. An electric field of 400 V/cm was introduced after the 6 min pressure propagation and maintained throughout the remainder of the experiment. Black traces represent temporal propagation pattern/electropherograms of the equilibrium mixture containing 437 nM of Exo1 and 100 nM of the 15 nucleotide inhibitor. Blue traces illustrate the temporal propagation pattern/electropherogram of the inhibitor controls, and red traces depict pressure propagation/electropherogram of the heat denatured equilibrium mixture.

[Figure 38] Temporal propagation patterns of the Exo1-15 nucleotide inhibitor complex after 10-cm and 40-cm pressure-driven propagations using an uncoated capillary using a 50 mM Tris acetate (pH 8.2) run buffer. The equilibrium mixture containing 437 nM Exo1 and the 100 nM 15 nucleotide inhibitor was prepared to ensure complete binding and propagation of the pure complex peak.

[Figure 39] Two substrate competition assays investigated in a 102 cm capillary. Exo1 was incubated with the Alexa-488 labeled N40 DNA library and the Alexa-647 labeled 15 nt inhibitor. Fluorescence emission at 520 nm and 655 nm were detected simultaneously using a two channel filtration system. Green traces correspond to Alexa-488 emission after separation through a 520 nm band-pass filter. Black traces correspond to Alexa-647 emission following the separation through a 655 nm band-pass filter. The top panels illustrate results of the competition assay after the 5 min incubation with the inhibitor followed by a subsequent 15 min incubation with both substrates. All experiments were performed in a 50 mM Tris-acetate (pH 8.2); 50 mM KCl; 5 mM EDTA incubation buffer and a 50 mM Tris-acetate (pH 8.2) run buffer. (A) 96.7 nM Exo1; 100 nM 15 nt inhibitor; 100 nM N40 library. (B) Magnified image of panel A illustrating poor peak resolution. (C) 96.7 nM Exo1; 300 nM 15 nt inhibitor; 100 nM N40 library. (B) Magnified image of panel B illustrating poor peak resolution.

List of Tables

Chapter 1: Introduction and General Overview

1.1 Non-covalent Biomolecular Interactions

Non-covalent molecular interactions are central to all biological systems, where they govern fundamental processes necessary for cellular function and viability. All chemical bonding exists as an energetically favorable balance between the opposing forces of attraction and repulsion at the atomic level.[4] Covalent bonds are strong electrostatic forces generated between a pair of electrons and positively charged nuclei, which hold individual atoms together as a molecule.[5] They are formed though the direct sharing of electrons and are characterized by fixed angles and distances between the bonding atoms.[6] These bonds dictate the structural foundation of all biological molecules and function as a potential energy reservoir during cellular metabolism. In contrast, non-covalent bonds are much more dynamic and result from a diverse set of weak electromagnetic interactions. Non-covalent bonding occurs through a wide range of distances, providing the structural flexibility found in all macromolecules, and the specificity needed for intermolecular recognition. Although these bonds are individually weak and exist only transiently at physiological temperatures, collectively they allow for highly stable and specific intermolecular binding, as well as complex three dimensional structure formation. There are four major types of non-covalent forces prevalent in biomolecular interactions: (i) ionic interactions (ii) van der Waals forces (iii) hydrogen bonding and (iv) the hydrophobic effect. It is these basic interactions that control a myriad of cellular events ranging from signal transduction, gene regulation, cell recognition, the catalytic activity of enzymes and the immune response.[7,8]

1.1.1 Ionic Interactions

Ionic interactions emanate from a variety of electrostatic forces of attraction or repulsion that can exist between charged and partially charged particles. The strength of such forces is highly dependent on the distance between the interacting species, which is generally dictated by the molecular structure rigidity. Charge-charge interactions occur when ionized particles of opposite charge are within close spatial proximity. Forces of this type are relatively strong and can occur through the widest range of distances in comparison to all other non-covalent electromagnetic interactions. Charged particles can also interact with polarized neutral species if they exist as molecular dipoles where the charge density is physically separated within itself. The nature of such forces depends on how the dipole is positioned relative to the neighbouring ion as alternate orientations result in either an attractive or repulsive force.[9]

1.1.2 Van der Waals Forces

Two electrically neutral particles may also experience relatively weaker forces of attraction and repulsion, known as van der Waals forces, based solely on the polarity or polarizability of each molecular partner. These forces are derived though an unequal charge distribution where the electron density is shifted towards an atom of greater electronegativity, thus forming a molecular dipole. Two molecules with permanent dipole moments may experience notable forces of attraction when their mutual spatial orientation is in agreement. Although these forces are weaker than the aforementioned ionic interactions, they are still quite prevalent in many affinity-based binding. It is also possible for a point charge or permanent dipole to induce a dipole in a nearby species with polarizable molecular properties. The induced dipole moment would otherwise not exist in the absence of the inducing agent (i.e. the ion or

dipole) with which it is interacting. Although the van der Waals force involving inducible particles is not necessarily weaker than those found between permanent charges of the same type, they exhibit a much greater dependency on the interatomic distances between opposing charges. Accordingly, the occurrence of such interactions is often enforced by the three-dimensional organization of each molecule and their structural complementarities.[10] Dispersion forces are the weakest type of van der Waals interaction which typically occurs between overlapping electron clouds in aromatic molecules. These forces are derived through the mutual synchronization of fluctuating electric charges which then leads to the simultaneous production of two induced dipoles.[11,12]

1.1.3 Hydrogen Bonding

Hydrogen bonding is a specialized type of dipole-dipole interaction which involves a hydrogen atom covalently attached to a highly electronegative atom (i.e. N, F, or O). The electron deficient hydrogen atom retains a partial positive charge and serves as a hydrogen donor capable of binding to a nearby electron rich acceptor atom. Although the major energetic source of the hydrogen bond is electrostatic and dipole-based, the interaction also possesses a significant covalent character. The covalent nature of the hydrogen bond is conveyed through its relatively short and fixed bond lengths which cannot be explained solely through overlapping van der Waals radii. Moreover, hydrogen bonds have a linear directionality and are aligned at predictable interatomic orientations, a feature analogous to covalent-based interactions.[13] The strength of these interactions is intermediary to van der Waals forces and covalent bonds, with molar enthalpies ranging from 0.2[14] to 39[15] kcal mol^{-1}. Hydrogen bonding confers the stability found in complex macromolecular structures such as the DNA double helix. It also has a fundamental

influence on higher-order protein folding and is a crucial element needed for α-helix and β-sheet formation.[16]

1.1.4 Hydrophobic Effect

Non-polar molecules or molecular residues demonstrate a rather low solubility when submerged in an aqueous environment and tend to aggregate together to form clusters. Unlike the previously described electromagnetic forces of attraction and repulsion, the hydrophobic 'interaction' is misleading as it does not involve any true bonding character between hydrophobic species. Rather, the mechanism of non-polar molecular ordering is thermodynamically driven through the mutual exclusion of the surrounding polar solvent. This phenomenon, referred to as the hydrophobic effect, is a spontaneous process determined primarily through an entropy based increase in systems overall free energy. The aqueous solution found in most biological systems is predominantly composed of liquid water. The structural polarity of water molecules results in the assembly of inherently dynamic hydrogen bonding networks with neighboring water molecules or other polar species. If the non-polar solute were completely hydrated by the solvent, this would disrupt the hydrogen bonding network and reduce the configurational space that would otherwise be available for hydrogen bonding. This effectively reduces the number of accessible microstates for each water molecule in the system. Since water makes up the majority of the solution, this results in a notable entropy increase in the system as a whole. As a result, non-polar molecules tend to associate in aqueous solutions in order to minimize the surface area exposed to the solvent.[17]

1.2 Reversible Binding Kinetics

Affinity-based biomolecular bonding generally exists through a variety of non-covalent interactions, which collectively define the overall binding strength. When two molecules that share a common affinity are combined together in solution and left to equilibrate, a distinct time-dependent association will exist between the unbound species and the molecular complex. The rate of this reversible interaction is concentration dependent and obeys the simple binding reaction as follows:

$$T + L \underset{k_{off}}{\overset{k_{on}}{\rightleftharpoons}} TL$$

Here T refers to a large biomolecule, typically a protein, and L refers to any substance, typically a smaller molecule, which binds to the protein to form a binary complex, denoted as TL. In this report the binding partners, T and L, are referred to as target and ligand, respectively. Since the reaction is reversible, it does not reach completion and a combination of all three species (T, L and TL) will exist in solution at any given time. Although the reaction is never static, during equilibrium the average concentration of each component is maintained. To fully appreciate the dynamic interplay of a given interaction, it is important that the kinetic rates of complex formation and dissociation, k_{on} and k_{off}, be properly characterized. These kinetic rate constants are interconnected with the concentrations of each species and can be mathematically defined through the law of mass action (**equation 1**).

$$\frac{d[TL]}{dt} = k_{on}[T][L] - k_{off}[TL] \qquad (1)$$

$$k_{on}[T][L] = k_{off}[TL] \qquad (2)$$

At chemical equilibrium, the rate of complex formation is equivalent to the rate of its dissociation, represented by **equation 2,** where $[T]$, $[L]$, and $[TL]$ refer to the equilibrium concentration of T, L, and TL respectively.[18]

1.2.1 Equilibrium Constant of Dissociation

When investigating the binding kinetics between a given target and ligand, a parameter known as the equilibrium constant of dissociation, K_d, is used to quantitatively define the strength of such interaction. Mathematically, K_d is defined through **equation 3** and is measured in units of concentration. If the equilibrium ratio between bound to free target or ligand (i.e. either $[T]/[TL]$ or $[L]/[TL]$) is measured experimentally with reasonable certainty, the K_d value can be calculated. This constant is especially useful in areas of biochemistry and pharmacology as it numerically conveys the natural inclination towards complex dissociation under a given set of conditions. More specifically, K_d is defined as the ligand concentration at which half of the available target molecule is bound.

$$K_d = \frac{k_{off}}{k_{on}} = \frac{[T][L]}{[TL]} \tag{3}$$

$$r = \frac{[L]}{K_d + [L]} \tag{4}$$

The position of any chemical equilibrium can be shifted by altering the initial concentrations of either component; however, the K_d value itself is independent of such considerations. In fact, the calculated K_d is contingent solely on external factors such as temperature and reaction solvent, making it a very useful parameter for conveying the strength of interaction. The ratio of bound target to total target present during equilibrium can be described through a parameter

known as fractional occupancy (**equation 4**), which can be mathematically derived from the initial ligand concentration and intrinsic K_d value (see **appendix** for complete derivation). [19]

By convention, the equilibration time is determined experimentally as the time needed for 90% of the ligand to bind to the excess target. The K_d is established through several equilibrium experiments where the concentration of target is kept constant and that of the ligand is varied from well below the target concentration up until complete saturation is achieved.[20,21] Generally this process is quite lengthy and requires an exhaustive set of experiments to establish a numerically accurate K_d. Although saturation experiments remain the classical approach affinity analyses, alternative techniques are available with added advantages. Experimental approaches may or may not require the separation of free ligand from bound. Although separation-free approaches such as spectroscopy, isothermal titration calorimetry and surface plasmon resonance are capable of affinity measurements, alternative separation-based techniques, including chromatography, membrane filtration, precipitation, surface plasmon resonance and capillary electrophoresis are generally preferred as they can also assist in affinity purification[22]. Several separation-based kinetic methods must take caution to ensure that equilibrium is maintained throughout the separation in order to obtain a reliable K_d measurement. In addition, methods which require target immobilization must ensure that the attachment process does not lead discrepancies in affinity measurements caused by surface adsorption, structural alterations or steric hindrance.[23]

1.3 Aptamers as Ligands

Aptamers are small single stranded (ss) oligonucleotide or peptide-based ligands, which adopt specific three-dimensional structures capable of binding a target molecule with high

affinity and selectivity.[24,25] With nucleic acid-based aptamers, secondary structure is largely established by their distinctive nucleotide sequences and their corresponding base-pair complementarity. It is the unique secondary structure of an aptamer that imparts the binding selectivity towards its target. Their molecular recognition capacity has been shown to parallel that of antibodies, and as a result, aptamers serve as a viable substitute in therapeutic, diagnostic and analytical assays which require such high affinity probes. In addition, aptamers offer unequivocal advantages over traditional affinity probes due to their ease of synthesis, low production cost, amenability to chemical manipulations, and ability to undergo *in vitro* selection.[26,27] Due to their irrefutable versatility, aptamers are now used in several diagnostic and therapeutic applications ranging from biosensory affinity probes[28] to drug candidates[29] and drug delivery vehicles.[30]

1.3.1 Systematic Evolution of Ligands by Exponential Enrichment

In 1990, the laboratories of Jack Szostak and Larry Gold independently developed the first artificially selected nucleic acid ligands from large combinatorial libraries *in vitro,* using an iterative procedure now known by the acronym SELEX (systematic evolution of ligands through exponential enrichment).[31,32] Using *in vitro* selection, aptamers can be isolated from large DNA (or RNA) libraries that consist of roughly $10^{12} - 10^{15}$ unique sequences of potential target binders. Each nucleic acid belonging to the library contains a distinct region of 40 to 80 randomized nucleotides flanked on each side by two constant regions (~20 nucleotides in length) that are intended to serve as binding complements to PCR primers. SELEX begins by briefly incubating a target of interest with the DNA (or RNA) library for a fixed time period to ensure that the mixture has reached chemical equilibrium. Target-binding sequences are isolated from the free DNA in a partitioning step and then used as a template for PCR amplification. The

amplified DNA sequences then serve as an aptamer-enriched library from which the subsequent round of selection is made. The cycle of incubation, partitioning and amplification is repeated for multiple rounds until aptamers with the desired binding parameters are obtained [**Figure 1**].

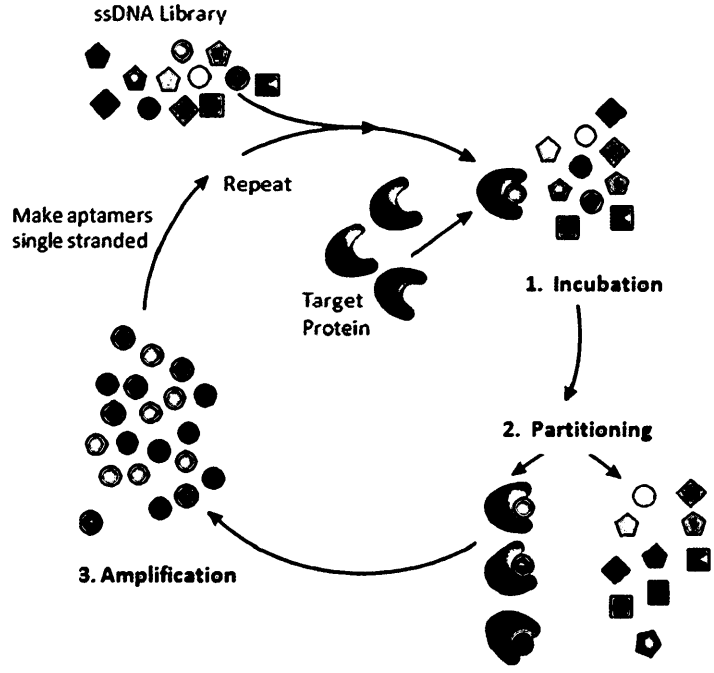

[Figure 1] Schematic representation of the three steps involved in the iterative SELEX procedure: (i) Incubation (ii) Partitioning, and (iii) Amplification.[33,34]

The partitioning of potential aptamers from non-binding sequences is arguably the most crucial step in the SELEX process. Inefficiencies during sequence separation can lead to the unwanted collection of non-specific DNA as well as loss of potential high affinity aptamers, both of which are highly detrimental to *in vitro* selection. By convention, nitrocellulose filtration is frequently elected for partitioning when working with protein targets. Other common sequence partitioning methods include target immobilization approaches such as affinity chromatography and immunoprecipitation. The efficiency of partitioning not only determines the number of rounds needed to produce high affinity aptamers, but it is also central to the success of aptamer development in general. With the advent of SELEX technology, aptamers have been developed

towards a diversified set of targets including inorganic ions[35,36], small molecules[37-40], peptides[41,42], proteins[43-48], nucleic acids[49], viruses[50-52] and even whole cells[53-56]. Still, there are a number of limitations with the procedure and, although aptamer development is promising, it is not guaranteed, and many potential targets are abandoned due to these shortcomings.

1.4 Overview of Electrophoresis

Electrophoresis is a separation technique widely used in clinical chemistry and cell biology for the analysis of charged molecular species. Under the application of a uniform electric field, ionized particles tend to travel towards the electrode of opposite charge. This basic principle can be illustrated in **Figure 2A**, which represents an arbitrary mixture of ions that vary size and charge in the absence of an electric field. An external electric field, E, is produced when an electrical potential, V, is passed through fixed distance, d, which is established through the separation of two electrodes (**equation 5**).

$$E = \frac{V}{d} \tag{5}$$

This results in the voltage activated migration of cations towards the cathode and anions towards the anode as shown in **Figure 2B**. [57]

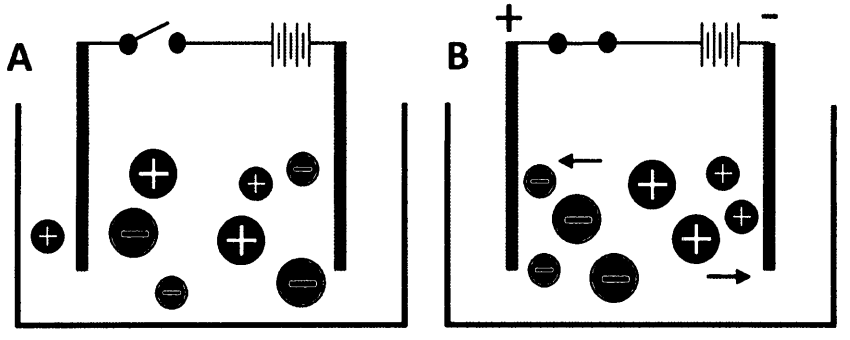

[Figure 2]. A contained solution of assorted electrolytes in both the absence (A) and presence (B) of a voltage-stimulated external electric field.[58]

1.4.1 Electrophoretic Mobility of Charged Analytes

The differential migration between charged analytes relative to the surrounding fluid or gel matrix provides the basis of separation in electrophoresis. The electrophoretic force, F_{ep}, which induces analyte migration, is a function of both the overall molecular charge, q, and electric field strength, E (**equation 6**). As the molecule accelerates, it experiences an additional frictional force, F_f, which resists the forced electrophoretic migration. The frictional force is defined in terms of a frictional coefficient, f, and the particles electrophoretic velocity, v_{ep} based on Stokes' law. For a spherical particle, f can be described in terms of the solution viscosity, η, hydrodynamic radius, r_h, and the numerical constant, 6π (**equation 7**). Once the system reaches mechanical equilibrium and the analyte no longer accelerates, the net force is set to zero and the frictional force is said to equal the electrophoretic force (**equation 8**). Here, the electrophoretic velocity, v_{ep}, is constant and its numerical value can be resolved experimentally for any detectable analyte. Since v_{ep} is a function of the electric field strength, an additional proportionality constant, referred to as the electrophoretic mobility, μ_{ep}, is used to characterize the intrinsic mobility of a given macromolecule, independent of external conditions (**equation 9**).[59]

$$F_{ep} = qE \tag{6}$$

$$F_f = -fv_{ep} = -6\pi\eta r_h v_{ep} \tag{7}$$

$$qE = 6\pi\eta r v_{ep} \tag{8}$$

$$\mu_{ep} = \frac{v_{ep}}{E} = \frac{q}{6\pi\eta r_h} \tag{9}$$

And so it directly follows, that the electrophoretic mobility strength increases with the overall charge magnitude, q, and decreases with a larger hydrodynamic radius, r_h or frictional coefficient, f. This principle can also be visualized in **Figure 2**, where similarly charged ions appear to travel at different velocities depending on their physical dimension and mass.

1.4.2 Joule Heating Effects

Electrophoretic separations are always performed in the presence of a buffer system, which supplies the ions necessary to support electrical conductivity and aids in maintaining a stable pH. The voltage-generated current that travels through the given separation media conforms to Ohm's law of electrical dynamics (**equation 10**), which relates current, I, to voltage, V, through a proportionality constant known as resistance, R. Resistance is defined as a force which acts in opposition to the current flow, and is a direct function of the support media and buffers used during electrophoretic separation. Consequently, background electrolytes of high ionic strength have lower electrical resistance and produce a higher current.

$$V = IR \tag{10}$$

$$Q \propto P = I^2R \tag{11}$$

When an electrical current passes through a resistor, some of the potential energy is dissipated within the resistor and released as heat though a phenomenon known as Joule heating. The rate at which electrical energy is converted into alternate forms is referred to as electrical power, P, which can be expressed mathematically in terms of I and R (**equation 11**). The rate at which thermal energy is absorbed by the electrophoretic resistor, Q, is directly proportional to the total power distributed across the entire system.[60] Joule heating can have detrimental effects

on electrophoretic separation ranging from band distortion, excessive diffusion, and sample denaturation or dissociation.

In free solutions, separation is especially limited by the severe thermal convection associated with the voltage-induced current flow. Since a well-established current is a fundamental requirement in electrophoresis, the associated thermal energy must be efficiently dissipated to avoid excessive heat production within the separation media. Therefore, a gel matrix is usually employed to improve separation capacity as the increased ratio of surface area to volume allows for better heat dissipation. In electrophoresis, shorter separation times are beneficial as this tends to result in narrower bands and greater resolution due to the reduced time-dependent sample diffusion. In theory, this increased band resolution can be achieved by simply increasing the potential difference between electrodes, which would lead to a higher current and shorter separation times. Unfortunately, at high voltages the additional thermal energy cannot be entirely dissipated through the surface and is instead manifested as excessive sample dispersion and uneven temperature gradients which may lead to buffer boiling. This undesirable complication places an upper limit on the operating voltage, and subsequent resolving power, associated with any electrophoretic separation system. [61-63]

1.5 Capillary Electrophoresis

Capillary electrophoresis (CE) is based on the same theoretical principles as slab electrophoresis, yet it is conducted in a narrow-bore (20-300 μm, i.d.) capillary. The small inner diameter of the capillary imparts several advantages over traditional electrophoretic separations. The much larger surface area to volume ratio leads to highly efficient heat dissipation, thereby enabling the use of electric field strengths that are unattainable in conventional electrophoresis.

The use of strong electric fields allows for faster separation, and the effective heat removal minimizes sample diffusion, which collectively results in improved resolution and analytical quality separation. Furthermore, the capillary format offers the added advantages of rapid analysis times, smaller sample volume requirements, gel-free separation and method automation.[64,65]

1.5.1 Basic Instrumental Setup

The typical instrumental setup used in CE is illustrated in **Figure 3**. It consists of a few basic components: a capillary, two electrodes submerged in buffer reservoirs, a high voltage power supply (0-30 kV), a light source, and an on-column detector coupled to an output device. The power supply is physically connected to each electrode and prompts the formation of an electric field across the entire capillary length, from inlet to outlet. Analytes are then carried across the capillary based on their unique migration velocity, and detected as they pass the detection window located near the outlet.[59] Some on-column detection modalities commonly used in CE include UV-absorbance, laser-induced fluorescence, electrochemical or refractive index based approaches. Laser-induced fluorescence (LIF) is the most sensitive mode and is generally preferred when the sample can be chemically derivatized with a fluorescent agent. If sample modification is undesirable or impractical, UV-absorbance is generally used as less-sensitive alternative. Information pertaining to the absorbance or emission of luminescence is detected with a photomultiplier tube, where the output is then read and transmitted through a computer interface.[65,66]

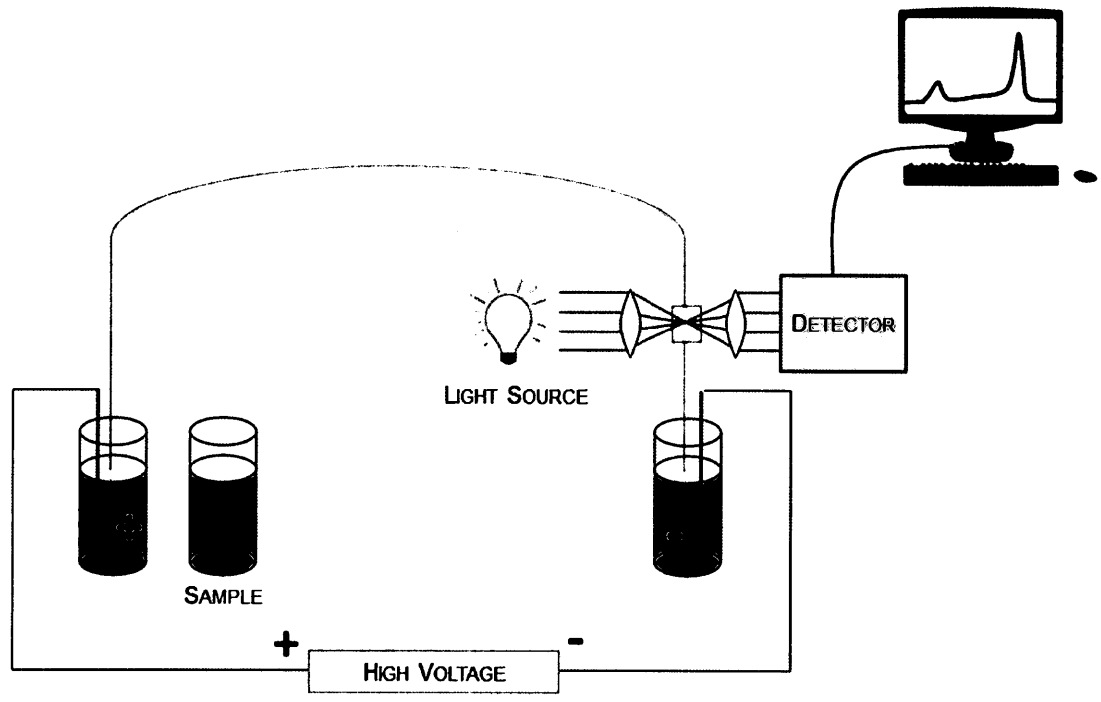

[**Figure 3**] Schematic representation of the basic capillary electrophoresis instrumental set-up including a high voltage power supply, two electrodes, fixed-length capillary, light source and on-column detection system.

In CE, the sample can be injected into the capillary either hydrodynamically through a pressure difference between each end, or electrokinetically by an applied electric field. In each method, the sample is introduced by momentarily transferring the capillary inlet from the buffer reservoir into the sample containing vial. It is possible to accurately control the amount of sample injected at the inlet by adjusting either the voltage or pressure settings of the instrument. Separation is then initiated by replacing the capillary inlet into a reservoir filled with the electrolytic separation buffer under the influence of an external electric field. As the time progresses, the molecular species present within the injected sample plug continue to separate according to their differential migration velocities. In free zone electrophoresis, the apparent velocity of an individual molecule is a direct function of its size to charge ratio in a given

separation buffer. The electrophoretic separation of two negatively charges analytes, denoted as A and B, is illustrated in **Figure 4**.[58]

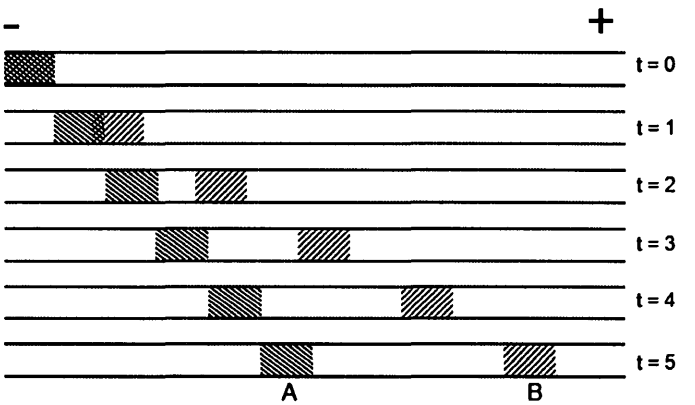

[Figure 4] The time progression of the electrophoretic separation of a sample plug that contains two unique analytes: A and B. The apparent velocity of B is considerably faster than A with complete resolution being achieved by t=2.

1.5.2 The Electrical Double Layer

Fused-silica is, by far, the most common base material used for capillary fabrication due to its inherent flexibility, physical strength and chemical inertness. The outer capillary tubing is often coated with synthetic polyimide to provide added mechanical strength and durability. At physiological pH, the silanol groups of the inner capillary surface retain a considerable negative charge (average pK(SiOH) = 5.3)[67]. Therefore, when completely filled with the separation buffer, the ions present within the electrolyte experience a strong attraction towards the charged silica surface. This leads to the manifestation of two parallel layers with opposing charge at the solid-liquid interface, known as an electrical double layer (EDL). The first layer corresponds to the negatively charged silanol groups which are homogeneously distributed along the capillary surface, while the second layer is formed with the counter ions dispersed within the electrolytic solution. The aqueous layer can be further sub-divided into two distinct regions: an immobile layer and a diffuse layer. The inner region, also termed the immobile or Stern layer, consists of

electrostatically adsorbed cations that are firmly affixed to the capillary surface and remain motionless in the presence of an electric field. The outer region, termed the diffuse layer, also retains a net positive charge but extends out further into the solution and is capable of thermal and electrical motion. Although the immobile layer holds a positive charge, its magnitude is insufficient to neutralize the negative charge of the capillary, and ions within the diffuse layer are needed to completely balance the residual surface charge.[68]

Within the diffuse layer, there exists a hypothetical boundary that separates ions based on their gravitational or electrical motion relative to the stationary surface. This boundary is referred to as the Shear plane. Any ion beyond this theoretical interface will respond favorably to an applied voltage and supply an electrical current across the capillary. The electric potential that exists at the surface and along the edge of the immobile layer, are referred to as the surface potential, Ψ_0, and stern potential, Ψ_δ, respectively. A more useful parameter is the zeta potential, ζ, which refers to the electric potential along the outer limit of the shear plane[69] (see **Figure 5** for EDL interpretation). The zeta potential numerically describes the potential difference between the stationary surface and the mobile dispersion media. In colloidal systems, ζ is used to infer the stability of the suspension and gauges its propensity to form aggregates. In capillaries, ζ is useful as it provides the energetic basis for the electroosmotic flow (EOF), a defining feature of CE.[70]

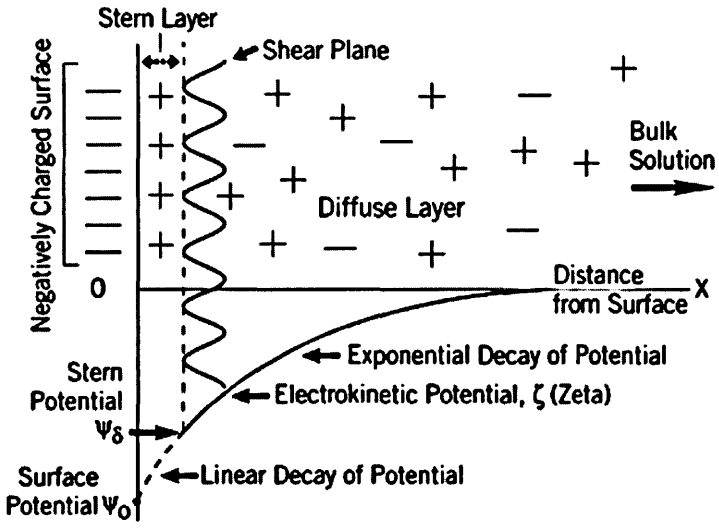

[**Figure 5** Simplified Stern Model of the electrical double layer formed along a fused-silica surface when an aqueous background electrolyte completely permeates the inner capillary. The surface potential decreases linearly with the distance from surface until reaching the Stern potential, after which an exponential decay in potential energy is observed. $\Psi_0$denotes the surface potential of the capillary and the Stern potential,Ψ_δ, corresponds to the energetic potential that exists along the outer limit of the immobile layer. ζ refers to the potential that exists along the Shear plane.[70]

1.5.3 The Phenomenon of Electroosmosis

CE has several advantages compared to other commonly used separation techniques, such as chromatography and filtration, all of which are attributed to the phenomena of electroosmosis. EOF is produced whenever an aqueous solution, in contact with a charged surface, is placed within an electric field. The flow itself is represented as the bulk movement of liquid originating from the shear plane interface in any electrophoretic system. Although an EOF exists in all electrophoresis-based separations, it is generally insignificant and assumed to be negligible in non-capillary formats. It is the high surface-to-volume ratio associated with capillaries that significantly contributes to the added electroosmotic velocity found in CE. The electroosmotic velocity, v_{eo}, depends on a number of external parameters, and is generally modeled using the Smoluchowski approximation[71] listed in **equation 12**. Since the v_{eo} is dependent on the

externally applied electric field, E, a parameter referred to as the electroosmotic mobility, μ_{eo}, is preferred when reporting the EOF of an experimental separation (see **equation 13**).

$$v_{eo} = \frac{\varepsilon\zeta}{4\pi\eta}E \tag{12}$$

$$\mu_{eo} = \frac{v_{eo}}{E} = \frac{\varepsilon\zeta}{4\pi\eta} \tag{13}$$

$$\mu_{ap} = \mu_{eo} + \mu_{ep} \tag{14}$$

$$\mu_{ap} = \frac{v_{ap}}{E} = \frac{L_d/t_m}{V/L_t} \tag{15}$$

Here ε and η refer to the dielectric constant and viscosity of the background electrolyte, respectively, and 4π is a numerical constant. The magnitude of ζ is a function of the capillary surface charge, and is inversely proportional to the valence charge of the counterion and the square root of its concentration. In addition, ζ is highly pH dependent, given that the capillary surface charge is directly coupled to the p*K*a of fused silica. Ultimately, as the electrolyte pH increases, additional silanol groups become ionized creating a more negatively charged surface and, thus, a more negative ζ. In addition to the EOF-dependent mobility, charged analytes also exhibit unique electrophoretic motilities based on their size to charge ratio as denoted in **equation 9**. Therefore, in CE, the apparent mobility of a given analyte, μ_{ap}, is a combination of the electroosmotic mobility of the separation buffer, μ_{eo}, and electrophoretic mobility of the analyte in question relative to the bulk solution, μ_{ep}. Through **equation 14**, it is evident that presence of an EOF allows for the continuous movement of neutral species ($\mu_{ep} = 0$) across the capillary, enabling its detection. An additional benefit of the EOF is the ability to simultaneously

separate positive, negative and neutral molecules based on their size to charge ratio – a feat that is unattainable with alternative separation methods.

In CE, the apparent velocity, v_{ap}, of a particular analyte can be measured experimentally by dividing the capillary length from the inlet to the detector, L_d, by the time needed for that same analyte to reach the detection window (referred to as the migration time), t_m. The electric field strength is determined by dividing the applied voltage by the total length of the capillary, L_t (**equation 15**). The electroosmotic mobility is easily determined experimentally by the monitoring the migration of a detectable neutral marker ($\mu_{ap} = \mu_{eo}$). The concept of electroosmosis and its relationship with the apparent mobility of charged and neutral species is illustrated in **Figure 6**.[58,59,65,72]

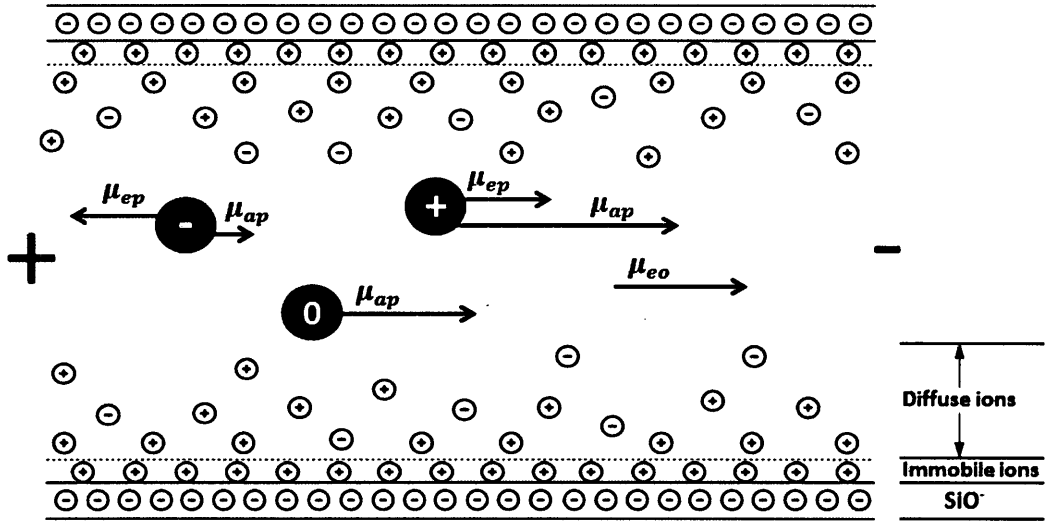

[**Figure 6**] Illustrative depiction of the concurrent free zone CE separation of charged and neutral species in the presence of an electroosmotic flow. The bulk solution travels towards the cathode at a measureable rate, defined through the μ_{eo}

1.5.3.1 Electroosmotic Flow Profile

Another element that favors CE separation over pressure-based separations is the flat cross-sectional flow profile associated with electroosmotic driven fluid propagation. In methods such as liquid chromatography, separation is induced through a uniform pressure application across the column inlet. Although the directed pressure is consistent across the capillary diameter, the liquid in contact with the surface experiences an additional frictional force, which opposes the applied pressure. This then results in a laminar flow profile that is parabolic in nature, where the central fluid travels at a considerably faster rate than that located near the edges. A parabolic profile is undesirable for analytical separations, as it results in increased band broadening and a reduction in the peak resolving capacity of the system. The flat profile produced by through electrically driven flow is a key contributor to the remarkable efficiency and peak resolution in CE separations. The cations that constitute the aqueous portion of the EDL form strong interactions with neighbouring water molecules and exit as closely interconnected bonding networks. When a potential difference is introduced across the capillary, the solvated cations begin to migrate towards the cathode. Since these counterions are clustered mainly along the capillary surface, they tend to drag the bulk solution, including the associated anions, in this direction though viscous forces, which then drives the EOF. Since the flow originates from the thin cationic layer along the surface, the bulk electrolyte tends to travel at a constant rate across the capillary cross-section, and thus, yields inherently flat plug profile (see **Figure 7** for illustration).[65,73]

[**Figure 7**] Illustration of the flow-profiles associated with pressure-driven and electrically driven separation methods. The parabolic profile linked to pressure-based separation methods results from the discontinuous pressure gradient is created by the frictional drag experienced along the capillary edges.[65]

1.5.4 Separation Efficiency and Resolution

In separation sciences, the quality of sample partitioning is generally measured using the number of theoretical plates, which numerically defines the maximal efficiency of a given separation. This value is quantified using parameters which are characteristic to both the sample and its physical surroundings. Conceptually, separation efficiency is linked to the extent of band broadening and the subsequent peak variance that occurs across the column. As a result, the number of theoretical plates, N, achieved during a separation, is a direct function of two parameters (i) the capillary length from inlet to detector, L_d, and (ii) the peak dispersion within the sample, σ (see **equation 16** for relationship).

$$N = \frac{{L_d}^2}{\sigma^2} \tag{16}$$

$$N = \frac{\mu_{ap} V}{2D} \tag{17}$$

$$R_s = \frac{1}{4}\sqrt{N}\frac{\mu_1 - \mu_2}{\bar{\mu} + \mu_{eo}} \tag{18}$$

Ideally, the only source of peak dispersion is the time-dependent longitudinal diffusion experienced by a given analyte across the capillary. The relationship between a molecules diffusion coefficient, D, the applied voltage, V and N is described through **equation 17** (see

appendix for derivation). Large molecules that experience little diffusivity, are better separated in CE and produce a greater N value than small molecules which diffuse readily. Since the total amount of diffusion depends on the time given for separation, theoretically, the efficiency can be controlled through the applied voltage. Resolution, R_s, describes the quality of separation between adjacent peaks, based on their average widths along the baseline. In the presence of an EOF, the resolution between peaks can be calculated with **equation 18**, as first derived by Giddings[74] and later adapted by Jorgenson[75] (see **appendix** for derivation). Here μ_1 and μ_2 represent the electrophoretic mobilities of the two analytes being separated and $\bar{\mu}$ refers to the average mobility of both analytes. Based on this equation, optimal resolution is attained only when the electroosmotic mobility and average electrophoretic mobilities are of similar magnitude but of opposite direction (i.e. when $\bar{\mu} + \mu_{eo}$ approaches zero)

1.6 CE-Based SELEX

Efficient partitioning is essential for the development of high-quality aptamers, since inadequate separation leads to the contamination of protein-bound sequences with unbound DNA. Heterogeneous partitioning methods, such as filtration and affinity chromatography, are limited in their ability to separate and collect DNA sequences which display a strong affinity towards the target. As a result, multiple rounds of SELEX are required to generate aptamers with the desired binding parameters. Moreover, since each partitioning step is characterized by a certain amount of aptamer-loss, a greater dependency is placed on PCR amplification, which in turn, increases the yield of undesirable products.[76]

The well-controlled high-performance separation ascribed to CE, can facilitate the partitioning of aptamers from any non-aptamers present in the equilibrium mixture, and thus,

simplify the SELEX process. Since unbound DNA and protein-bound DNA have unique electrophoretic velocities, highly efficient aptamer partitioning can be achieved in this approach. In 2004, Bowser and Mendosa first introduced CE as a powerful partitioning approach that positively compliments aptamer development through SELEX technologies. The free solution separation imparted by CE, eliminates complications common in two-phase partitioning such as linker bias and non-specific binding to the substrate.[77-80] In 2005, the Krylov group expanded CE-based SELEX to include kinetic and equilibrium measurements via kinetic capillary electrophoresis (KCE) methods. KCE refers to several separation-based affinity methods that function as a platform for the kinetic analysis of non-covalent molecular interactions.[22,81] This is beneficial during aptamer selection as it enables the comprehensive characterization of binding affinity between the protein target and isolated aptamer pools. The ability to elucidate the kinetic and equilibrium constants of interaction (k_{on}, k_{off}, K_d) after each round of selection makes KCE methods ideal in SELEX. One to four rounds of KCE-based partitioning is generally sufficient to complete the selection process,[82-85] while other partitioning methods typically require more than 10 rounds. The high efficiency of KCE methods allows the intermediary PCR steps to be excluded during aptamer selection, by an approach entitled Non-SELEX.[86-88] In addition, KCE methods uniquely allow for the selection of smart aptamers- aptamers with predefined binding parameters.[89,90]

1.6.1 Non-Equilibrium Capillary Electrophoresis of Equilibrium Mixtures

Non-equilibrium capillary electrophoresis of equilibrium mixtures (NECEEM) is the most widely used KCE method for SELEX partitioning[91] and is frequently referred to within this report. NECEEM begins by introducing a sample plug containing the equilibrium mixture (EM) into the capillary (**Figure 8a**). In the case of KCE-SELEX, this EM contains unbound protein,

unbound aptamers and protein-aptamer complex, which separate during electrophoresis. When the sample undergoes separation, equilibrium is perturbed, prompting complex dissociation. Throughout the course of separation, the sample is shifted further from the equilibrium conditions, and the complex undergoes further dissociation. The rate of dissociation depends largely on the binding affinity an individual aptamer has towards the protein. Aptamers with a high affinity will remain bound and be detected as a complex peak, while any aptamers that have dissociated will be observed as a decay curve (**Figure 8b**). Since the DNA aptamers are fluorescently tagged, the CE migration time of unbound aptamer, protein-DNA complex, and aptamer that has dissociated from the complex can be visualized in LIF detection modes (**Figure 8c**). By integrating the areas of the unbound aptamer (A_1), aptamer-protein complex (A_2), and aptamer dissociated from the complex (A_3) the equilibrium dissociation constant (K_d) can be determined using **equation 19**, where $[P]_0$ is the initial concentration of protein and $[DNA]_0$ is the initial concentration of aptamer (see **appendix** for derivation). NECEEM can also be used to establish the first order rate constant of dissociation, k_{off} by applying **equation 20** (see **appendix** for derivation).[92,93]

$$K_d = \frac{[P]_0 - [DNA]_0\{1 - A_1/(A_1 + A_2 + A_3)\}}{(A_1 + A_2 + A_3)/A_2 - 1} \tag{19}$$

$$k_{off} = \frac{1}{t_{P \bullet DNA}} \ln\left(\frac{A_2 + A_3}{A_3}\right) \tag{20}$$

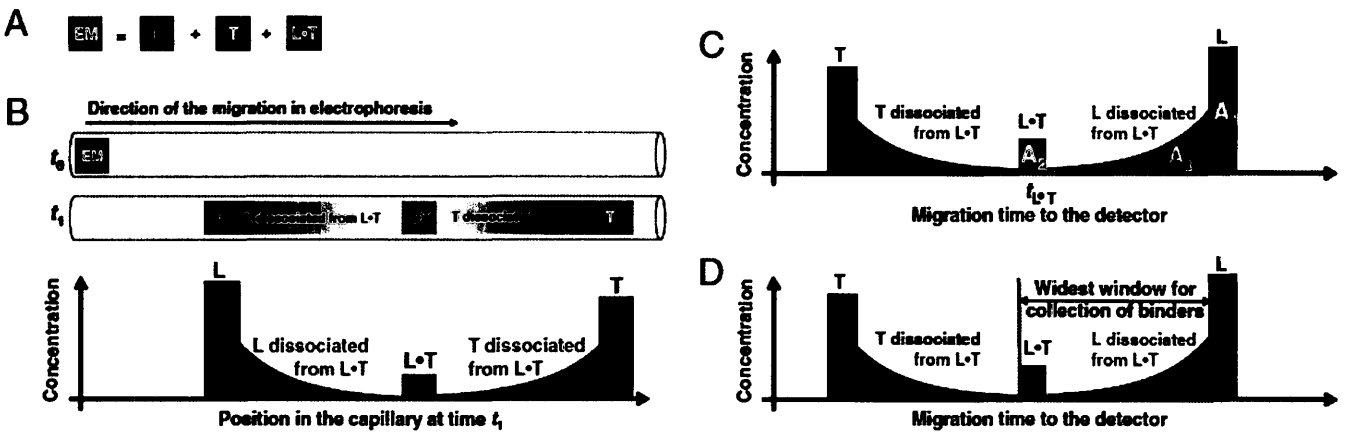

[Figure 8] Illustration of non-equilibrium capillary electrophoresis of equilibrium mixtures (NECEEM). (a) Components of the equilibrium mixture where L represents free ligand (or aptamer), T represents free target (or protein) and T · L represents target-ligand complex (or protein-aptamer complex). (b) NECEEM-based separation of T, L and T · L during electrophoreses. A short plug of the equilibrium mixture is introduced at time, t_0, and is the subjected to separation by applying a high voltage. In this case, the target/protein mobility is greater than that of the ligand while the target-ligand complex is intermediate. Any target or ligand that remained in an unbound state at equilibrium will migrate as individual peaks and their mobility is constant during the separation. Since the target-ligand complex was formed under equilibrium conditions, some dissociation will occur due to the introduction of non-equilibrium conditions, shown as the decay curves. Only a fraction of the target-ligand complex remains in the bound state at the time of detection. (c) Illustration of the quantitative parameters used in K_d calculation (equation 19) (d) Displays the widest window that can be chosen for aptamer selection as it selects for all ligands that were bound to the target during equilibrium.[93]

In order to physically isolate aptamers form non-aptamers present in the EM, a well-defined window for aptamer collection must be established. Aptamer collection boundaries can be optimized by performing pre-selection steps which identify the electrophoretic mobility of the protein, DNA library and most importantly, the protein-aptamer complexes. The widest collection window that can be chosen for aptamer selection, **Figure 8d**, spans from the beginning of the complex peak up until the region of free DNA.

1.7 Nanopore DNA Sequencing

DNA sequencing technologies have undergone rapid advancements and the introduction next generation sequencing has led to impressive scientific achievements. However, there are still a number of challenges that need to be addressed before complete genome analysis can be

routinely practiced. Current sequencing approaches require multiple copies of the DNA sample which are generated through PCR amplification. This step introduces limitations to both the speed and quality of genome sequencing as the replication process is time consuming and can produce artifacts or errors.[94,95] Moreover, conventional detection platforms rely on fluorescent labeling which requires DNA modifications and add to the overall mechanistic complexity. A label-free, single molecule detection system, combined with high-throughput analysis would radically simplify genomic sequencing. Nanopore-based DNA sequencing is an emerging technology which has the potential to analyze the entire genome in minutes at a relatively low cost. A collaborator at Oxford University, Hagan Bayley, has been developing nanopore sequencing using a pore-forming protein toxin secreted by *Staphylococcus aureus,* known as α-hemolysin (α-HL). *In vitro,* α-HL spontaneously inserts into artificially synthesized lipid bilayer thereby creating a small pore within the membrane. The pore then serves as a channel which separates two reservoirs of buffered salt solution. If a voltage bias is applied across the membrane, a current can be generated through the pore by the surrounding electrolytic solution. When a particle is momentarily drawn through the nanopore, a transient interruption in ion conductance can be recorded and quantified electrically.[96] Each DNA base is capable of generating a characteristic reduction in current as it passes through the pore, allowing for direct detection in real time. Since the α-HL pore can harbour 10-15 nucleotides at any given moment, the single stranded DNA must first be processed into its individual bases to ensure correct identification upon pore entry.[97]

1.7.1 Exonuclease I (*E.coli*): A Potential Target for KCE-SELEX

Exonuclease I (Exo1), a protein native to *Escherichia coli,* processively cleaves single stranded DNA from the 3' end resulting in the sequential release of its nucleotide

constituents.[98,99] If Exo1 is closely connected to α-HL, each individual base can be readily delivered through the nanopore in a well-controlled manner.[100] The attachment between the two proteins should be highly specific, localized and reversible, to allow for optimal orientation and easy Exo1 replacement. Artificially selected aptamers could provide the ideal linkage leading to the project's success. If a suitable aptamer can be developed towards Exo1, nanopore sequencing may quickly progress into a reality. However, Exo1 is a difficult target for aptamer selection as the single stranded DNA library will serve as a substrate and will ultimately degrade upon incubation with the active protein. There are many factors that need to be considered when dealing with this specific target. First, conditions where Exo1 activity is suppressed need to be established. Second the aptamer should be selected towards the proteins native conformation to ensure binding to the active form. Thirdly, the aptamer should not bind near the active centre as this will lead to enzymatic inhibition. Although the target is complex, by employing the appropriate pre-selection optimization, the KCE-SELEX process can be enhanced, even for difficult targets. This project will also lay down some general framework for aptamer development towards exonuclease targets which may eventually assist in nanopore-based DNA sequencing.

Chapter 2: Enhancing KCE-SELEX through Protein Labeling

2.1 Pre-Selection Optimization

KCE-based aptamer selection can be optimized in three distinct steps: (i) finding conditions under which the protein does not interact with the capillary inner wall, (ii) maximizing the separation between the target protein and the DNA library, and (iii) determining the aptamer-collection window (**Figure 9**).[3]

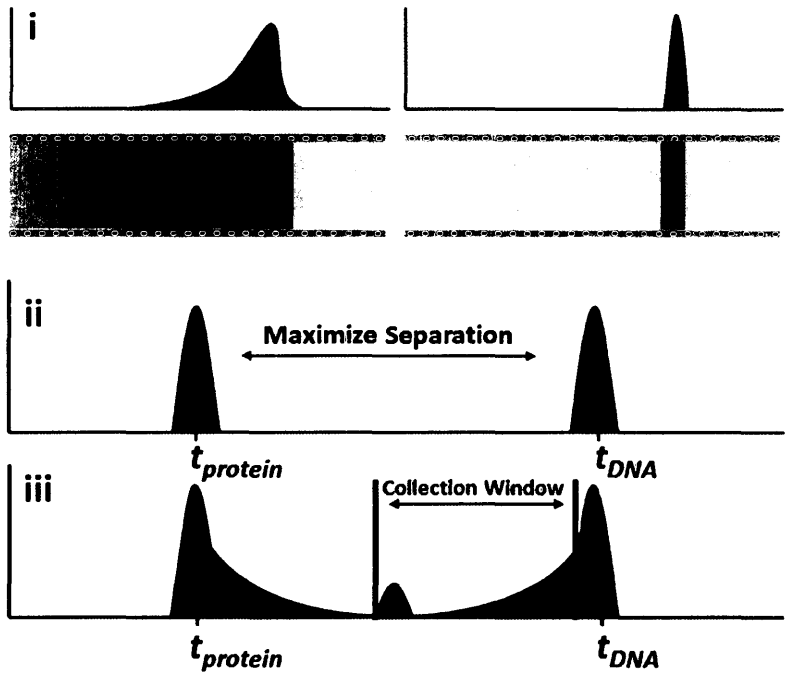

[Figure 9] Schematic illustration of the three steps of optimization in KCE-based aptamer selection: prevention of protein adsorption to the inner capillary wall (i), maximizing the protein-DNA separation window (ii), and determination of the aptamer collection window (iii).[3]

To perform these three steps of pre-selection optimization, both the DNA library and protein target or complex must be detected. In the analysis of biomolecules, ultraviolet (UV) absorbance and laser induced fluorescence (LIF) are the most widely used CE detection modes.

Although LIF is markedly more sensitive, UV absorbance is often used when fluorescent tagging is not a possibility due to alterations in analyte structure and CE mobility.

In KCE methods, DNA can be easily tagged with a fluorescent label while maintaining its native electrophoretic properties; therefore, both UV absorption and LIF can be used for library detection. As for the protein, earlier studies on fluorescent labeling of proteins had resulted peak broadening and a significant shift in CE migration times, making the labeling procedure unsuitable for optimizing KCE-based aptamer selection.[101] Therefore, only a single means of protein detection, light absorption in the UV region of the spectrum, has been used to facilitate the selection process. This creates a problem in all three steps of optimization. Since the path length across the injected sample is restricted to the small diameter of the capillary, UV detection often lacks the sensitivity needed to accurately identify target peaks at low micromolar concentrations. Due to the multistep nature of protein purification, the concentration of many proteins are below the detection limit for UV absorbance at 280 nm, and at 214 nm the protein peak is often indistinguishable from those attributed to buffer components or sample contaminants. In these cases, optimization steps 1 and 2 cannot be carried out when using detection by light absorbance.

The inability to detect the protein can also present a challenge in step 3, which typically relies on the fluorescently labeled DNA library. Under ideal circumstances, the labeled DNA is sufficient to detect both the complex and DNA which will, accordingly, establish the aptamer collection window (see **Figure 9C**). However, if the protein has nuclease activity, as with Exo1, the library may become partially degraded during the incubation period and these products of degradation can be mistaken for the complex.

It is also possible that the complex peak remains undetected during the bulk affinity assay even at the highest available target concentrations. In these situations, the mobility of the pure protein is used as a reference for boundary determination, which again relies on UV absorbance. If not optimized, KCE-based aptamer selection has a much lower chance of success. If the target protein can be fluorescently labeled so that it is compatible with KCE-based SELEX, aptamer development can be facilitated.

2.2 Protein Labeling and KCE-SELEX

Labeling reagents typically react with positively charged ε-amine groups on the exposed lysine residues and alter the protein's charge upon conjugation. If the proteins charge-to-size ratio is affected by the labeling procedure, it corresponding electrophoretic velocity will be shifted making the observed migration time unreliable. Some of the best-studied and most widely used labeling reagents tend to neutralize the charged residues with which they react. Consequently, the migration of the labeled product cannot be used to accurately extrapolate any mobility information on the native molecule. Furthermore, conjugation reactions are often incomplete and the fluorescently labeled products generally vary in the number of reacted lysine residues. Therefore, protein labeling has largely been avoided during the pre-selection optimization steps of KCE-SELEX.

2.2.1 Chromeo P503 as a Labeling Reagent

Recently, a new series of fluorescent pyrylium dyes, termed Chromeo, have become commercially available.[102] These dyes can enable fluorogenic labeling without changing the proteins charge during the process. Dovichi and coauthors demonstrated that Chromeo dyes can be successfully used in capillary isoelectric focusing, as the proteins p*I* is maintained.[103,104]

Ideally, for KCE-SELEX applications, protein labeling should include three specific properties. First, it cannot significantly shift the proteins migration with respect to the time-window chosen for aptamer collection. Second, labeling should not prevent protein-DNA binding. Third, the labeling reaction should be compatible with commonly used amino-containing buffers such as Tris, glycine, etc. Each of these three properties of protein labeling was investigated using a dye from the Chromeo family. Chromeo P503 was chosen to test these three properties of protein labeling given that its quantum yield increases by a factor of 50 when bound to the protein. This feature effectively eliminates any background signal, allowing for sensitive detection. Chromeo P503 offers additional advantages over other Chromeo dyes, which can be attributed to its unique spectral properties. The excitation wavelength at 503 nm is similar to both the FAM and Alexa488-labeled DNA libraries, while its emission is shifted to a much longer wavelength [**Figure 10**]. This would allow both the protein and DNA to be excited simultaneously by the same laser source yet detected though different channels by using the appropriate band-pass filter.

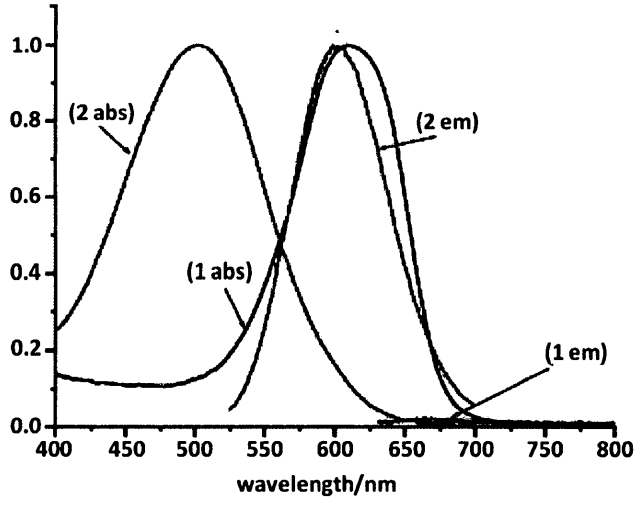

[Figure 10] Spectral properties of the pyrylium dye Chromeo P503 as listed by the manufacturer. The blue lines labeled (1 abs) and (1 em) refer to the absorbance and emission spectrums of the free label prior to protein conjugation, respectively. The absorbance and emission spectra of the conjugated dye are represented through the pink spectral data labeled (2 abs) and (2 em), respectively.[102]

2.2.2 Limits of Detection for Labeled and Unlabeled Proteins

First, it was confirmed that the fluorescent labeling of proteins with Chromeo P503 considerably improved their detection in CE when compared to light absorbance of the native protein. Due to the significant variations which exist in the physical-chemical properties of proteins, a series of proteins models were analyzed; bovine serum albumin (BSA), human serum albumin (HSA), α_1- acid glycoprotein (AGP), myoglobin, and α-lactalbumin. This range of protein standards secures the reliability of the experimental conclusions and enables a reasonable power of prediction. The results, shown in **Table 1**, suggest that the lower limit of detection improves (for the five proteins studied) from an average value of 1620 to 35 nM when switching from UV light absorbance of the unlabeled proteins to fluorescence detection of the labeled proteins (see **supplementary information** for details).

[Table 1] Limits of detection of unlabeled and Chromeo-labeled proteins detected with UV absorbance and fluorescence, respectively.

Protein	Limit of detection (nM)	
	UV Absorbance	**Fluorescence**
AGP	2600	3
BSA	500	2
HSA	400	1
Myoglobin	3100	120
α-lactalbumin	1500	60

This detection limit is suitable for KCE-based aptamer selection since proteins are typically available, and often used, at concentrations higher than 35 nM. Thus, for the majority of proteins, Chromeo-labeling can facilitate the optimization of aptamer selection provided that the label does not influence the proteins electrophoretic mobility to a great extent.

2.2.3 Mobility Shift of Chromeo-Labeled Proteins

In order to quantify the mobility shift attributed to the Chromeo label, we measured the difference in the migration times of native and Chromeo-labeled proteins with respect to the separation window between the protein and DNA library. These experiments were performed using the five previously listed proteins, as they were available at concentrations high enough to produce a reliable signal when using UV absorbance for detection.

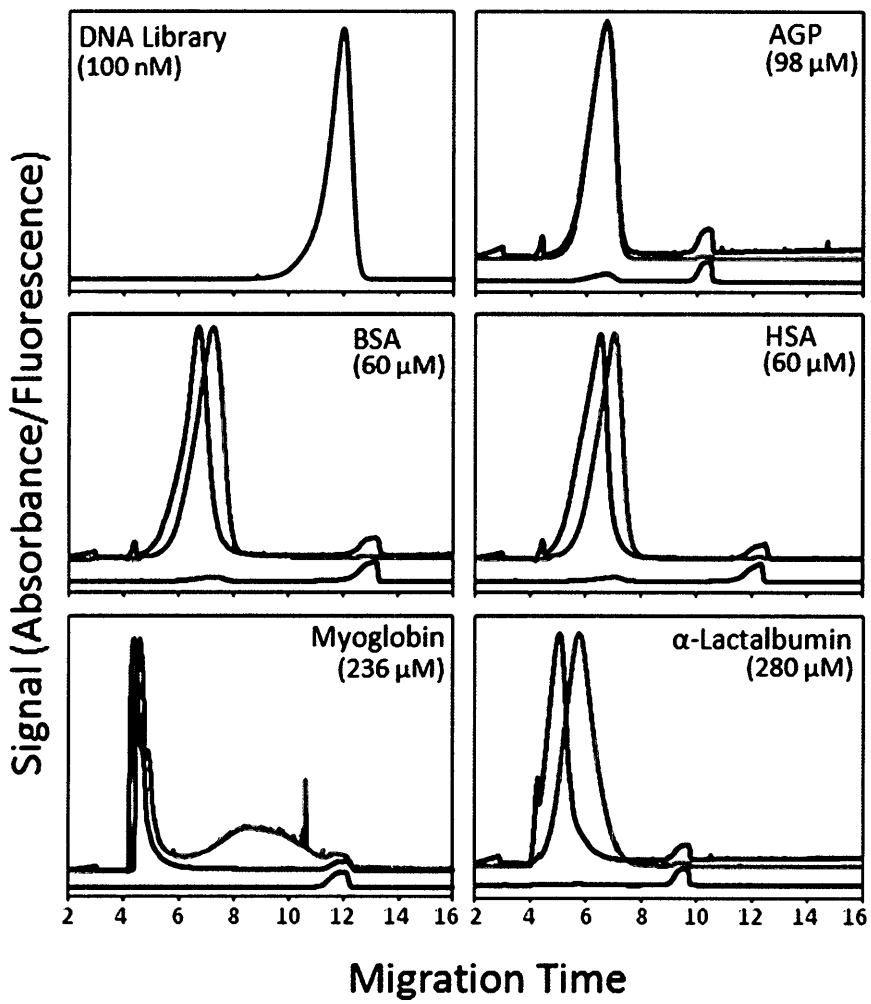

[Figure 11] Effect of Chromeo labeling on protein mobility in CE. Unlabeled proteins were detected by UV absorbance at 214 nm using 50 μM fluorescein as a migration standard (blue traces). Chromeo-labeled proteins were prepared at the same concentrations which were used for UV absorbance detection. Fluorescence of labeled proteins was excited by a 488 nm solid-state laser and detected using a 610 nm filter (red traces). Fluorescence of the migration standard, 10 nM fluorescein, and the DNA library were excited using the same 488 nm laser and detected through a 520 nm filter (black traces).

The top left panel in **Figure 11** shows the electrophoretic mobility of the library; the remaining panels demonstrate the CE migration of the unlabeled and Chromeo-labeled proteins, detected using UV absorbance and LIF, respectively. For each protein tested, only a marginal shift in the electrophoretic mobility was observed following the labeling reaction. α-Lactalbumin expressed the greatest shift in electrophoretic migration upon labeling, which was found to be approximately 10% of the protein-library separation window. Moreover, Chromeo P503 does not lead to labeling products with heterogeneous mobility since all labeled proteins migrate as individual peaks with widths similar to those of the native proteins, a result which could not be obtained by FQ-labeling.[101] From these results, we conclude that Chromeo-labeled proteins can be used in the first two steps of optimization for KCE-based aptamer selection.

2.2.4 Labeling Influence on Protein-Aptamer Interactions

For step 3 of the optimization process (determining the aptamer collection window), the labeling process should not significantly perturb protein-DNA binding. **Figure 12** illustrates how protein labeling influenced aptamer binding by using two proteins for which aptamers were readily available: thrombin[105] and AlkB[106]. NECEEM experiments were performed, to determine the equilibrium (K_d) and rate (k_{off}) constants of dissociation for the protein-aptamer complex.[92,107-109] With the use of a 520 nm filter, only the fluorescence emitted by the DNA library was detected and shown in each trace.

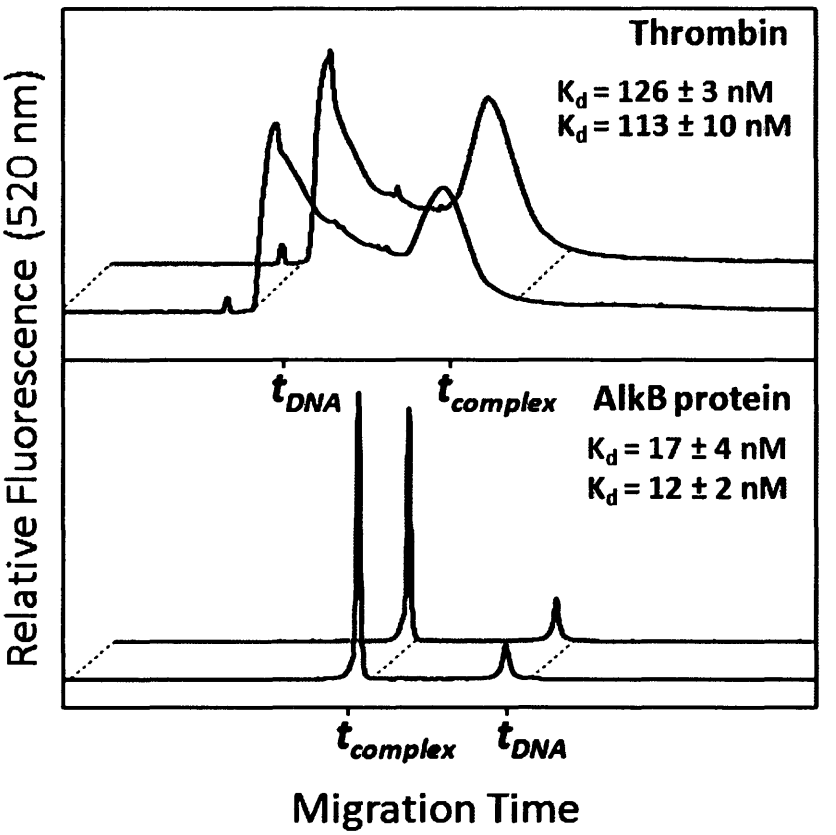

[Figure 12] Influence of Chromeo-labeling on aptamer binding and affinity for thrombin (upper panel) and AlkB protein (lower panel). NECEEM binding assays were performed by using equilibrium mixtures containing labeled aptamer and either labeled (red lines) or unlabeled (black lines) protein. The concentrations of thrombin and its aptamer were 0.5 and 0.1 μM, respectively. The concentrations of AlkB protein and its aptamer were 80 and 30 nM, respectively. Only DNA is detected when fluorescence is measured at 520 nm.

We can easily see that the NECEEM electropherograms are similar for both the Chromeo-labeled and unlabeled proteins in both aptamer/protein models. This result was unexpected but is not counterintuitive. Indeed, while labeling can affect biomolecular interactions, the wide use of fluorescently labeled antibodies suggests that when it comes to binding other molecules, proteins have a relatively high tolerance toward the labeling of a limited number of residues. Our observation certainly does not prove that Chromeo labeling will be this inert to all protein-aptamer pairs. However, during step 3 of optimization, which relies on the interaction of the protein with the entire library (known as bulk affinity assays), the influence of Chromeo-labeling is expected to be negligible for the majority of proteins. The library

provides and incredibly large number of DNA structures, and even if labeling prevents the interaction of some structures, it may equally increase the protein's affinity to others. Since the bulk affinity assay is done prior to both the collection and amplification steps, the labeled protein can be used initially for optimization and predictive purposes while the unlabeled protein is subsequently used for aptamer selection. This approach would enhance the selection process and ensure that the aptamers will bind tightly to the native protein. Therefore, it is possible to use Chromeo-labeled proteins in step 3 of the optimization process.

2.2.5 Identification of the Protein-Aptamer Complex

Chromeo-labeling of the protein target can also be used to correctly identify the protein-DNA complex from other unknown peaks such as library-degradation products. This distinction can be made by simultaneously detecting the protein and DNA at two different wavelengths. Both the Chromeo-labeled protein and Alexa-labeled DNA can be excited using the same 488 nm laser line; however, their emission wavelengths are unique, 610 nm for the protein and 520 nm for the DNA. Thus, with the use of a two channel detection system, the fluorescence emitted from both the DNA and protein can be separated into two distinct electropherograms. The principle of complex distinction is based on the fact that the protein-DNA complex will fluoresce only at a single wavelength, unless bound to the protein. To illustrate this approach, we conducted an experiment in which we used either Chromeo-labeled or unlabeled thrombin and its Alexa-488 labeled aptamer, with fluorescence detection at both 520 nm and 610 nm. NECEEM experiments were performed in which we expect to observe two main peaks: unbound aptamer and protein-bound aptamer.

When the unlabeled protein is used in the equilibrium mixture (upper panels in **Figure 13**), only DNA fluoresces and, ideally, we expect to see no signal in the 610 nm channel.

However, the channel picks up the spectral tail of Alexa fluorescence from the DNA and records a signal similar to that in the 520 nm channel but at a much lower intensity. The similarity can be confirmed by normalizing the signals from the two channels; the normalized signals are identical. The peak located at the right side of each panel in **Figure 13** is tentatively assigned to the protein-DNA complex but it may potentially be a product of DNA degradation that migrates differently from the intact DNA.

To test whether or not this assignment is correct, we used the Chromeo-labeled thrombin (lower panels in **Figure 13**). In this case, the signals at the two wavelengths are not similar; in the 610 nm channel, the right-hand side peak is higher relative to the left-hand side peak. This becomes clearly evident when the signals are normalized. Both the Chromeo label of the protein and the Alexa label of the DNA contribute to this peak while the left peak is solely the spectral tail of DNA fluorescence. This allows us to accurately conclude that the right-hand side peak is the complex and not any other product such as aptamer degradation. This simple model experiment proved that Chromeo labeling of the protein can facilitate the simple identification of the protein-aptamer complex from all other possible peaks. This distinction is crucial during the determination of the aptamer-collection window, step 3 in the optimization process, and throughout the course of selection.

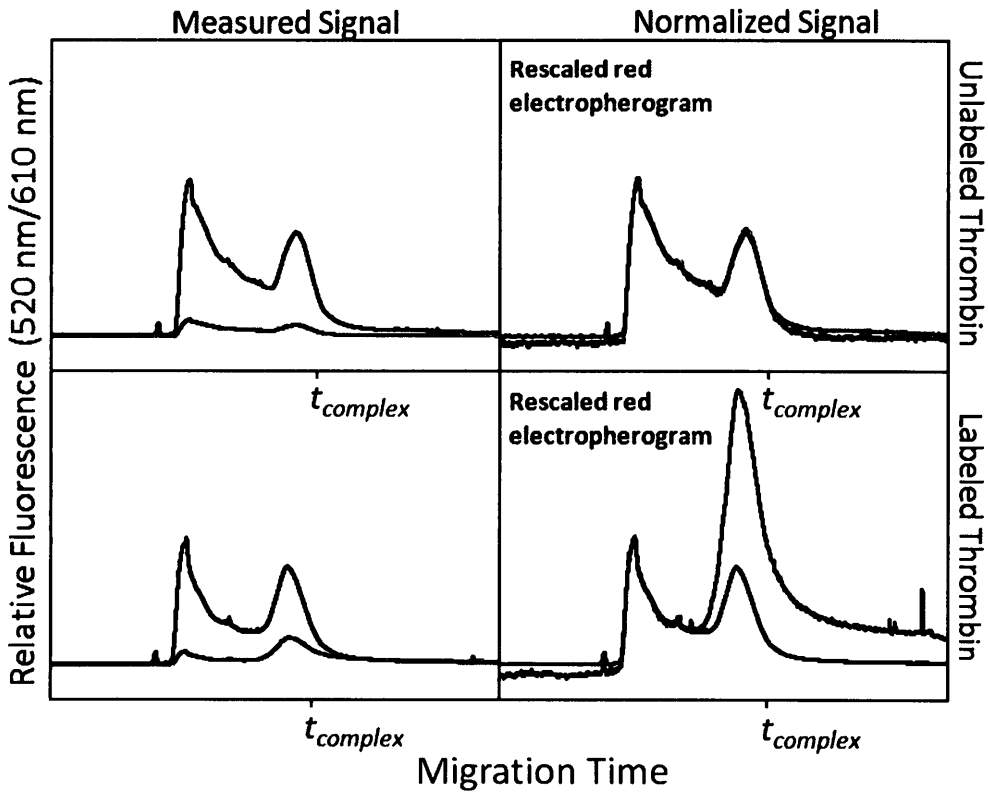

[Figure 13] Peak identification of the thrombin-aptamer complex through the combined use of Chromeo-labeled thrombin and Alexa488 labeled aptamer. Back traces depict fluorescence at 520 nm while the red traces represent fluorescence at 610 nm. Upper panels show NECEEM electropherograms obtained with the native thrombin; lower panels show NECEEM electropherograms obtained with the Chromeo-labeled thrombin. The left panels show the measured signals, while the right panels show the same data with the red electropherograms rescaled to have the heights of the left peaks identical for the black and red electropherograms. The concentrations of thrombin and aptamer were 0.5 and 0.1 μM, respectively.

2.2.6 Chromeo-labeling with Amine-containing Buffers

Aptamer selection by KCE methods is often conducted in buffers containing amino-groups, such as Tris and glycine. Since Chromeo dyes react with primary and terminal amino groups present on the proteins, they can potentially react with amino groups present in buffer components. The labeled buffer can, in turn, interfere with protein detection. To test this potential problem, we performed a labeling reaction using Exo1, which was stored in a Tris-containing buffer. By comparing the electropherogram of the labeled protein to that of the labeled storage buffer containing the Tris-component, the migration of the pure protein can be

inferred. It is evident from **Figure 14,** that the Tris buffer, which is present at a much higher concentration than Exo1, produced a much smaller peak relative to the protein. This suggests that Chromeo-labeling is compatible with amino-containing buffers.

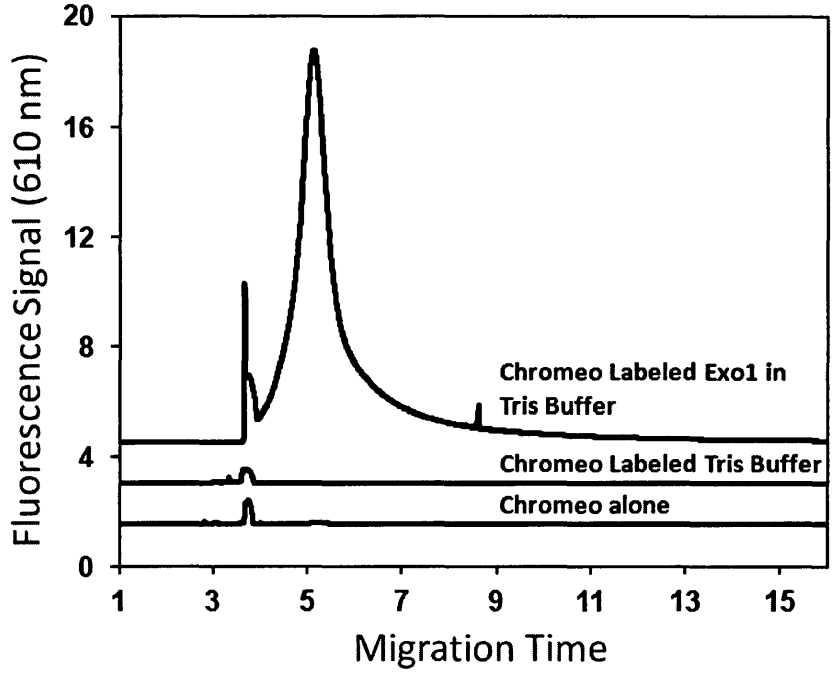

[Figure 14] Negligible effect of amino-containing buffer components on fluorescence signal from Chromeo-labeled Exo1 protein. The top trace shows the electropherogram obtained from the Chromeo-labeled Exo1, which was stored in buffer containing 10 mM Tris-HCl. The middle trace is a control illustrating how this Tris buffer reacts with the Chromeo dye. The bottom trace is a second control which illustrates the peak obtained from the Chromeo dye alone.

2.3 Experimental

2.3.1 Materials

Uncoated fused-silica capillaries with 75 μm inner diameter (375 μm outer diameter) were purchased from Polymicro (Phoenix, AZ). Chromeo P503 pyrylium dye was purchased from Active Motif (Burlington, ON, Canada). AlkB and Exo1, both native to *E.coli* was provided from collaborators at Oxford University and Oxford Nanopores, respectively. Human-

α-Thrombin was purchased from Haematologic Technologies Inc. (Essex Junction, VT). Bovine Serum Albumin (BSA), Human Serum Albumin (HSA), α_1- Acid glycoprotein (AGP), Myoglobin, α-Lactalbumin and all other chemical reagents were purchased from Sigma Aldrich (Oakville, ON, Canada). The HPLC purified fluorescently labeled AlkB aptamer (5'-FAM/TGC CTA GCG TTT CAT TGT CCC TTC TTA TTA GGT GAT AAT A-3') and thrombin aptamer (5'Alexa488/CGC TTG GTG TGG TTG GAA AAA AAA AAA AAA AAA AAA AAA A-3') were purchased from Integrated DNA technologies Inc. (Coralville, IA). The DNA was dissolved in 10mM Tris-acetate buffer, pH 7.5 to obtain a high stock concentration which was then stored at -20°C until use. All other solutions were prepared in deionized water and filtered through a 0.22 μm filter (Millipore, Nepean, ON, Canada)

2.3.2 Instrumentation

All experiments were conducted using a P/ACE MDQ capillary electrophoresis instrument (Beckman-Coulter, Fullerton, CA) equipped with either a photo-diode array (PDA) or LIF detector. A 488 nm solid-state laser was used to excite Alexa-488/ FAM labeled DNA and Chromeo labeled proteins. A two-channel detection system was implemented in order to detect both the protein and DNA simultaneously. A 520 nm filter was used to detect the fluorescently labeled DNA through one channel, while a 610 nm filter was used to detect the Chromeo-labeled proteins through the second channel.

2.3.4 Electrophoresis Conditions

The separation buffer used in all CE experiments was 50 mM Tris-acetate (pH 8.2). Prior to each run, the uncoated capillary was conditioned by rinsing with 0.1 M HCl, 0.1 M NaOH, ddH_2O, followed by 50 mM Tris-acetate (pH 8.2) using a pressure of 20 psi for 2 min. The

polyvinyl (PVA) coated capillary was rinsed with ddH_2O and 50 mM Tris-acetate (pH 8.2) at 10 psi for 4 min. A total of 50 nL of the sample was introduced into the capillary using a 0.5 psi pressure pulse for 10s. The cartridge temperature was controlled at 15°C for each run.

2.3.5 Protein Labeling using Chromeo P503

Proteins that were available in lyophilized powder form (BSA, HSA, AGP, Myoglobin and α-Lactalbumin) were dissolved in 100 mM $NaHCO_3$ (pH 8.3) to a concentration of 4 mg/ml. The solution was then divided into two 200 µL aliquots, one of which was labeled with 2 µL Chromeo P503 working solution. The protein was left to incubate at room temperature for 30 min to complete the conjugation reaction, which was observed by a colour change from blue to red. Proteins that were already stored in a storage buffer (Exo1, AlkB, and Thrombin) were labeled by diluting the protein stock in a 1 to 100 mixture of the Chromeo working solution and 100 mM $NaHCO_3$ (pH 8.3), respectively. The final protein concentration present in the labeling was greater than 5 µM in each case. The labeling reaction was left to incubate overnight at 4°C to maintain protein structure and activity. The Chromeo-labeled-Tris buffer was prepared in a similar manner to Exo1; however, the storage buffer containing 10 mM Tris-HCl (pH 8.0) was used in replace of the protein.

2.3.6 Migration Shift of Labeled proteins

50 nL of the unlabeled protein solution and 50 nL of 50 µM fluorescein, diluted in 0.1 M $NaHCO_3$ (pH 8.3), were co-injected into a 50 cm uncoated capillary (75 µm i.d.). The sample was separated using 20 kV, and detected with a PDA detector at 214 nm with the temperature controlled at 15°C. 50 nL of the labeled protein and 50 nL of a 10 nM fluorescein, diluted in 0.1

mM $NaHCO_3$ (pH 8.3), were co-injected into the same 50 cm capillary, separated using 20 kV and detected with LIF through both the 520 nm and 610 nm channels.

2..3.7 NECEEM-Analysis of Protein-Aptamer Interaction

With the use of a thermal cycler (Eppendorf, Hamburg, Germany), 1 μM of the aptamer was heated to 95 °C for 1 min followed by a controlled decrease in temperature at a rate of 0.5°C per second until the sample reached 25°C. This temperature treatment, or "annealing", is necessary as it promotes the proper folding of the ssDNA aptamers.

A mixture containing 0.5 μM of labeled/unlabeled thrombin and 0.1 μM thrombin aptamer was prepared in a 20 mM Tris-acetate (pH 8.2) buffer supplemented with 5 mM KCl and 1 mM $MgCl_2$. The mixture was left to incubate for 15 min at room temperature prior to separation in a 50 cm PVA coated capillary, which was used to reduce protein adsorption to the inner capillary surface. A voltage of 10 kV was used for the first 5 min of the separation in order to avoid sample overheating in the uncooled region of the capillary.[110,111] The voltage was then increased to 20 kV for the remainder of the run.

A mixture containing 80 nM labeled/unlabeled AlkB protein and 30 nM AlkB aptamer was prepared in a 50 mM HEPES (pH 7.5) buffer containing 50 mM NaCl. Following a 15 min incubation, the equilibrium mixture was injected into a 50 cm uncoated capillary. A voltage of 10 kV was applied for the first 5 min of the run, which was subsequently increased to 20 kV.

2.4 Conclusions

The above described protein-labeling approach was shown to assist in the latter two steps of pre-selection optimization. The pyrylium dye, Chromeo P503, can facilitate the sensitive

detection of the target in CE without significantly affecting its electrophoretic mobility or DNA-binding capacity. These findings, along with the low reactivity toward amino-groups present in common buffer solutions and the ability to correctly identify protein-aptamer complex peaks from products of DNA degradation or contaminants, makes Chromeo labeling an useful addition to the tool-box of KCE-based aptamer selection. This opportunity has the potential to significantly increase the success-rate in KCE-based aptamer selection, and thereby, contribute to the further development of aptamer-based diagnostic and therapeutic tools

2.5 Supplementary Information

2.5.1 Establishing the Limit of Detection

Solutions of labeled and unlabeled BSA, HSA, AGP, myoglobin and α-lactalbumin were prepared as serial dilutions in a 100 mM $NaHCO_3$ (pH 8.3) dilution buffer. 50 nL of the sample was introduced into a 50 cm uncoated capillary (75 μm i.d.) and protein migration was induced by applying 20 kV. A PDA detector was used to detect the protein at 214 nm, while fluorescence emission at 610 nm was used to detect the labeled protein. The standard deviation of the background signal height (within the 1 to 2.5 minutes time frame) was determined for each sample. The standard deviation was then multiplied by 5 to determine the LOD in relative fluorescence units. This value was converted into units of concentration by normalizing it to the protein peak intensity at a known concentration. For each protein, detection limits obtained with UV absorbance and fluorescence were averaged and tabulated in **Table 1** of the main text. LOD experiments are shown in **Figures 15,16,17,18** and **19** with fluorescence detection shown in the top panel and UV detection shown in the lower panel.

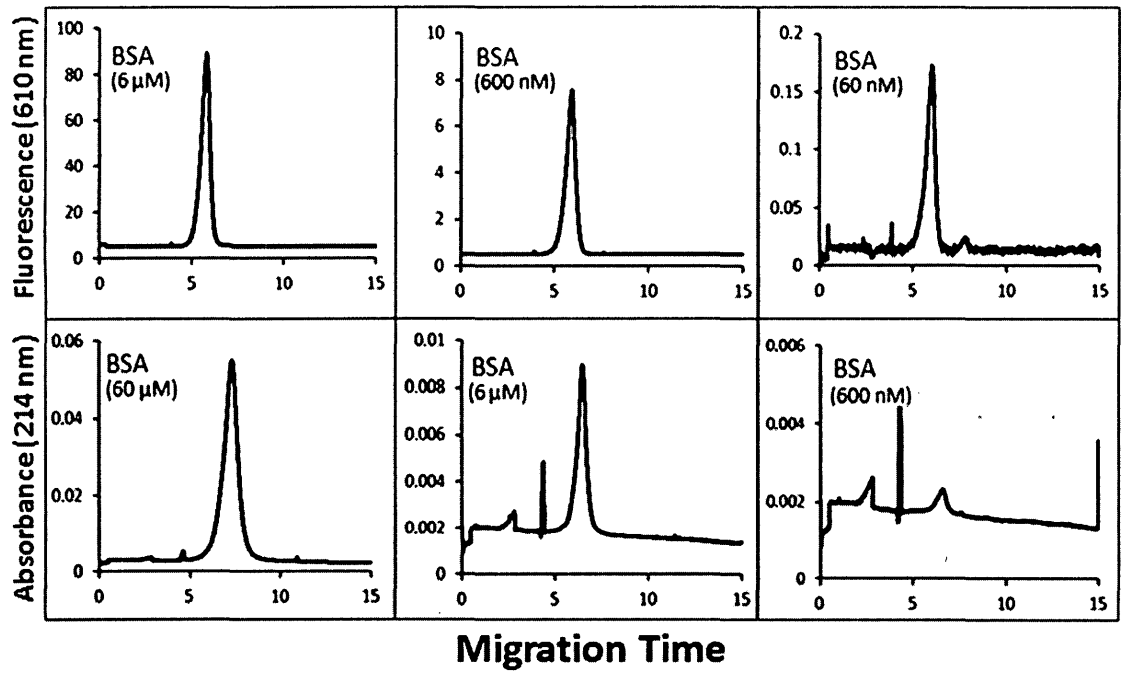

[Figure 15] Electropherograms illustrating the improvement in CE detection of BSA by labeling protein with Chromeo P503. The top panel shows the data obtained using fluorescence detection while the lower panel illustrates the data obtained using UV absorbance detection. The respective concentrations are indicated in the right corners.

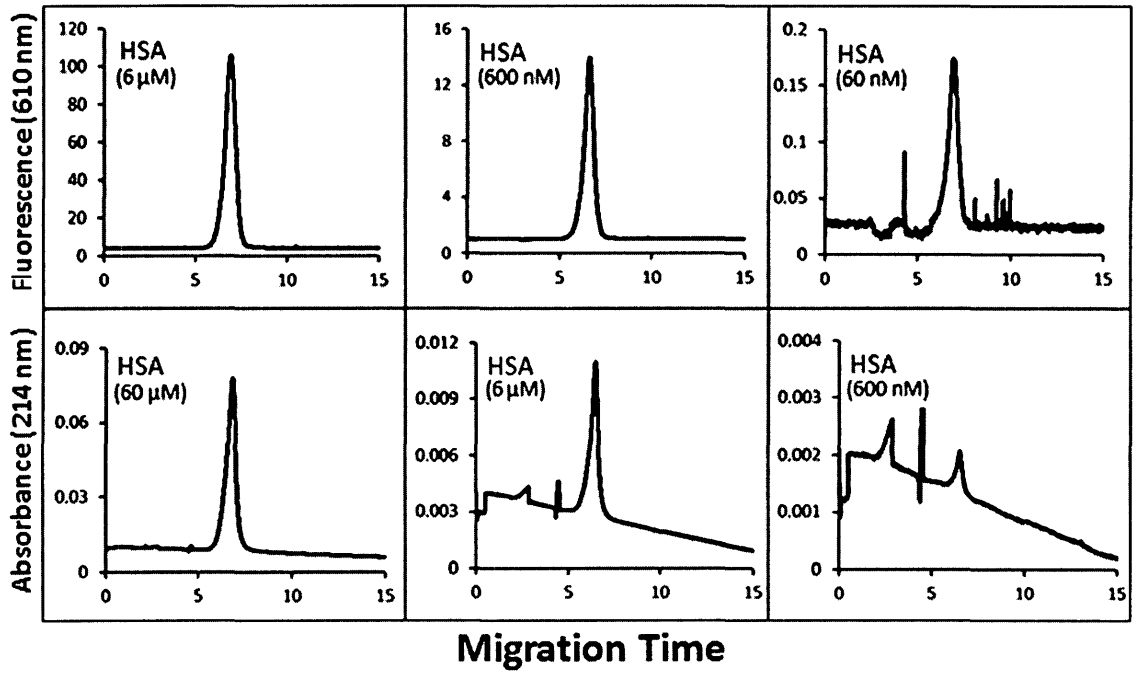

[Figure 16] Electropherograms illustrating the improvement in CE detection of HSA by labeling protein with Chromeo P503. The top panel shows the data obtained using fluorescence detection while the lower panel illustrates the data obtained using UV absorbance detection. The respective concentrations are indicated in the right corners.

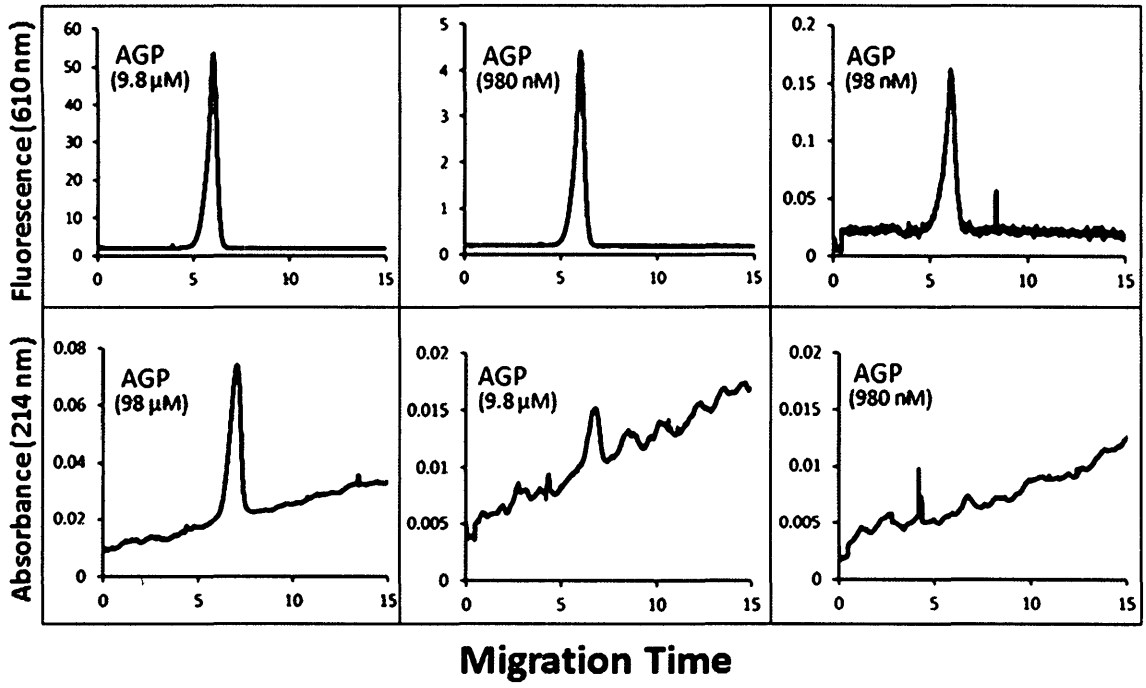

[Figure 17] Electropherograms illustrating the improvement in CE detection of AGP by labeling protein with Chromeo P503. The top panel shows the data obtained using fluorescence detection while the lower panel illustrates the data obtained using UV absorbance detection. The respective concentrations are indicated in the right corners.

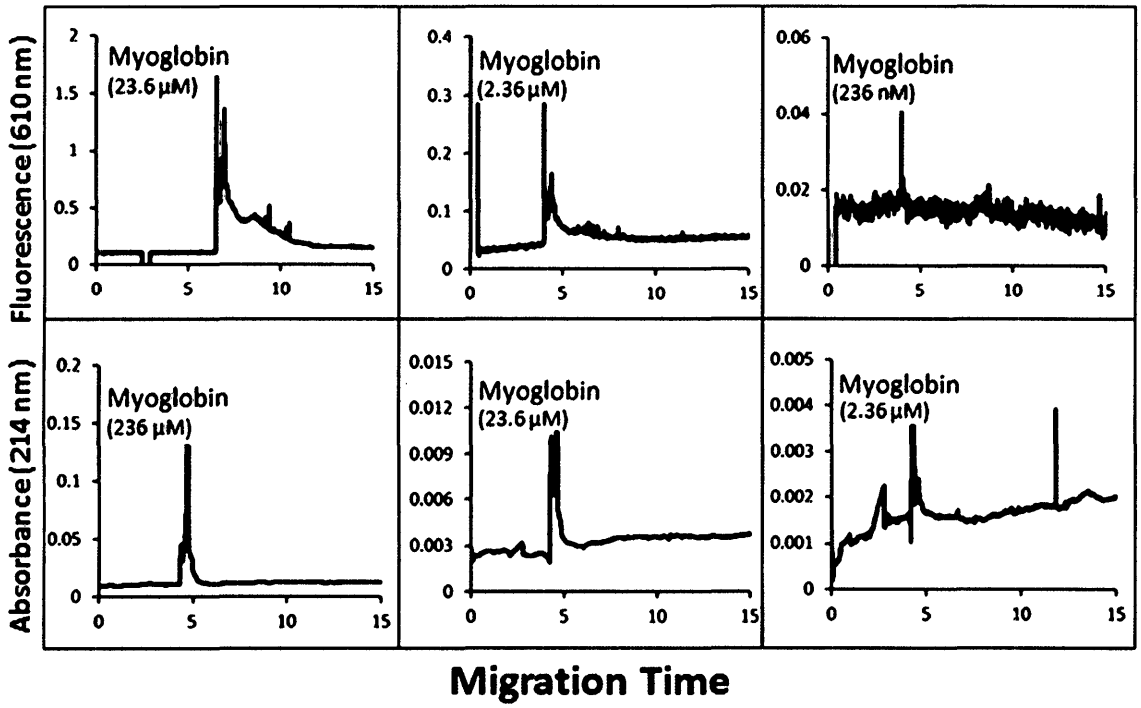

[Figure 18] Electropherograms illustrating the improvement in CE detection of myoglobin by labeling protein with Chromeo P503. The top panel shows the data obtained using fluorescence detection while the lower panel illustrates the data obtained using UV absorbance detection. The respective concentrations are indicated in the right corners.

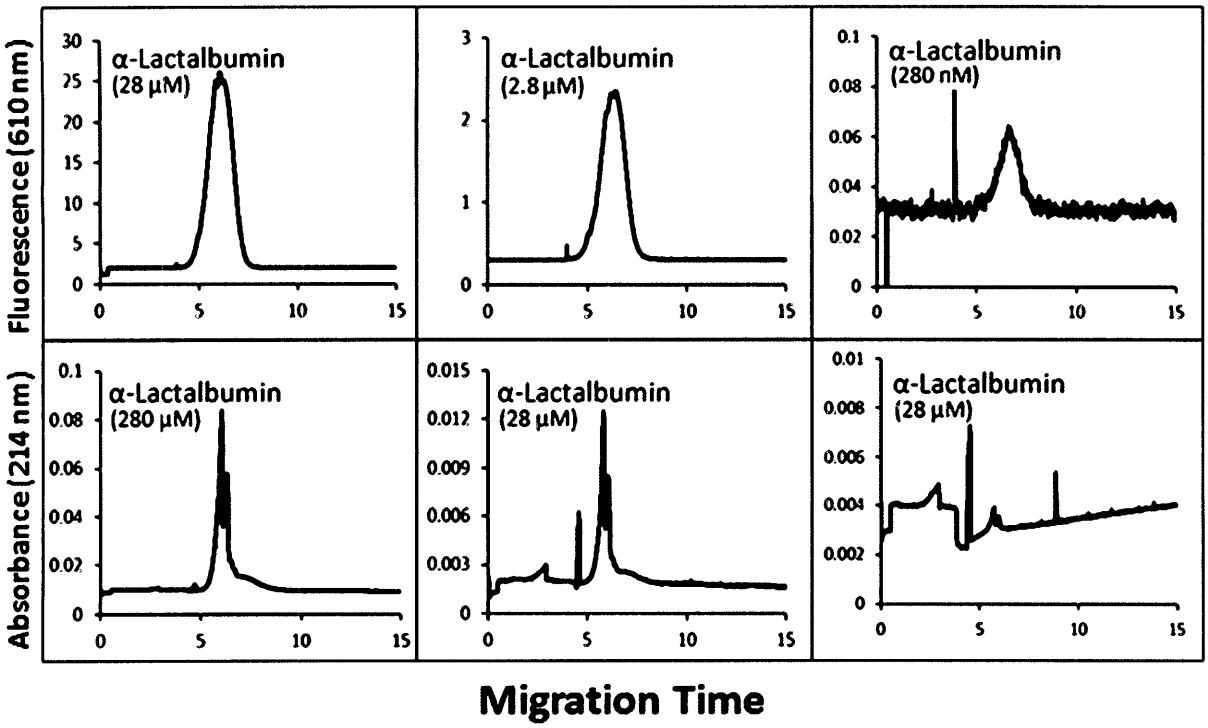

[Figure 19]. Electropherograms illustrating the improvement in CE detection of α-lactalbumin by labeling protein with Chromeo P503. The top panel shows the data obtained using fluorescence detection while the lower panel illustrates the data obtained using UV absorbance detection. The respective concentrations are indicated in the right corners.

Chapter 3: Pressure-based Approach for Protein Adsorption Analysis

3.1 Protein Adsorption to Capillary Surfaces in CE

Protein adsorption to the inner capillary surface creates a major obstacle in all applications of capillary electrophoresis involving protein samples. The problem is especially severe in KCE methods, such as aptamer selection, which demand near-physiological conditions during separation. At pH values greater than 3, the silanol groups of the inner capillary surface retain a considerable negative charge. Being amphiphilic molecules, many proteins have locally contained regions of net positive charge that experience significant ionic attraction to the capillary surface. The multisite protein-capillary interaction obscures the CE separation of free aptamer from the protein-aptamer complex and, depending on the protein affinity towards the surface, may completely inhibit the selection of aptamers for therapeutically important targets. Protein adsorption also creates a challenge in the general KCE analysis of protein-ligand interactions and often leads to peak broadening, poor separation efficiency and analyte depletion which then complicates accurate kinetic measurements.[112-114] Therefore, protein adsorption must be eliminated prior to the KCE analysis of the equilibrium mixture, which contains both the protein and ligand/aptamer components.

One approach to reduce the surface interaction is to adjust the pH of the background electrolyte to either extremely acidic or extremely basic conditions. Low pH buffers significantly reduce the charge of the inner capillary surface and effectively eliminate any electrostatic attraction that would otherwise occur with the protein sample.[115]

Alternatively, increasing the pH to a value above the protein's isoelectric point promotes the Coulombic repulsion between the protein and the negatively charged capillary surface.[116] Although this presents a relatively simple solution, protein-ligand interactions are highly pH sensitive and physiological conditions are necessary to ensure proper protein structure as well as suitable ligand binding.

A more practical approach used to prevent the adsorption of basic proteins is to mask the highly dense negative surface charge with dynamic modifiers of permanently bound coatings. Since the adsorption of proteins is generally a cooperative process, a reduction in the surface charge should yield an exponential decrease in the strength of the protein-capillary interactions.[117,118] When analyzing basic proteins in CE, a common approach is to completely reverse the surface charge of the capillary through the use of cationic chemical additives or coatings.[119-123] However, charge reversal becomes problematic in KCE analysis of protein-ligand interactions if the ligand is negatively charged at neutral pH. This is exactly the case with DNA (or RNA) aptamers, which experience a strong electrostatic attraction to positively charged capillary surfaces. Both proteins and ligands vary in their physical-chemical properties, and each component will demonstrate a unique interaction with a surface coating at the molecular level. As a result, there is no simple and universal solution to prevent analyte adsorption that is compatible with KCE studies on biomolecular interactions. Many proteins of therapeutic and diagnostic importance tend to adsorb to the inner capillary surface, which prevents both the KCE analysis and KCE-based aptamer selection until the proper coating or buffer additive is selected.

3.2 Protein-Capillary Interactions and KCE Analysis

Selecting the appropriate coating requires a direct comparison of their antiadhesive properties toward the protein (and ligand) of interest. Generally, in CE, the extent of adsorption

is monitored indirectly by assessing the separation efficiency during electrophoresis.[124] This approach is unreliable when it comes to ranking capillary coating effectiveness. Many factors influence a proteins electrophoretic migration pattern, the most notable being buffer conductivity and capillary surface charge. Both of these elements may be altered with the use of dynamic or covalent modifiers and lead to peak broadening and a reduction of the EOF even without the added complication of protein adsorption. Proteins themselves have also been shown to alter both the EOF and peak width due to high affinity interactions with the capillary surface. The experimentally acquired electropherograms, depicted in **Figure 20**, demonstrate how the varying degree of protein adsorption influences the EOF in an untreated fused-silica capillary. Although proteins which hold negligible surface affinity are able to maintain the predicted EOF, it drastically reduces as the protein-surface interaction intensifies. Hence, electromigration is not a reliable approach when it comes to screening a series of coating and buffer additives.

Although techniques for detecting irreversible capillary adsorption have been developed, they cannot be applied to KCE, as information related to the reversible surface interactions are neglected.[123-127] For accurate kinetic measurements, both the reversible and irreversible interactions along the capillary wall must be minimal, and thus, a single method is needed to detect both types of interaction.

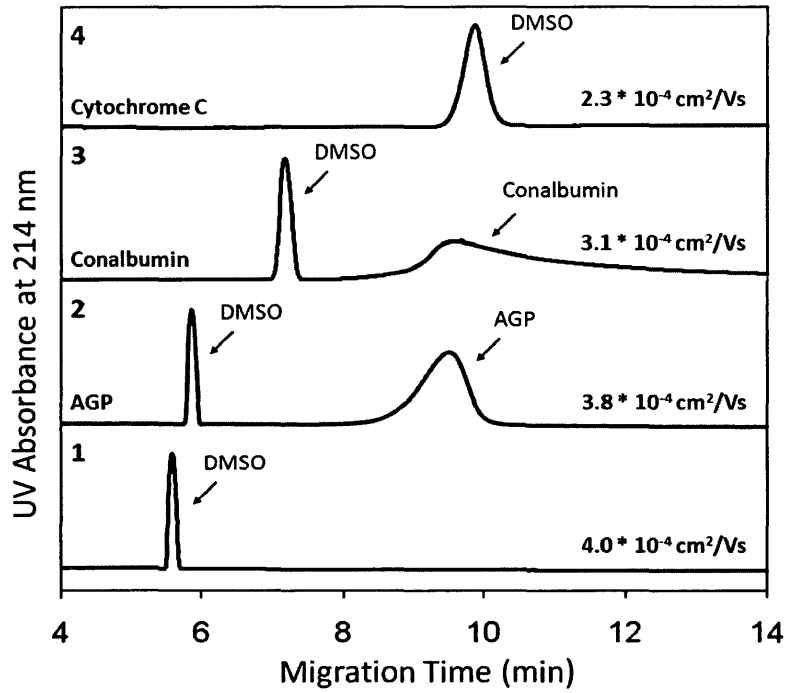

[Figure 20] UV absorbance data demonstrating how protein adsorption influences the EOF in an untreated fused-silica capillary. CE separation was performed at 300 V/cm using 50 mM Tris acetate (pH 8.2) run buffer. In each trace, 0.2% DMSO was used as a neutral EOF marker. Trace 1 presents DMSO migration in the absence of any protein. The calculated EOF values are shown on the right of each electropherogram. Traces 2-4 present results where protein samples of varying adsorptive properties are introduced into the capillary. AGP was selected as an example of a nonadsorptive protein (2), conalbumin as a moderately adsorptive representative (3), and cytochrome *c* as a highly adsorptive protein (4). All proteins were diluted to the same final concentration of 4 mg/mL and injected into the uncoated capillary together with DMSO. For cytochrome *c*, no protein peak is visible due to irreversible adsorption at the inner capillary surface and the limited detection capabilities of UV absorbance.

The described difficulties motivated us to develop a simple pressure-based approach for the accurate characterization of protein adsorption. Conceptually, a short plug containing the protein solution is injected into the capillary and carried to the detector by applying a low pressure. The temporal propagation pattern is then analyzed by comparing the peak area and symmetry to a nonadsorptive control. To accurately characterize the degree of protein adsorption, we combined this pressure propagation technique with a dual-detection approach, first described by Towns and Regnier.[108] Although the original method uses a modified instrument with two on-capillary detectors, we employed a pseudo-dual-detection approach, later adapted by Tran et al.,[128] which does not require the use of a customized instrument.

While the concept of two detection points on a single capillary is well-established, it has always been coupled with electromigration to monitor the progress of sample adsorption. Using pressure-driven sample propagation, rather than electrophoresis, immediately eliminates any complications that may arise from variations in EOF introduced by the coating or additive itself. This simple independence of EOF allows us to draw conclusions directly on the coatings ability to prevent protein adsorption.

By comparing the change in peak areas and shapes at each detection point, we can qualitatively assess the coating's antiadhesive properties for the protein and ligand of interest. The method can be enhanced if the proteins are fluorescently labeled with Chromeo P503 to improve the detection sensitivity.[103,104] The fluorescent labeling of the proteins enables the use of lower protein concentration, which can then more effectively define the protein's surface affinity.

3.2.1 Pressure Propagation and Plug Symmetry

If the pattern of pressure-driven protein propagation across a capillary is used to rank coating efficiency, the applied pressure itself should not significantly influence its peak shape and symmetry. When a uniform forward pressure is introduced along the capillary cross-section, a parabolic laminar flow profile is produced with each injected plug. If the applied pressure is relatively high, the extent of transverse diffusion along the sample interface, with respect to the longitudinal propagation, is minimal and the sample will retain a parabolic shape as it reaches the detector.[129] This parabolic profile will distort the peak shape of the protein and is undesirable given that the migration pattern is used to assess protein adsorption. This peak deformation can be reduced to an insignificant level if the buffer velocity is slow enough to maximize the Taylor

dispersion during the migration time between the initial and final (at the detector) positions of the plug (**Figure 21**).

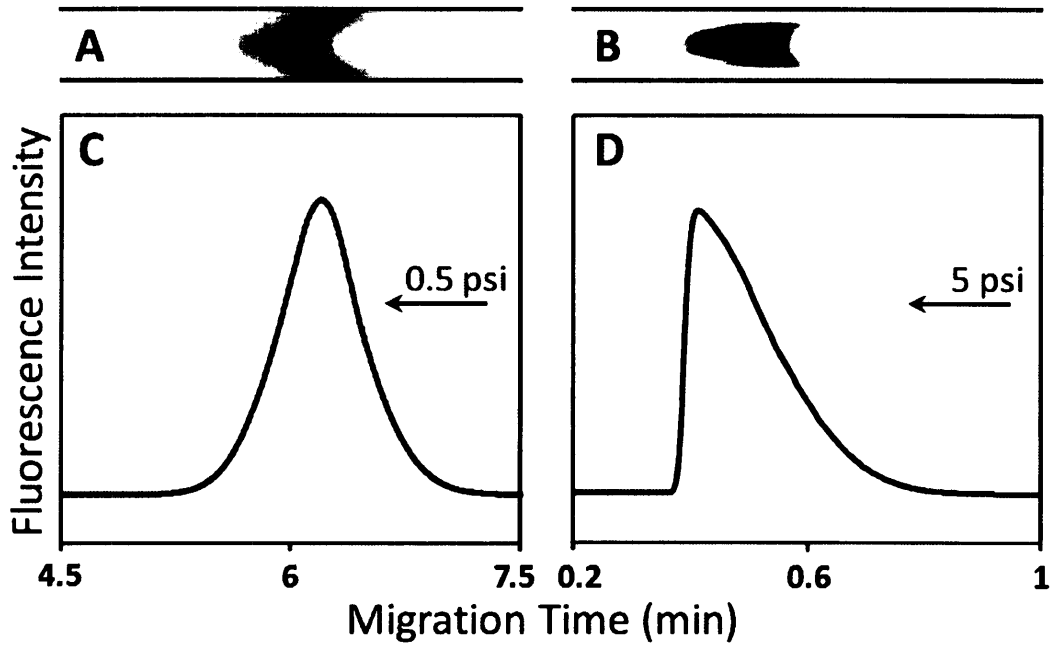

[Figure 21] Pressure-driven migration profiles of the 100 nM thrombin-binding aptamer by applying either a low or high forward pressure. Sample plug schematics were created using COMSOL Multiphysics modeling. The resulting parabolic pressure profiles were generated for pressures of 0.5 (A) and 5 (B) psi. Experimental electropherograms (C,D) are shown below the corresponding schematic representations. Tris acetate (50 mM, pH 8.2) was used as the run buffer, and the fluorescent emission was detected at 520 nm.

The amount of convection-diffusion obtained within the sample plug can be quantified in terms of its Péclet number, *Pe*. Provided that the analyte displays negligible adsorption to the capillary, Péclet values of:

$$Pe \equiv \frac{rv}{D} \ll \frac{L_d}{r} \qquad (21)$$

will imply almost complete diffusion (**equation 21**). Here, D is the diffusion coefficient, r is the capillary radius, v is the average velocity, and L_d is the distance from the injection end of the capillary to the detector. To assess how the applied pressure is correlated with the plug diffusivity, we chose a representative biomolecule (a thrombin binding DNA aptamer) which had

expressed a negligible affinity towards the surface of untreated fused-silica capillaries in the chosen run buffer. This allowed us to attribute any peak asymmetries to inadequate sample diffusion during the analysis time. By reducing the pressure, and corresponding flow rate, the detection time increases, thereby allowing for more effective diffusion. For the thrombin binding aptamer, the pressure-induced migration pattern was measured using a range of separation pressures to establish an optimal pressure value that guarantees adequate sample diffusion (representative results shown in **Figure 21**). It was found that, at a pressure of 0.5 psi, the DNA peaks appeared to be consistently symmetrical, and so, subsequent plug propagation experiments were performed at this pressure.

3.2.2 Semi-quantitative Analysis of Adsorption using Pressure-based Approach

To semi-quantify the irreversible protein adsorption at the capillary surface, we adapted a simplified variation of the two-detector approach described by Tran et al.[128] This technique can accurately estimate the amount of irreversible protein adsorption by performing two experiments using the same sample and capillary. First, the sample is injected from the capillary inlet and carried toward the detector using a low forward pressure. In the second experiment, the sample is injected from the capillary outlet and then travels to the detection window by applying a pressure of the same magnitude but in reverse direction. In the commercial instrument used for this study, the detection window is located at a fixed position of approximately 10 cm from the outlet end. However, the total distance from the inlet to the detector can be varied and is generally dependent on the experimental goals. In KCE-based methods such as aptamer screening, the total length is typically ~50 cm, leaving a 40 cm propagation distance to the detection point. By integrating the peak area obtained at each distance (10 and 40 cm), the amount of protein

adsorbed during a 30 cm propagation across the capillary can be calculated. **Figure 22** illustrates a significant reduction in peak area obtained with a lysozyme sample, which suggests that the sample plug had been depleted due to strong irreversible interactions that the protein likely experienced at the surface.

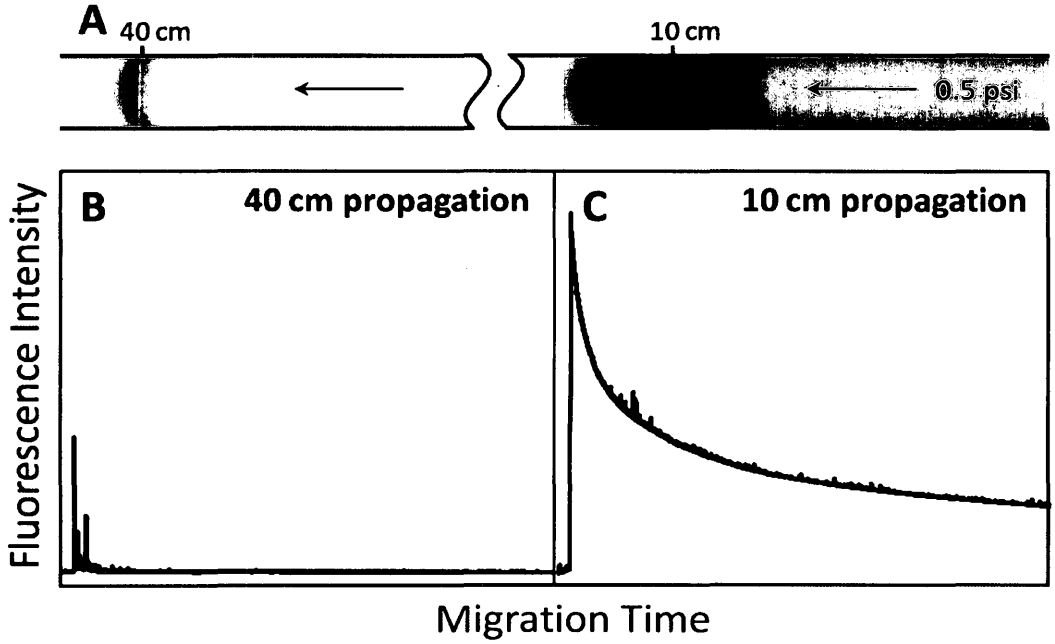

[Figure 22] (A) Schematic representation of extensive protein adsorption which may occur within the capillary and how a reduction in sample concentration can be analyzed by using the two-detector pressure-driven approach. Panels B and C show the experimental migration pattern obtained from the 40 and 10 cm propagations of 274 μM Chromeo-labeled lysozyme, respectively. Protein fluorescence was detected at 610 nm using a 50 mM Tris acetate (pH 8.2) run buffer.

Often the peak shape itself provides some insight into the extent of protein adsorption. Proteins that demonstrate high surface adsorption typically produce a wide pressure-driven propagation profile with a substantial amount of tailing that occasionally coincides with a stepwise increase from the baseline. Therefore, the analysis of the temporal propagation pattern may also be used to assess the degree of reversible adsorption.

3.2.2.1 Capillary Surface Screening and Antiadhesive Ranking

To demonstrate the applicability of this technique, we tested five proteins, each expressing different physical and chemical surface properties (α_1 acid glycoprotein (AGP), conalbumin, cytochrome *c*, thrombin, and lysozyme). Each protein was first injected into an uncoated capillary using the dual-detection, pressure-driven propagation method. It was determined that conalbumin, cytochrome *c*, thrombin and lysozyme all experienced a high level of capillary adsorption. The protein-capillary interaction for lysozyme, thrombin, and cytochrome *c* was especially severe as they each exhibited complete analyte loss during the 40 cm propagation, and the 10 cm propagation resulted in extremely broad peaks of negligible or low intensity (see **Figures 24-28** in the **Supplementary Information**).

We then evaluated the antiadhesive properties of three coatings, two permanent and one dynamic, toward each of the five model proteins. Dynamic coatings are relatively easy to implement as they consist of simple additives which slightly modify the chemical composition of the background electrolyte. Dynamic additives range from ionic/non-ionic surfactants to polymers and amine-containing molecules, each of which reversibly adsorbs to the negatively charged silanols of the inner capillary wall. Since the attachment is based on temporary interactions with the capillary surface, the coating agent, present at sufficiently high concentrations, tends to out-compete the protein for the available surface binding sites.[130] The dynamic coating used in this study, CElixir, is a commercially available, double-layer coating system which is offered in a range of pH values. The coating is applied by first rinsing the bare capillary with a polycationic initiator solution to form a stable positively charged surface. A second layer is then introduced by rinsing the capillary with a solution containing a buffered polyanion at the selected pH.

CElixir was originally developed as a means of achieving a stable and reproducible EOF, independent of the buffer pH. This fixed EOF is obtained by adjusting the negative charge density along the capillary surface to compensate for the variation in EOF that typically results from changes in pH.[131,132] For KCE methods, physiological pH is required to maintain the proteins native conformation, and for this purpose, a pH of 8.2 was selected.

We found that CElixir helped in suppressing the level of protein adsorbed for all five proteins tested. Although this dynamic modifier resulted in a major improvement compared to bare silica, it was not an infallible means of preventing protein adsorption as each protein had demonstrated its own unique response to the coating. In particular, lysozyme had shown significant tailing and substantial loss of the protein sample between the 10 and 40 cm propagations (see **Figures 24-28** in **Supplementary Information**). This persistent adsorption is likely attributed to the protein interaction with the anionic polymer that is temporarily retained along the capillary surface.

Permanent coatings, based on covalently or physically bound surface modifiers, have proven to be quite effective in the elimination of any protein-capillary interactions. Using a capillary permanently coated with poly(vinyl alcohol) (PVA) and another which was covalently bonded with linear poly(acrylamide) (LPA), we employed the pressure-driven propagation method for each of the five representative proteins. It is clear from **Figures 24-28** in the **Supplementary Information**, that PVA considerably reduced protein adsorption for conalbumin, cytochrome *c*, thrombin and lysozyme. Lysozyme still displayed a positive interaction with the PVA surface; however, there is a notable improvement from both the uncoated and dynamically coated capillaries. The capillary coated with LPA did not perform as well as the PVA-coated capillary or the capillary coated with the dynamic modifier CElixir,

though it still demonstrated an improvement to the bare-silica surface. Covalently bound poly(acrylamide) is typically quite efficient at preventing protein adsorption in CE. However, the run buffer used in all of the described experiments had a pH value of 8.2, which may have prompted LPA hydrolysis and reduced the coatings effectiveness.[133]

To rank each coating, the peak shape, width and intensity were first analyzed. If no clear visual distinction can be made, then the amount of protein adsorbed was estimated by integrating the peak area and then comparing the values obtained between the 10 and 40 cm propagations for a given protein and coating. In the case of AGP, both the uncoated capillary and capillary coated with CElixir were 100% effective in preventing protein adsorption, and thus, both surface chemistries were given equal rankings.

Due to its anionic properties, AGP (p*I* = 2.8-3.8) demonstrated minimal interaction with the fused-silica surface, and thus, an uncoated capillary suffices for its CE analysis. For conalbumin, both PVA and CElixir coatings produced similar results in terms of protein loss (each a significant improvement from the uncoated capillary) and were also given equal rankings. The results shown in **Table 2** suggest that different proteins respond differently to the same coating, and there may be no simple and universal solution to prevent protein adsorption at neutral pH. Proteins themselves vary in their overall charge and structure and each will experience a unique interaction with different wall chemistries.

[Table 2]: Antiadhesive ranking of capillary surface chemistries with respect to individual protein samples.

Protein	**Capillary Surface**			
	SiOH	**CElixir**	**PVA**	**LPA**
AGP	1	1	2	2
Conalbumin	3	1	1	2
Cytochrome *c*	4	1	2	3
Lysozyme	4	2	1	3
Thrombin	4	2	1	3

3.2.2.2 Method Validity in KCE Applications

To further verify the advantages of this technique, and demonstrate how a proteins temporal propagation pattern can facilitate KCE-based analysis, we performed a set of NECEEM experiments using the thrombin-aptamer binding pair as kinetic model. The kinetic and equilibrium parameters were obtained by integrating the areas which correspond to free aptamer (A_1), aptamer-thrombin complex (A_2), and aptamer that has dissociated from the complex during separation (A_3)[92,134] **[Figure 23]**. We performed consecutive NECEEM experiments using two different capillary surfaces, one demonstrating strong thrombin adsorption and the other having only a negligible affinity. As indicated in **Table 2**, the PVA coating ranked the highest in terms of its antiadhesive properties while the uncoated capillary ranked lowest with respect to the thrombin sample; therefore, these two capillary surfaces were chosen for the NECEEM analysis.

When using the uncoated capillary and performing separation with the cathode at the capillary outlet, we would expect the complex to migrate faster than the free aptamer and, under ideal conditions, reach the detector first. However, as seen in **Figure 23**, the areas of free aptamer and aptamer dissociated from complex are indefinable, and no clear complex peak was observed. The experiment was then repeated using PVA-coated capillary, with the anode at the outlet due to the absence of an EOF. The acquired results were precisely as expected, with the aptamer peak reaching the detector first, followed by the aptamer dissociated from the complex and finally the intact complex. The areas were easily integratable and enabled accurate kinetic analysis of the thrombin-aptamer interaction. These results confirm that the pressure-driven protein propagation can be used to improve the quality of KCE analyses that involve adsorptive protein samples.

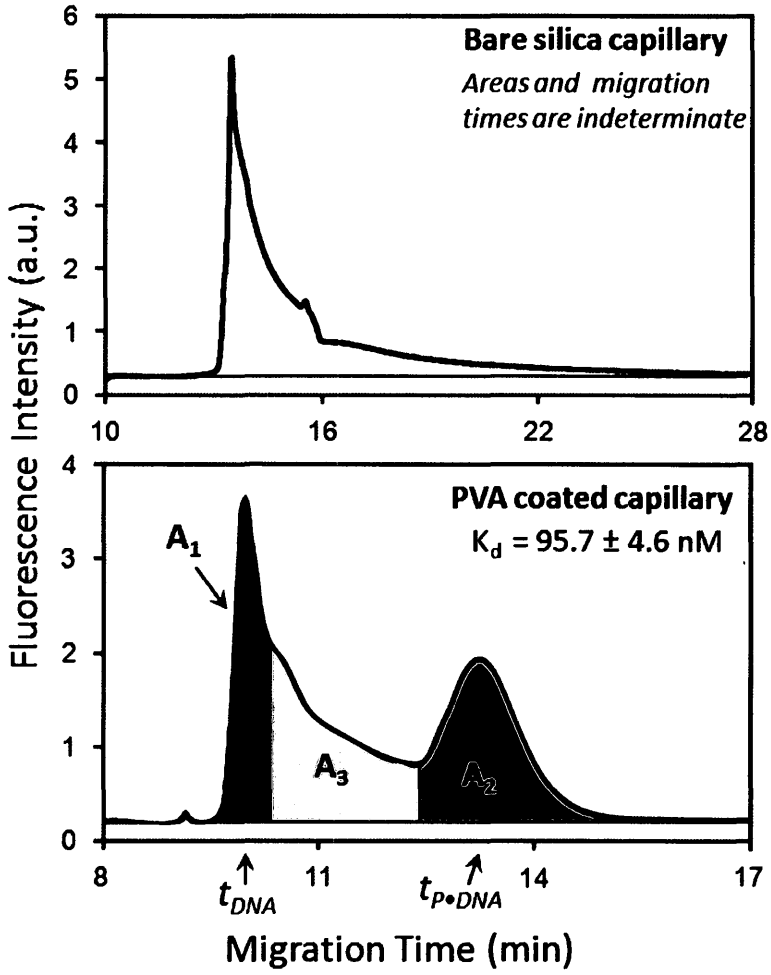

[Figure 23] NECEEM electropherograms produced using the thrombin-aptamer binding system in an uncoated capillary (top panel) and PVA-coated capillary (lower panel). The equilibrium mixtures consisted of 455 nM thrombin and 91 nM TBA and separated using normal polarity in the uncoated capillary and reverse polarity with the PVA coating. The areas corresponding to free aptamer (A_1), aptamer dissociated from the complex (A_3), and intact complex (A_2) are identified in the electropherogram produced using the PVA-coated capillary. The uncoated capillary could not be analyzed as the areas are poorly defined.

Due to its versatility, the described method can easily be applied for both coating and buffer screening. In an additional project, not described in this report, we expanded the pressure-propagation method to evaluate the effectiveness of a semi-permanent coating[135,136] in various background electrolytes.[3] Often, the buffer choice alone can dramatically alter the proteins tendency to adsorb, as this surface interaction is connected to many protein-specific factors such as p*I* and the external amino acid composition. The extent of protein adsorption is determined collectively by a number of parameters such as electrolyte pH, the electromagnetic interactions

with buffer ions, and hydrophobic effects. As a result, it is not possible to generalize coating and buffer efficiency, as different proteins will demonstrate a unique response and this must be determined empirically.

3.3 Experimental

3.3.1 Materials

Chromeo P503 fluorescent labeling pyrylium dye was purchased from Active Motif (Burlington, ON, Canada). The HPLC-purified thrombin-binding aptamer (5'-Alexa488-CGG TTG GTG TGG TTG GAA AAA AAA AAA AAA AAA AAA AAA A-3') was obtained from Integrated DNA Technologies (Coralville, IA), dissolved to a concentration of 50 μM in 10 mM Tris-HCl (pH 7.5), and stored at -20°C until use.

Lyophilized protein samples (α_1 acid glycoprotein, conalbumin, cytochrome c, and lysozyme) and all other chemicals were purchased from Sigma-Aldrich (Oakville, ON, Canada), while Human-α-Thrombin was acquired from Haematologic Technologies Inc. (Essex Junction, VT). Solutions were made with deionized water and passed through a 0.22 μm filter by suction (Millipore, Nepean, ON, Canada). Uncoated fused-silica capillaries with an inner diameter of 75 μm (375 μm outer diameter) were purchased from Polymicro (Phoenix, AZ). Neutral capillaries covalently bonded with linear poly(acrylamide) (75 μm i.d., 365 μm o.d.) and the CElixir dynamic coating system consisting of initiator and accelerator (pH 8.2) solutions were purchased from MicroSolv Technology Corp. (Eatontown, NJ).

3.3.2 Instrumentation

All experiments were performed using a P/ACE MDQ capillary electrophoresis instrument (Beckman, Coulter, Fullerton, CA) equipped with either a laser-induced fluorescence (LIF) of photodiode array (PDA) detection system. For pressure-driven propagation experiments, a continuous 488 nm solid-state laser line was used to excite fluorescence of both the DNA and protein samples. Due to the considerable variation in their fluorescence emission spectra, a two-channel detector was employed to effectively separate the DNA and protein fluorescence into two discrete channels. Band-pass filters specific for 520 and 610 nm were used to isolate fluorescence signals from Alexa-488 labeled DNA and Chromeo P503-labeled proteins, respectively.

3.3.3 Protein Labeling

Lyophilized proteins (AGP, conalbumin, cytochrome c, and lysozyme) were dissolved in a 0.1 M solution of $NaHCO_3$ (pH 8.3) to a concentration of 4 mg/mL. A working solution of Chromeo P503 was added to each protein sample at a 1:100 ratio of dye to protein. Thrombin was labeled by diluting the protein stock in a Chromeo mixture, containing 1 μL of Chromeo P503 and 100 μL of 0.1 M $NaHCO_3$ (pH 8.3), to obtain a final thrombin concentration of 48 μM. All labeling reactions were left to incubate overnight at 4°C to complete the conjugation. Protein solutions were then aliquoted and stored at -20°C until use. All samples were then further diluted in 0.1 M $NaHCO_3$ (pH 8.3) to obtain the final concentrations.

3.3.4 Poly(vinyl alcohol) Coating

PVA (5%, w/v) was prepared by dissolving the polymer in boiling deionized water. An uncoated fused-silica capillary was sequentially flushed with 0.1 M NaOH and deionized water for 1 h under a 12 psi flow of nitrogen gas. The pretreated capillary was then flushed with the PVA solution for 10 min at 15 psi and emptied using a 10 psi gas flow for 10 min. PVA was immobilized on the capillary surface by drying overnight in an oven set at 140°C with the continuous flush of low pressure nitrogen. The detection window was made using a fuming solution of H_2SO_4 to preserve the integrity of the coating at the detection site.[137]

3.3.5 Experimental Conditions

All experiments were performed using a 50 cm capillary (40 cm to the detection window). Bare silica capillaries were pretreated by rinsing with methanol for 10 min at 20 psi. Prior to each run, the uncoated capillary was rinsed with RNAse AWAY solution using 20 psi for 5 min followed by a sequential rinse with 0.1 M HCl, 0.1 M NaOH, doubly distilled water (ddH_2O), and 50 mM Tris acetate (pH 8.2) at 20 psi for 2 min. Dynamically modified capillaries were prepared using the commercial CElixir double-layer system. The capillaries were preconditioned by first rinsing with the initiator and accelerator (pH 8.2) solutions at 20 psi for 1 and 2 min, respectively. This coating procedure was repeated prior to each run. Before each experiment, the permanently coated PVA and LPA capillaries were rinsed with ddH_2O and 50 mM Tris acetate (pH 8.2), each at 20 psi for 8 min.

All samples were introduced into the capillary by applying a 6 s pressure pulse of 0.5 psi. Pressure-driven propagation analyses were carried out using a 50 mM Tris acetate (pH 8.2) run buffer for both the uncoated and permanently coated capillaries, while the CElixir accelerator

solution (pH 8.2) was used in the dynamically modified capillary. A 0.5 psi forward pressure was applied for the 40 cm propagation, and a reverse pressure of the same magnitude was used for the 10 cm propagation experiments.

UV absorbance experiments were performed using an uncoated fused-silica capillary. Separation was carried out at 300 V/cm with 50 mM Tris acetate (pH 8.2) as the background electrolyte. Dimethyl sulfoxide (DMSO; 0.2%) was used as a neutral marker to measure the protein influence on the EOF. The electroosmotic mobility values shown in **Figure 20** were calculated using **equation 22**:

$$\mu_{eo} = \frac{L_t L_d}{V t_m} \tag{22}$$

where V is the applied voltage, t_m is the migration time to the detector, L_t is the total capillary length, and L_d is the distance from the capillary inlet to the detector.

3.3.6 NECEEM Analysis of the Thrombin-Aptamer Interaction

A 1 μM solution of the thrombin-binding aptamer was heated to 95°C for 1 min using a thermal cycler (Eppendorf, Hamburg, Germany) and gradually cooled to 25°C at a rate of 0.5°C/s to promote proper aptamer folding. An equilibrium mixture consisting of 455 nM thrombin and 91 nM aptamer was prepared in a 20 mM Tris acetate (pH 8.2) buffer containing 5 mM KCl and 1 mM $MgCl_2$. The mixture was separated using 10 kV for the first 5 min followed by an increase to 20 kV in the uncoated capillary to avoid sample overheating. When using the PVA-coated capillary, the same voltages were applied; however, the electric field polarity was reversed. The equilibrium dissociation constants were calculated using **equation 23**:

$$K_d = \frac{[P]_0 - [DNA]_0\{1 - A_1/(A_1 + A_2 + A_3)\}}{(A_1 + A_2 + A_3)/A_2 - 1} \quad (23)$$

where $[P]_0$ and $[DNA]_0$ are the initial protein and aptamer concentrations, respectively, and A_1, A_2 and A_3 correspond to the integrated areas of free aptamer, complex and aptamer dissociated from complex, respectively. The areas were corrected for differences in the migration velocities of free and bound aptamers.

3.4 Conclusions

We propose this simple and fast method for screening a series of coatings to help select the optimal conditions for KCE methods involving proteins. This method promises to help expand the number of biomolecular interactions studies by KCE and assist in KCE-based aptamer selection.

Pressure-driven propagation can be used to screen various capillary coatings and run buffers for protein analysis in KCE, and more specifically, in KCE-SELEX. We prove that this approach can be readily used to rank the antiadhesive properties of different capillary surfaces and buffer types for important protein samples. We illustrate the difficulties associated with the KCE studies involving adsorptive proteins and propose a method that will improve their analysis by selecting the appropriate capillary coating and buffer. This technique will undoubtedly assist in diversifying the number of protein-ligand interactions studied by KCE methods, and improve the efficiency of KCE-based aptamer selection

3.5 Supplementary Information

3.5.1 Capillary Surface Chemistry Influence on the Temporal Propagation Pattern of Several Proteins

Protein adsorption was characterized using the dual-detection pressure-driven propagation method as described in section 3.2. Representative proteins, each with unique surface properties and charge, were chosen as models to illustrate the applicability of this method. Chromeo labeled proteins were diluted in a 0.1 M $NaHCO_3$ (pH 8.2) buffer to obtain the following concentrations: 9.8 μM α_1- acid glycoprotein, 5.3μM conalbumin, 10.1 μM thrombin , 171 μM cytochrome C, and 137 μM lysozyme. 30 nL of the sample was injected into the capillary inlet and carried 40 cm to the detector using a low forward pressure of 0.5 psi to guarantee adequate diffusion between the sample and buffer plugs. The 10 cm propagation was performed using the same capillary however, the sample was injected from the outlet end and each pressure (injection and propagation) was applied in the reversed direction. The experimental analysis of protein adsorption was performed using capillaries with four different surface chemistries: (i) a bare silica capillary, (ii) a capillary coated with the CElixir dynamic modification system, (iii) a capillary with a permanently adsorbed poly(vinyl) alcohol (PVA) surface and (iv) a capillary with a covalently bonded linear polyacrylamide (LPA) surface. For the uncoated, PVA and LPA capillaries we had employed a run buffer of 50 mM Tris acetate (pH 8.2). The dynamically coated capillary used the commercially available CElixir accelerator solution at pH 8.2 as the run buffer. All experiments were performed in triplicates with less than 15% standard deviation in the integrated peak areas to ensure reproducibility. Protein adsorption was determined by comparing peak height, width and symmetry of each pressure propagation profile. In addition, the differences in peak area between the 10-cm and 40-cm propagation were

used to assess the degree of protein adsorption by calculating the amount of protein loss during the 30-cm migration. Representative results for each coating protein are shown in **Figures 24, 25, 26, 27** and **28**.

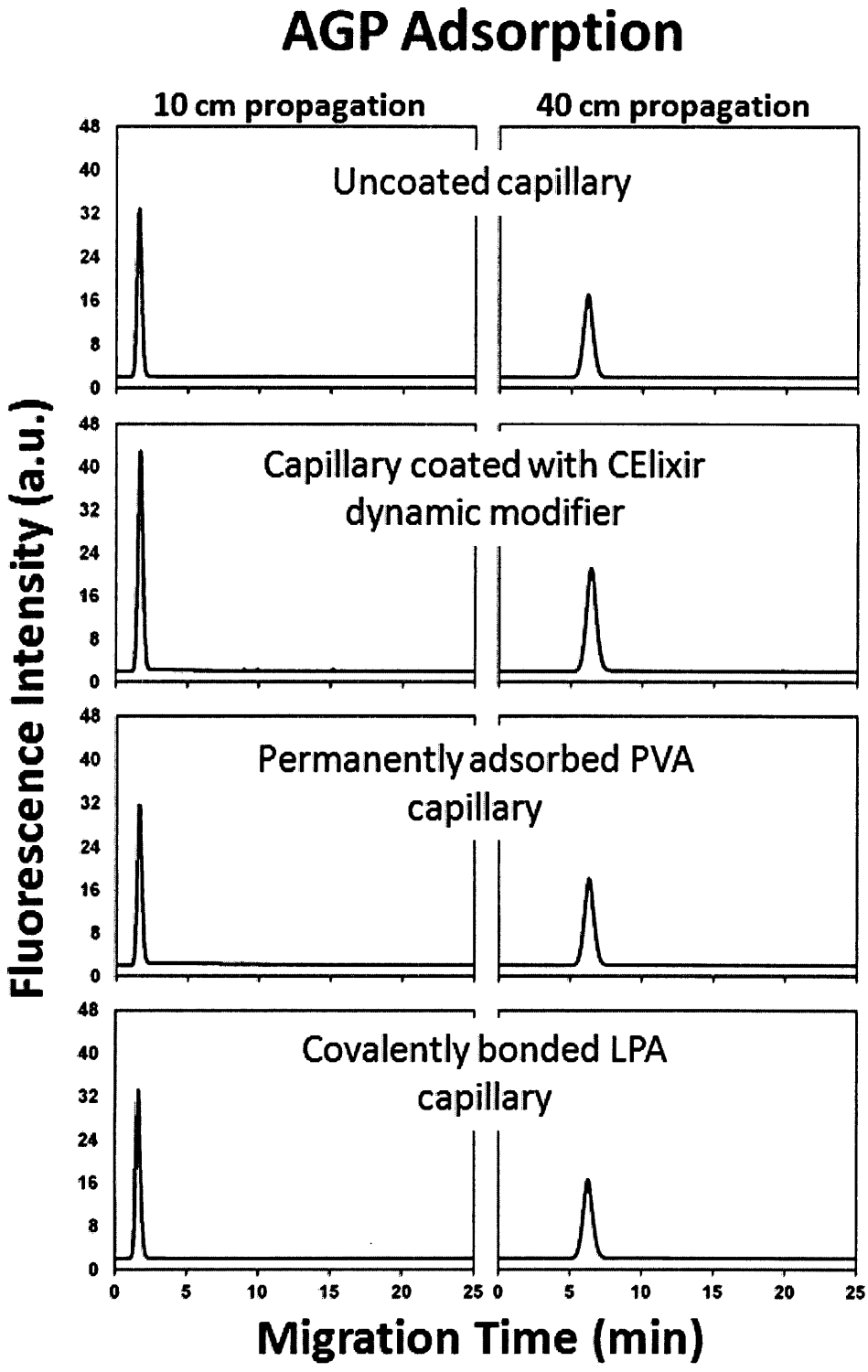

[Figure 24] Temporal propagation patterns of 9.8 μM Chromeo-labeled α_1-acid glycoprotein after 10-cm and 40-cm pressure-driven propagations using an uncoated capillary a capillary coated with CElixir dynamic modifier, a capillary with a permanently adsorbed PVA coating and a capillary covalently bonded with LPA.

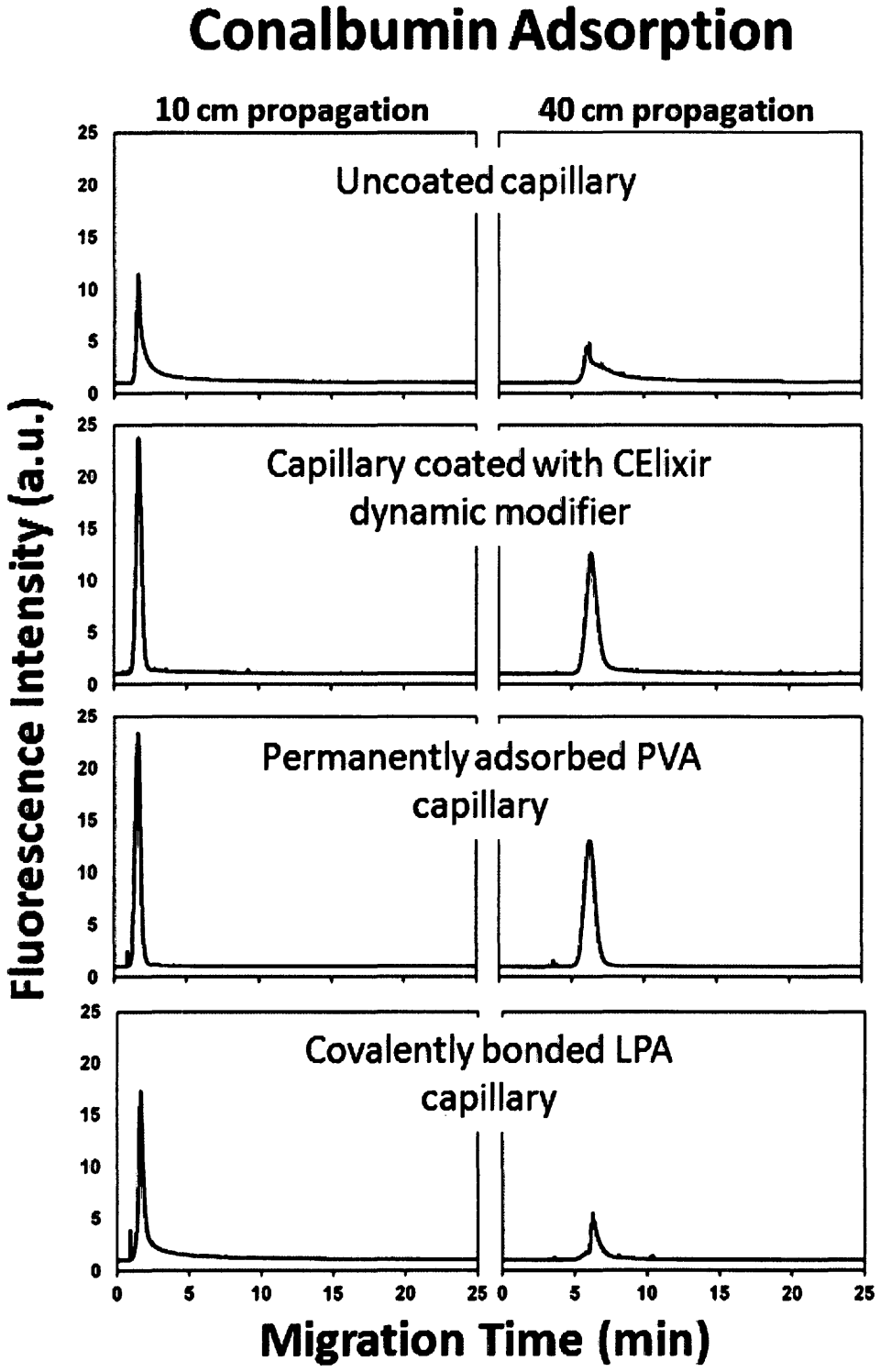

[Figure 25] Temporal propagation patterns of 5.3 μM Chromeo-labeled conalbumin after 10-cm and 40-cm pressure-driven propagations using an uncoated capillary a capillary coated with CElixir dynamic modifier, a capillary with a permanently adsorbed PVA coating and a capillary covalently bonded with LPA.

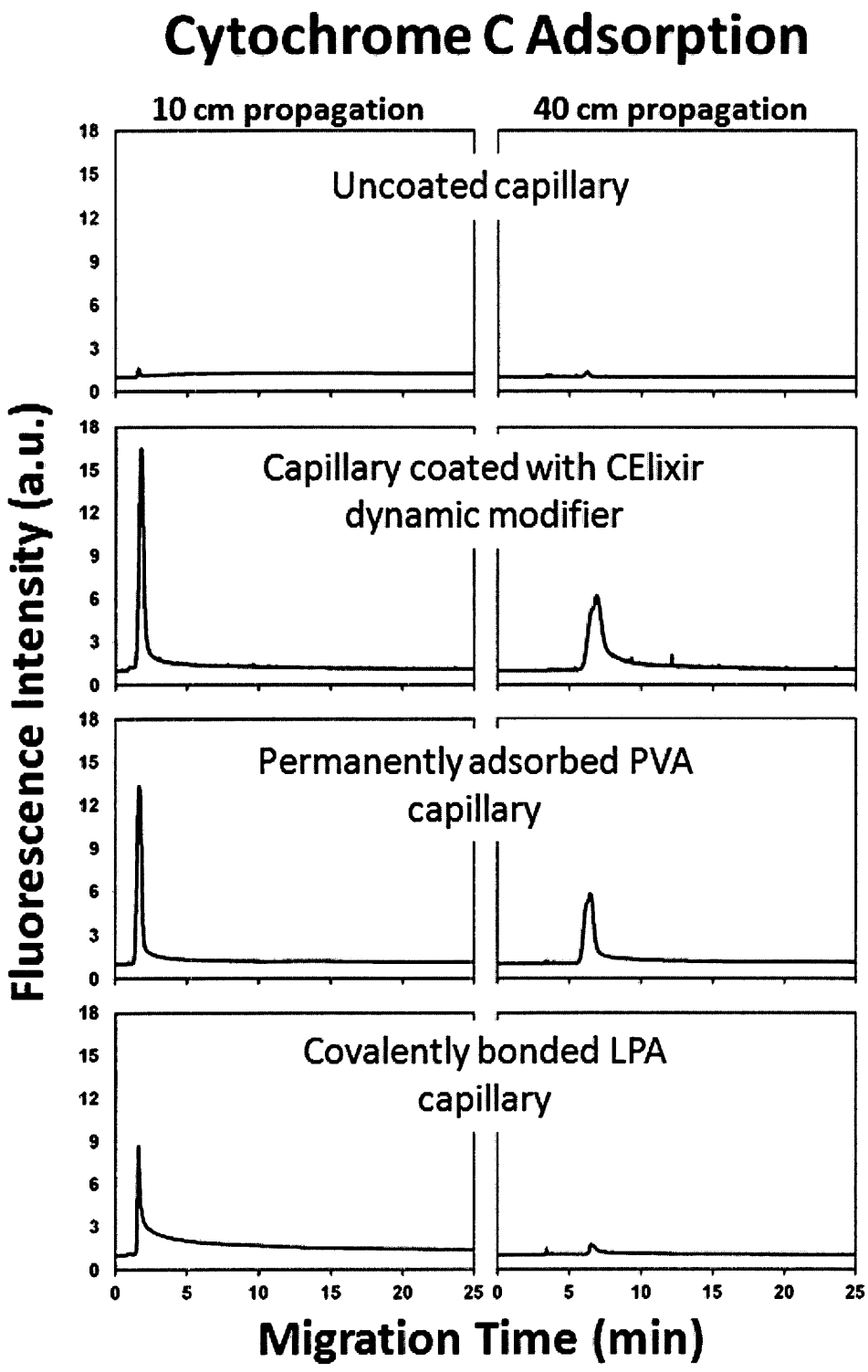

[Figure 26] Temporal propagation patterns of 171 μM Chromeo-labeled cytochrome C after 10-cm and 40-cm pressure-driven propagations using an uncoated capillary a capillary coated with CElixir dynamic modifier, a capillary with a permanently adsorbed PVA coating and a capillary covalently bonded with LPA.

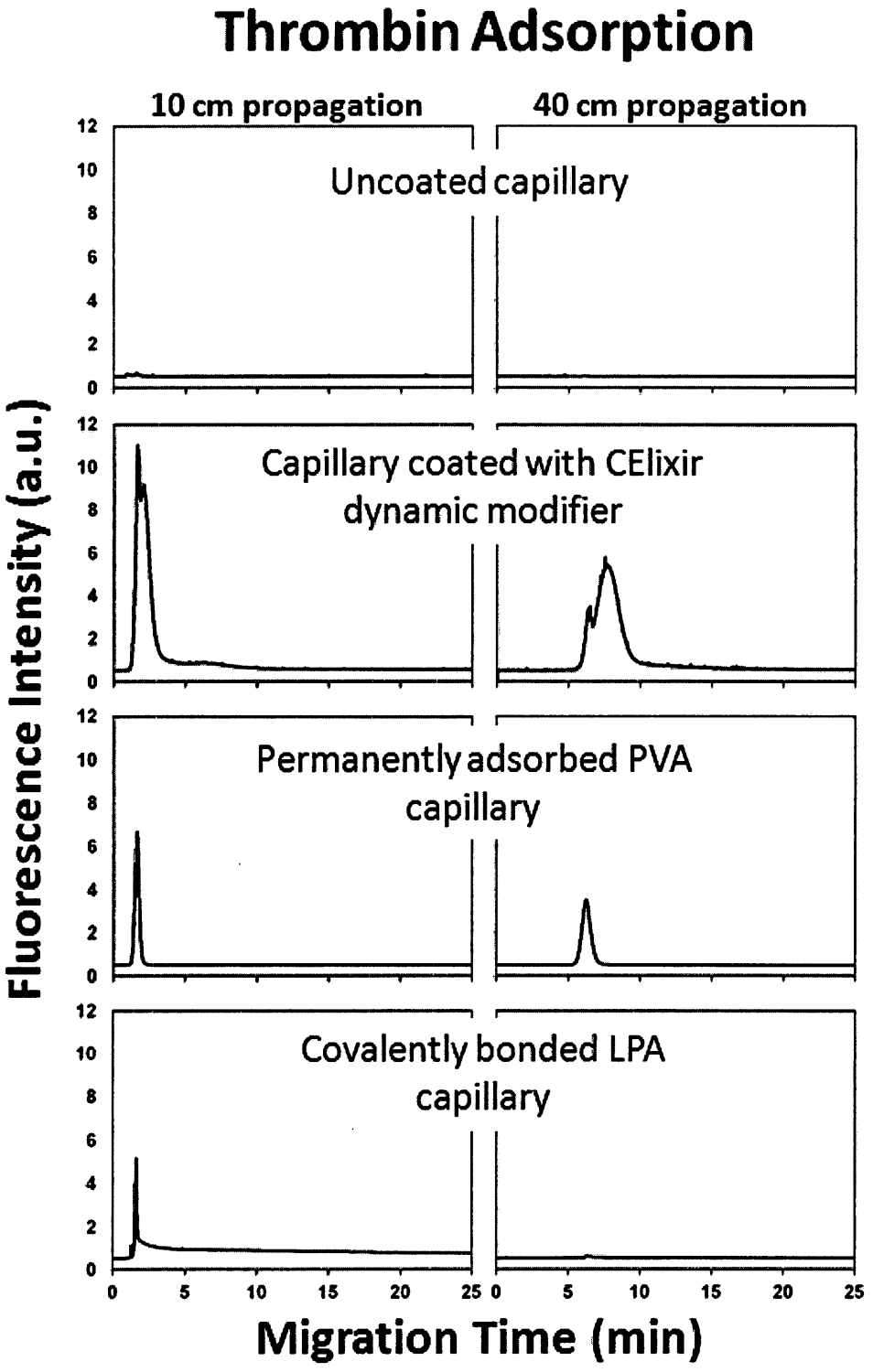

[Figure 27] Temporal propagation patterns of 10.1 μM Chromeo-labeled thrombin after 10-cm and 40-cm pressure-driven propagations using an uncoated capillary, a capillary coated with CElixir dynamic modifier, a capillary with a permanently adsorbed PVA coating and a capillary covalently bonded with LPA.

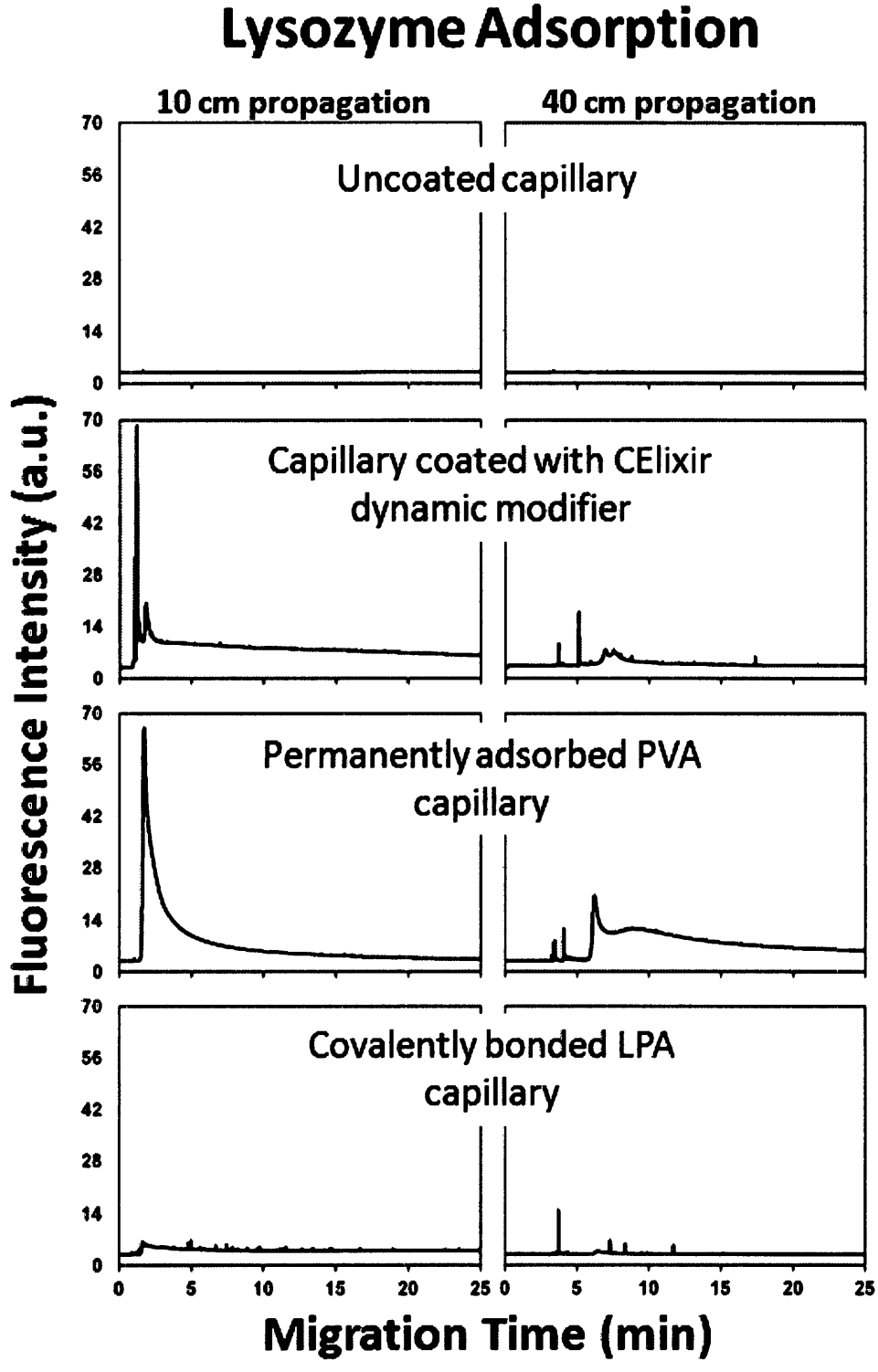

[Figure 28] Temporal propagation patterns of 137 μM Chromeo-labeled lysozyme after 10-cm and 40-cm pressure-driven propagations using an uncoated capillary, a capillary coated with CElixir dynamic modifier, a capillary with a permanently adsorbed PVA coating and a capillary covalently bonded with LPA.

Chapter 4: Target-Specific Optimization: Exonuclease 1

4.1 Aptamer Development for an Exonuclease

The previous two chapters described, in detail, novel methods of pre-selection optimization that should be implemented in KCE-SELEX for all protein-based aptamer targets. In this work, the target in question is an active exonuclease capable of degrading any potential aptamers which approach the proteins active site. This is problematic, as the entire DNA library serves as a substrate for enzymatic degradation by Exo1. Since Exo1 is known to be a highly processive DNA nuclease,[138] this would certainly lead to the selective degradation of high-affinity aptamers if activity is not controlled. Therefore, prior to performing any pre-selection optimization, conditions must be established where the exonuclease activity is suppressed. Literature indicates that Exo1 requires a Mg^{2+} cofactor for enzymatic activity,[98,99] therefore, chelating agents such as ethylenediaminetetraacetic acid (EDTA), may remove any residual Mg^{2+} from the enzymes active site, and prevent cleavage of the phosphodiester bond.

4.2 Magnesium-Dependent Nuclease Activity Assay

Exo1 activity was assessed using Gel CE as this technique can discriminate between DNA that differs in length by only 1 nucleotide (nt). If any significant DNA degradation were to occur, it would be clearly seen in the Gel CE electropherograms. A DNA ladder containing 20 nt, 37 nt, 56 nt and an 80 nt DNA markers was used as a control to assess the length of the DNA present in the sample of interest. **Figure 29A** shows an electropherogram of this DNA ladder. The 80 nt marker is useful, since the N40 DNA library (with 40 random nucleotides) is also 80 nt in length. By performing a co-injection of the equilibrium mixture and the DNA ladder,

degradation can be accurately assessed. If the 80 nt marker and DNA present in the EM co-elute, it can be confirmed that no DNA degradation has occurred. In order to accurately mimic the initial collection conditions in KCE-SELEX, the equilibrium concentration of the library was designed to be in great excess of the target (5μM N40 and 100 nM Exo1).

Figure 29B illustrates the extensive DNA degradation that arose after a 15 minute incubation with Exo1, when the equilibrium mixture is supplemented with 5 mM $MgCl_2$. It is evident from this electropherogram that Mg^{2+} does indeed promote an exonuclease activity. **Figure 29C** shows the Gel CE results obtained when Exo1 and the DNA library were incubated for over 1 hour in 50 mM Tris-acetate (pH 8.2), 100 mM NaCl buffer without any metal chelating agents. It is clear from this figure, that there is still some slight exonuclease activity, although not nearly as extensive as that found when Mg^{2+} was added to the buffer. When 5 mM EDTA was added to the 50mM Tris-acetate (pH 8.2), 100 mM NaCl incubation buffer, no DNA degradation was observed and the DNA library remained intact even after a 60 minute incubation **(Figure 29D)**. These results confirm that Mg^{2+} promotes enzymatic activity, while EDTA suppresses it.

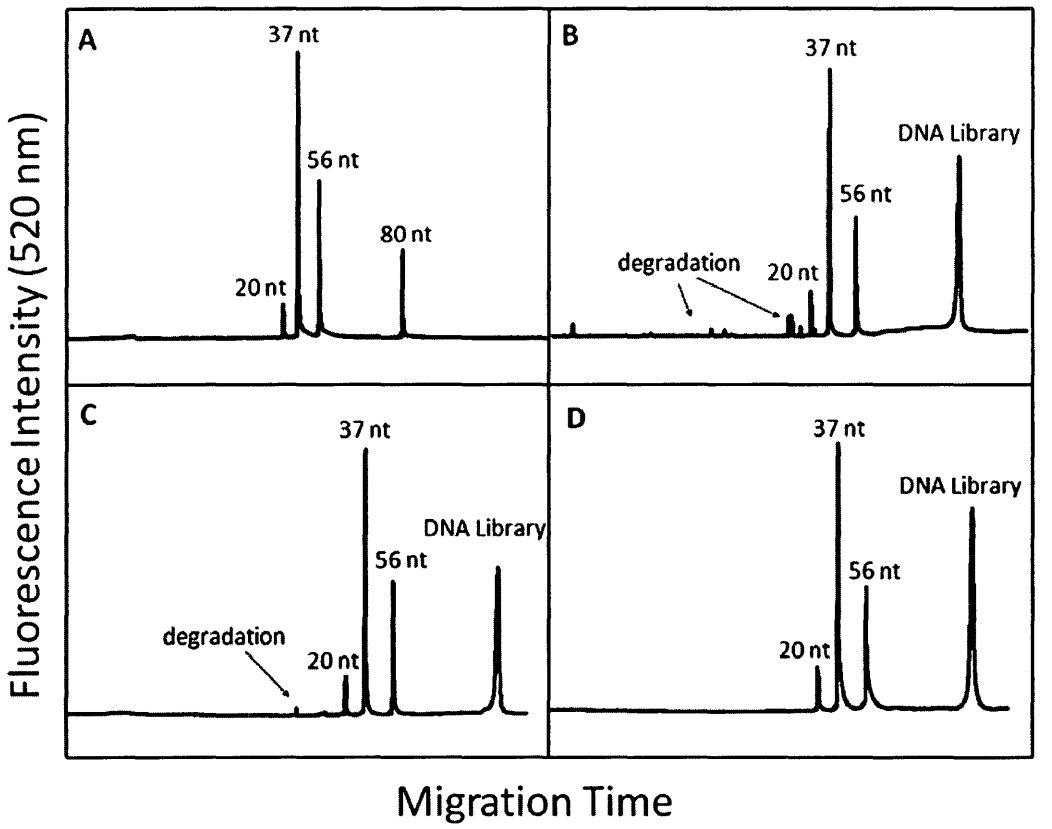

[Figure 29] Gel CE results illustrating Exo1 activity with various buffer additives. Panel A displays the DNA ladder containing 100 nM of the 20 nt sequence, 400 nM of the 37 nt sequence, 300 nM of the 56 nt sequence and 200 nM of the 80 nt sequence. Panel B shows the electropherogram obtained with a EM containing 100 nM Exo1 and 5 μM N40 DNA library incubated in a 50 mM Tris-acetate (pH 8.2), 100 mM NaCl, 5 mM $MgCl_2$ buffer for 15 minutes. The EM was co-injected with the DNA ladder in order to estimate the extent of DNA degradation. Panel C displays the electropherogram obtained with a EM containing 100 nM Exo1 and 5 μM N40 DNA library incubated in a 50 mM Tris-acetate (pH 8.2), 100 mM NaCl buffer incubated for 60 minutes and co-injected with the DNA ladder. Panel D shows the electropherogram obtained with a EM containing 100 mM Exo1and 5 μM N40 DNA library incubated in a 50 mM Tris-acetate (pH 8.2), 100 mM NaCl, 5 mM EDTA buffer incubated for 60 minutes and co-injected with the DNA ladder.

Although this result is somewhat intuitive, it is important to correctly identify the nominal concentration of EDTA necessary to avoid any library degradation. If the enzymatic suppression is incomplete, and residual exonuclease activity persists, this can result in the preferential degradation of high-affinity aptamers, making their collection and amplification impossible. From the gel CE results, 5 mM EDTA was found to be the optimal concentration required to completely inhibit the nuclease-induced degradation of the DNA library under collection conditions.

4.3 Bulk Affinity Analysis

In the classical KCE-SELEX protocol, a general bulk affinity assay is performed in order to numerically gauge the overall DNA-binding potential of the selected target. Bulk affinity is implemented experimentally through standard NECEEM assays where the equilibrium mixture consists of a low concentration of the DNA library and an excess of the target. The areas corresponding to any intact complexes, unbound DNA, and the DNA which is dissociated from the target can be easily determined through integration. Then, by substituting these areas into **equation 19**, a hypothetical K_d can be calculated to probe the relative abundance of target-binding sequences found within the heterogeneous DNA library. Although this bulk K_d does not offer any information on the binding capacity of individual aptamers, it can be used to monitor aptamer evolution after each round.

In order to estimate the general binding affinity Exo1 has towards the random DNA library, NECEEM experiments were conducted in a free solution running buffer (50 mM Tris-acetate (pH 8.2)). Exonuclease activity was also assessed through free zone CE in both the presence and absence of 5 mM EDTA. It can be seen from the results in **Figure 30**, that Exo1 experiences several high-affinity interactions with the heterogeneous DNA sequences in the N40 library. The left panel illustrates the bulk affinity in the absence of EDTA, while the right panel depicts the same experiment in the presence of 5 mM EDTA. In each panel, the black traces represent the electropherograms obtained from the equilibrium mixtures and blue traces are the N40 library in the absence of Exo1. After injection, the EM was subsequently heated to 95°C for 20 minutes to completely denature Exo1 and any complexes which had formed. This heating step was done to check for degradation products that may have been mistaken for complex peaks. The heat denatured EM was then re-run through the capillary using the same method, and

the results are illustrated as the red traces in each electropherogram. With an estimated bulk K_d value in the nanomolar range, it is clear that Exo1 recognizes then library as a substrate destined for degradation. It is further noted from **Figure 30A**, that EDTA is an essential component, if library degradation is to be avoided. However, in the presence of EDTA, multiple "complex" peaks are visible making the NECEEM electropherograms difficult to decipher and integrate with reasonable certainty.

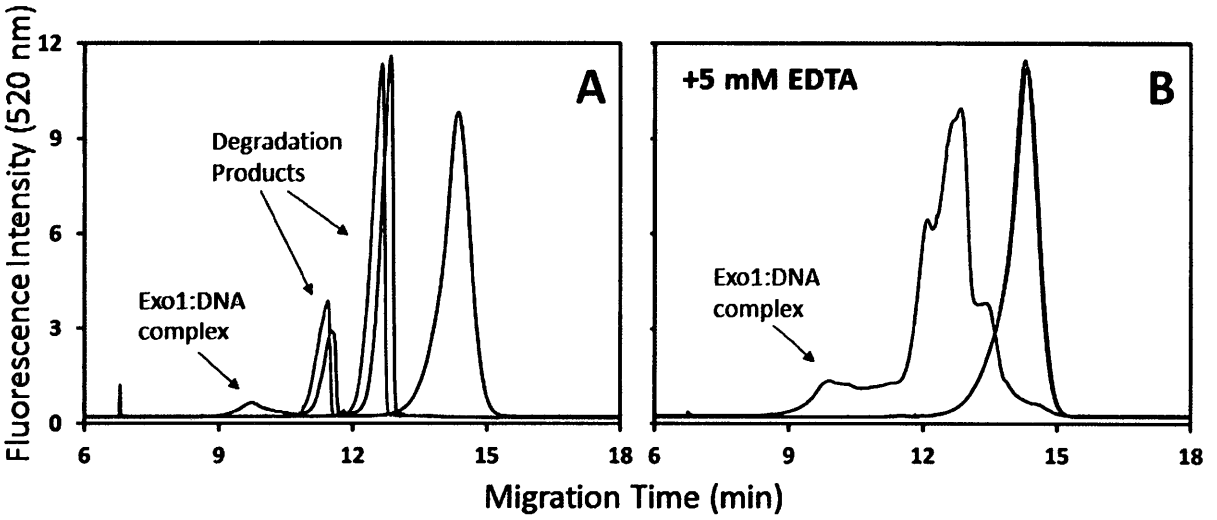

[Figure 30] NECEEM experiments performed to assess both Exo1-DNA affinity and exonuclease activity in the presence (b) and absence (a) of 5 mM EDTA. The black traces represent the NECEEM electropherograms of the equilibrium mixture. The blue lines show the DNA only control, and the red traces show the heat denatured protein-DNA mixtures. (a) EM containing 435 nM Exo1 and 100 nM of Alexa-488 labeled N40 DNA library in a 50 mM Tris-acetate (pH 8.2) incubation buffer supplemented with 50 mM KCl. (b) EM containing 435 nM Exo1 and 100 nM Alexa-488 labeled N40 DNA library in a 50 mM Tris-acetate (pH 8.2) incubation buffer supplemented with 50 mM KCl and 5 mM EDTA. In the presence of 5 mM EDTA the bulk K_d was estimated at 259 nM,

4.3.1 Complex Identification

In order to correctly identify the Exo1-N40 complex, NECEEM bulk affinity test was performed where unlabeled protein is replaced with the Chromeo P503 labeled counterpart. Fluorescence emission was detected through two separate channels, to help differentiate between the signals produced by Alexa488 and Chromeo P503. The electropherogram depicted in **Figure 31** illustrates the results of the NECEEM binding assay when using the Chromeo-labeled Exo1 and Alexa488-labeled DNA library, as the respective target and ligand. In each panel, the black traces depict emission signals acquired following the filtration through the 520 nm channel, specific for the Alexa-488-labeled DNA library, and the red traces represents the signal after being filtered through the 610 nm channel, specific for the Chromeo P503-labeled Exo1. As stated earlier, there is considerable fluorescence leakage of the 520 nm emission signal into the 610 nm channel due to an overlap in the emission spectra of each species. Therefore, the relative amount of fluorescence overlap must be accounted for when verifying the complex peak. This is done by adjusting the measured fluorescence signal, recorded through the 610 nm channel, so that the height of the rightmost peak, representing the unbound DNA library, exactly matches its complement detected through the 520 nm channel. Although the re-scaled electropherogram produces similar signals through both channels, it assists in recognizing certain complex peaks located at the leftmost region of the NECEEM electropherogram. From this result, it is evident that complexes exist; however, the mechanism of binding is likely non-sequence specific as the bulk K_d is quite strong. Moreover, complex mobility is rather broad and poorly separated from the DNA library. Both of these issues must be resolved prior to KCE-SELEX, in order to avoid collection contamination with unbound or non-specific DNA sequences.

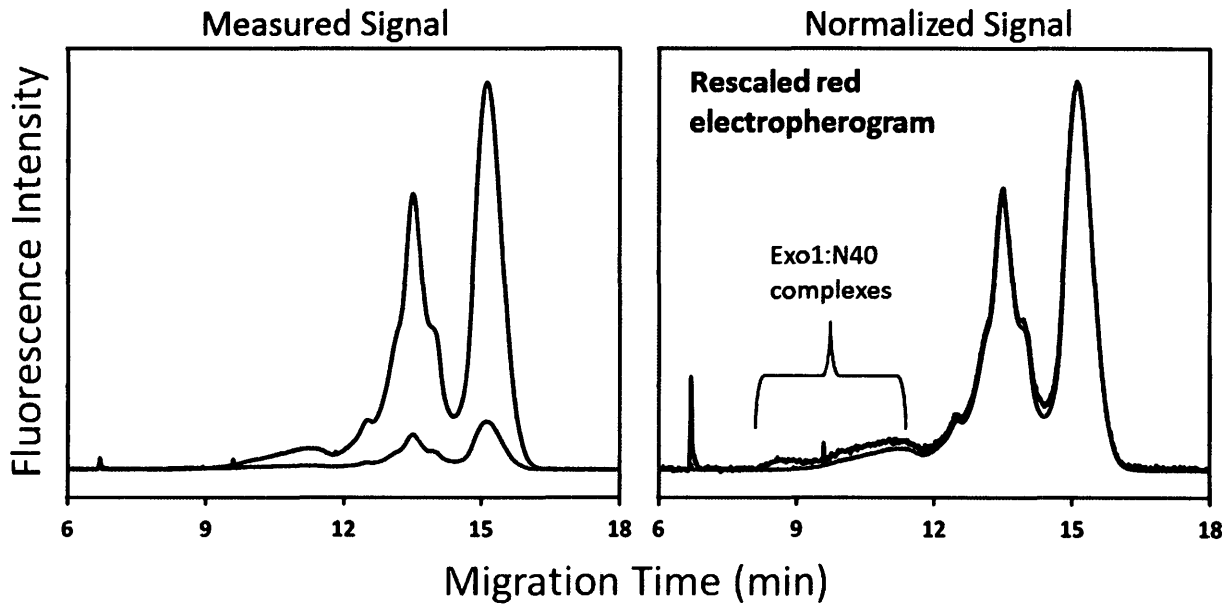

[Figure 31] Peak identification of the Exo1-N40 library complex through the combined use of Chromeo P503 labeled Exo1 and Alexa-488 labeled N40 DNA library. Black traces depict fluorescence at 520 nm while the red traces represent fluorescence through the 610 nm filtered channel. The left panel show the measured signal obtained through both channels, while the right panels show the same data with the red electropherograms rescaled so that the height of the rightmost peaks are equivalent for both the black and red electropherograms. The concentration of Exo1 and N40 library were 510 and 100 nM, respectively.

4.4 Short Oligonucleotides as Competitive Inhibitors

The non-specific binding of Exo1 to all single stranded DNA sequences, must be avoided as it will drastically hinder the entire SELEX process. It has been reported in the literature a free 3'hydroxyl group is necessary for exonuclease activity and polynucleotides with 3'-phosphoryl groups act as inhibitors.[98] This suggests that it is possible to generate a small single stranded oligonucleotide that can be used as a competitive inhibitor which blocks potential aptamers from binding in the active site. If the aptamers can be selected towards the inhibited protein, this would ensure that they are not bound to the active site as a substrate. Three polyT inhibitors were tested using NECEEM binding analysis **[Figure 32]**. It is shown, that they do prevent DNA degradation even when a small amount of Mg^{2+} was remained in the Exo1 storage buffer. This is most evident for the 5 nt inhibitor, which did not experience any degradation after a 15

minute incubation in 50 mM Tris-acetate (pH 8.2), 50 mM KCl buffer. Black traces refer to the NECEEM binding experiments, blue traces are the inhibitor controls, and red traces are the EM following heat denaturation. The 10 nt and 15 nt inhibitors had underwent some degradation in the 50 mM Tris-acetate (pH 8.2), 50 mM KCl buffer, however when supplemented with 5 mM EDTA, they remained intact. Moreover, the equilibrium dissociation constant calculated for the Exo1-inhibitor mixtures was lower than those calculated for the DNA library, suggesting preferential inhibitor binding. In panel **F**, it can be seen that no unbound DNA remained throughout the course of separation indicating a relatively low dissociation rate. Based on the calculated K_d values, the 15 nt inhibitor has the highest affinity towards Exo1. However, if all polyT inhibitors are equally effective at blocking the library from the active site, shorter strands may be preferred as they will likely minimize any repulsion of potential aptamers.

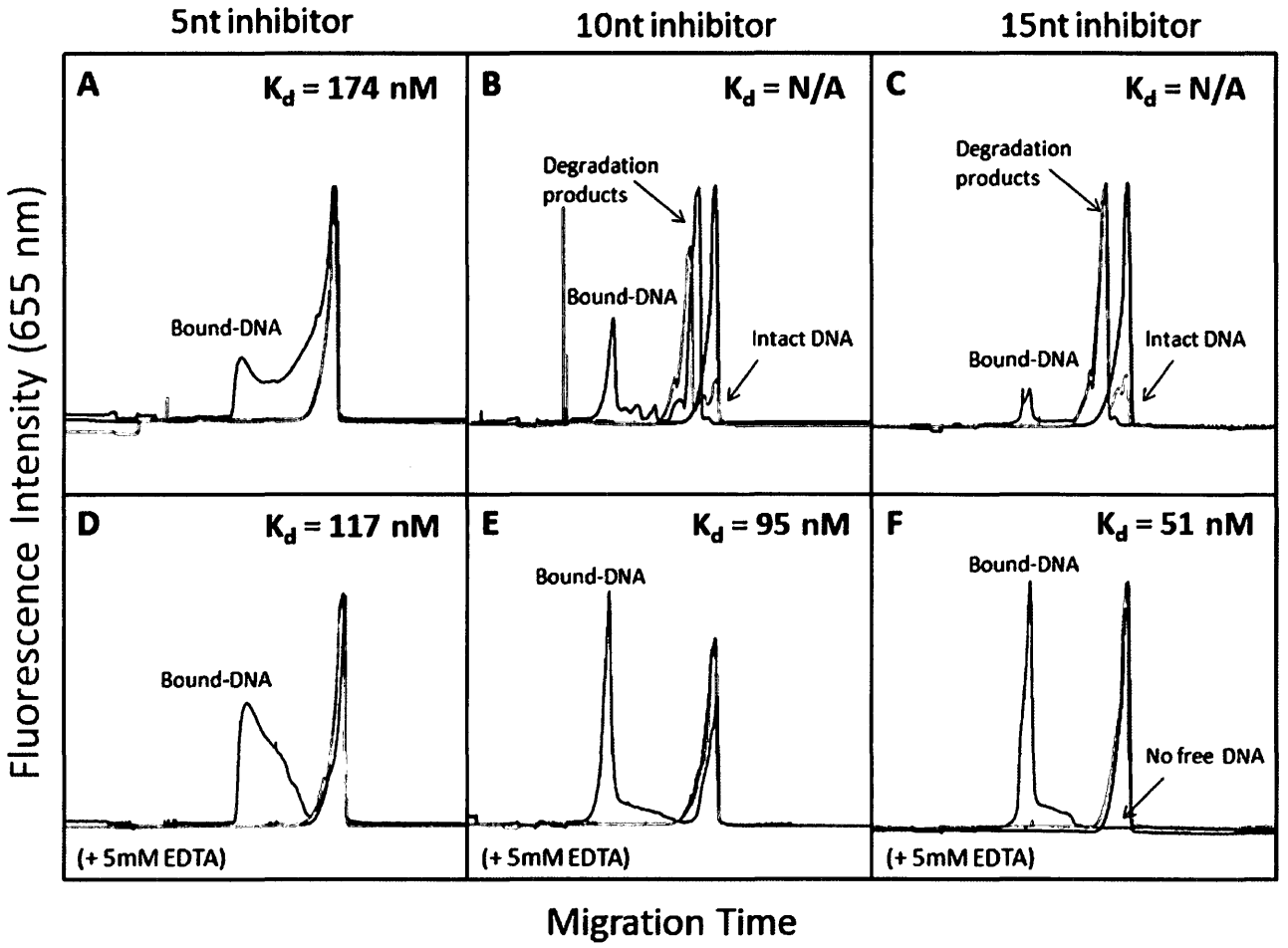

[Figure 32] NECEEM binding tests using Alexa-647 labeled 5nt, 10nt, and 15nt inhibitors as ligands towards Exo1. (A) 5nt DNA inhibitor in s 50 mM Tris-acetate (pH 8.2); 50 mM KCl run buffer. (B) 10nt DNA inhibitor in a 50 mM Tris-acetate (pH 8.2); 50 mM KCl run buffer. (C) 15nt DNA inhibitor in a 50 mM Tris-acetate (pH 8.2); 50 mM KCl un buffer. (D) 5nt DNA inhibitor in a 50 mM Tris-acetate (pH 8.2); 50 mM KCl; 5 mM EDTA run buffer. (E) 10nt DNA inhibitor in a 50 mM Tris-acetate (pH 8.2); 50 mM KCl; 5 mM EDTA run buffer. (F) 15nt DNA inhibitor in a 50 mM Tris-acetate (pH 8.2); 50 mM KCl; 5 mM EDTA run buffer. Black traces represent NECEEM electropherograms of the EM, blue traces illustrate the inhibitor controls, and red traces depict heat denatured equilibrium mixtures.

4.4.1 Ligand Competition Assay

Although the NECEEM binding assays indicate high-affinity binding with all three oligonucleotide sequences, their inhibitory properties are not guaranteed. In order to evaluate how effective each sequence is at blocking the enzymes active site, and thus, inhibiting any non-specific binding of the DNA library, a competition experiment was performed. The competition

assay was treated in a similar approach to all other single-ligand NECEEM experiments previously discussed. However, the equilibrium mixture consisted of the Exo1 and two potential ligands, the N40 DNA library and one of the polyT inhibitors. Since the DNA library is fluorescently labeled with Alexa-488, and the inhibitor with Alexa-647, synchronized excitation and detection is possible by using two distinct laser lines coupled with the appropriate dual-channel filtration. In **Figure 33**, all green traces represent fluorescence emission from the DNA library, while all black traces illustrate the signal obtained from the respective inhibitor as listed on the figure headings. Initially, an equimolar concentration of all three species (Exo1, library and inhibitor) was used to directly compare the enzymes relative affinity to each ligand. The electropherograms presented in panels **A, B**, and **C** of **Figure 33**, depict the result of the competition assay using a library concentration equal to that of the 5 nt, 10 nt and 15nt inhibitors, respectively. Panel **D**, represents the results from a competition assay where the 15nt inhibitor was present in a 3-fold excess to both the DNA library and Exo1. Panels **E, D, G,** and **F** illustrate the electropherogram acquired after heating the specified EM, displayed in the above panel, for 20 min at 95°C to inactivate and denature the enzyme. This denaturation step was performed in order to correctly identify any observed peaks as complexes (or dissociated complexes) as opposed to products of enzymatic degradation. The controls, depicted in panels **I, J, K** and **L** are shown in order to compare migration times of each ligand in the absence of Exo1. From **Figure 33A**, it is clear that in the presence of the 5 nt polyT sequence, Exo1 still exhibits a strong preference for the DNA library, and therefore, this is an ill-suited inhibitor. The 10 nt polyT sequence displayed a greater affinity to the active site and, slightly reduced Exo1's library binding capacity, as illustrated in **Figure 33B**. However, from **Figure 33C**, it is evident that the 15nt polyT sequence is a much more potent inhibitor, as the library binding is significantly

reduced in its presence. When used in excess, this inhibitor can completely out-compete the library for active-site binding [**Figure 33D**]. This result agrees with previous research, reporting an active site capable of harbouring ~13 nucleotides through two distinct domains.[139,140] The first domain is capable of binding up to 7 nucleotides, while the second binds nucleotides from positions 9 through 13.The 15 nucleotide inhibitor can exploit all possible binding sites and, accordingly, demonstrates maximal affinity towards Exo1.

Since nanopore DNA sequencing requires an unoccupied active site, the 15 nt inhibitor can assist in blocking this site during KCE-SELEX. Therefore, the Exo1-15nt inhibitor complex will serve as the target to which potential aptamers can bind. The introduction of an inhibitor is especially useful as it avoids any non-specific binding of the DNA library, and occupies the active site to promote aptamer binding elsewhere.

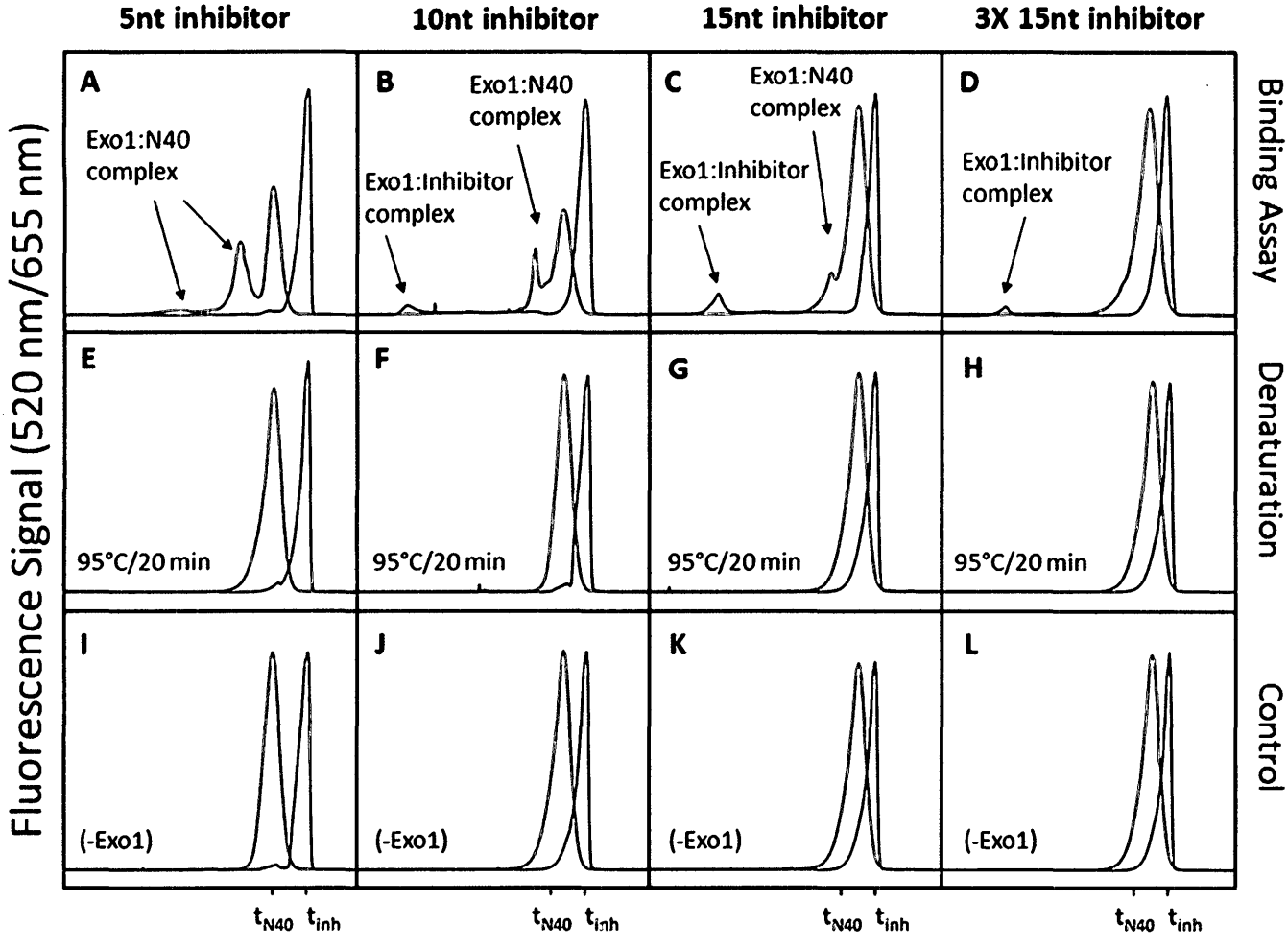

[Figure 33] Two substrate competition assays investigated through NECEEM. Exo1 was incubated with the Alexa-488 labeled N40 DNA library and either the 5 nt, 10 nt or 15 nt inhibitors, each labeled with the Alexa-647 fluorophore. Fluorescence emission at 520 nm and 655 nm were detected simultaneously using a two channel filtration system. Green traces correspond to Alexa-488 emission after separation through a 520 nm band-pass filter. Black traces correspond to Alexa-647 emission following the separation through a 655 nm band-pass filter. The top panels illustrate results of the competition assay after the 15 min incubation with both substrates. The middle panels illustrate the same equilibrium mixtures following complex denaturation through heat-induced Exo1 deactivation. The lower panels depict the controls where Exo1 was excluded from the EM. All experiments were performed in a 50 mM Tris-acetate (pH 8.2); 50 mM KCl; 5 mM EDTA incubation buffer and a 50 mM Tris-acetate (pH 8.2) run buffer (A) 96.7 nM Exo1, 100 nM N40 and 100 nM 5 nt inhibitor (B) 96.7 nM Exo1, 100 nM N40 and 100 nM 10 nt inhibitor (C) 96.7 nM Exo1, 100 nM N40 and 100 nM 15 nt inhibitor (D) 96.7 nM Exo1, 100 nM N40 and 300 nM 5 nt inhibitor (E) 96.7 nM Exo1, 100 nM N40 and 100 nM 5 nt inhibitor after heating at 95°C for 20 min (F) 96.7 nM Exo1, 100 nM N40 and 100 nM 10 nt inhibitor after heating at 95°C for 20 min. (G) 96.7 nM Exo1, 100 nM N40 and 100 nM 15 nt inhibitor after heating at 95°C for 20 min. (H) 96.7 nM Exo1, 100 nM N40 and 300 nM 15 nt inhibitor after heating at 95°C for 20 min. (I) 100 nM N40 and 100 nM 5 nt inhibitor (J) 100 nM N40 and 100 nM 10 nt inhibitor (K) 100 nM N40 and 100 nM 15 nt inhibitor (L) 100 nM N40 and 300 nM 15 nt inhibitor.

4.4.2 Exo1 Interaction with the 15 Nucleotide Inhibitor

Due to its high affinity for Exo1 and its powerful inhibitory capabilities, the 15 polyT sequence was selected for use in KCE-SELEX, with the target being the Exo1-inhibitor complex. Prior to aptamer selection, the binding affinity was further investigated in order to accurately measure both the equilibrium and unimolecular dissociation constants (K_d and k_{off}). The results are illustrated in **Figure 34**, with reported K_d and k_{off} values of 51 nM and 1.8 $*10^{-2}$ s^{-1}, respectively. In the lower panel, the black trace corresponds to the NECEEM electropherogram where the EM consisted of 131 nM of Exo1 and 50 nM of the 15 nt inhibitor. The red trace represent the EM following a heat treatment at 95°C for 20 min, and the blue trace is the control. The top panel is an enlarged image of the EM emphasizing the complex, unbound inhibitor and decay region.

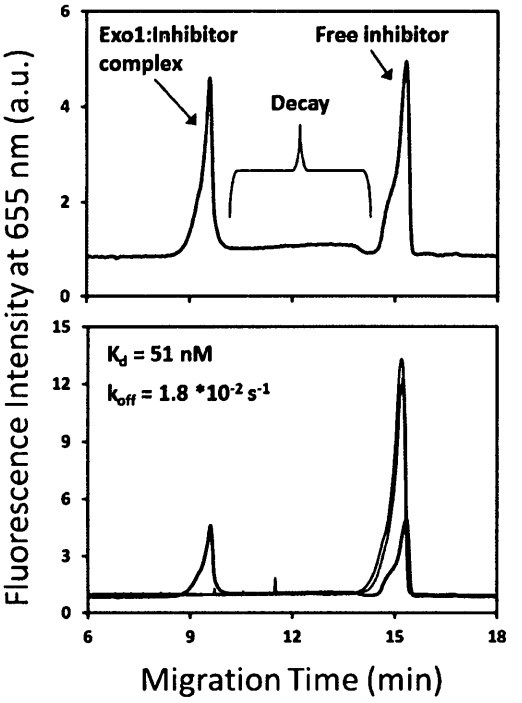

[Figure 34] NECEEM binding tests using Alexa-647 labeled 15nt PolyT DNA sequence an Exo1 inhibitor. The concentration of Exo1 and the 15nt inhibitor were 131 nM and 50 nM, respectively. Black traces represent NECEEM electropherograms of the EM, blue traces illustrate the inhibitor controls, and red traces depict heat denatured equilibrium mixtures. The top figure is a magnified image illustrating the Exo1-inhibitor interaction, highlighting the decay. Under these conditions, $K_d$was estimated at 51 nM and k_{off} at 1.8 $*10^{-2}$ s^{-1}.

As evident from **Figure 32F**, Exo1 is capable of binding all of the available inhibitor after a 15 min equilibration time. In order to further investigate the speed of complex formation, the incubation time was shortened to 5 min for comparison. During aptamer collection, all available Exo1 active sites should, ideally, be occupied with the inhibitor. Therefore, a pre-incubation step with the inhibitor must be performed prior to the incubation with the DNA library. The results shown in **Figure 35** highlight the apparent similarities between the 15 min and 5 min incubation times. This implies that a 5 min pre-incubation of Exo1 with the 15 nt inhibitor is suffice for maximal active site occupation,.

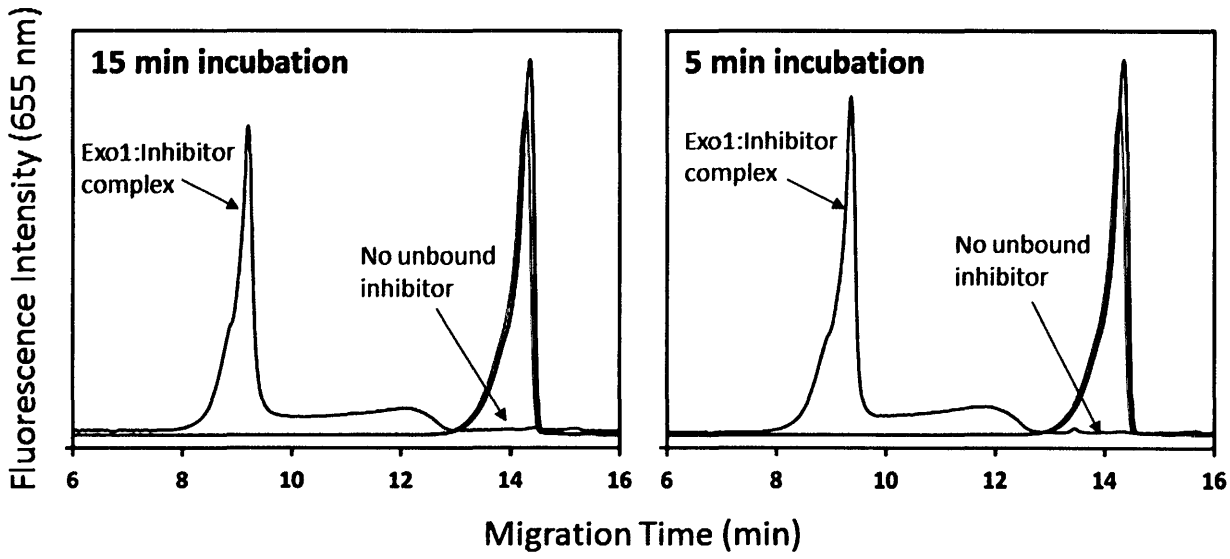

[Figure 35] NECEEM binding tests using Alexa-647 labeled 15nt PolyT inhibitor after 5 min and 15 min incubation times, shown in the right and left panels, respectively.. The concentration of Exo1 and the 15nt inhibitor were 435 nM and 100 nM, respectively. Black traces represent NECEEM electropherograms of the EM, blue traces illustrate the inhibitor controls, and red traces depict heat denatured equilibrium mixtures.

4.5 Pressure-based Propagation and Exo1 Surface Adsorption

It is known that target adsorption to the capillary surface can greatly hinder aptamer selection through KCE methods, and thus, should be minimized prior to commencement. From **Figure 14** in Chapter 2 of this report, the tailing of the Chromeo-labeled Exo1 peak, implies

protein interaction the inner wall of the capillary. The fluorescence signal eventually returns to the baseline, which suggests a weaker reversible interaction.

Although many buffer additives and coating techniques have proven to be effective in reducing the surface adsorption of protein analytes, the majority are poorly suited for kinetic-based applications such as binding analysis and aptamer selection due to apparent incompatibilities with the fundamental KCE requirements. A buffer, together with any additive or coating, must satisfy three conditions in order to study biomolecular interactions by CE: (i) complex formation must not be inhibited (ii) the adhesion of aptamer target and the DNA library must be suppressed, and (iii) the EOF should be sufficiently strong to ensure that both detectable components (ligand and complex) are carried past the detector, while still maintaining an ideal separation distance. The number of coatings compatible with KCE-SELEX is rather limited. While several dynamic additives such as amine-containing molecules, polymers and surfactants may satisfy the three requirements, they often lack the efficiency associated with more permanent coatings. Since their attachment is based on temporary interactions with the capillary, dynamic modifies tend to compete with the protein for surface binding sites, and thus, introduce an additional level of interaction. This will undoubtedly complicate both the kinetic analysis and aptamer selection, and should generally be avoided. Furthermore, only a selected number of covalently bound coatings are suitable for KCE, and often, these coatings require complex synthesis and lengthy derivatization processes.[141-143] Moreover the alteration in EOF can likely decrease the separation distance between the complex and unbound DNA, and thus, narrow the collection window. As a result, both the advantages and disadvantages must be carefully considered prior to coating and buffer selection.

The pressure propagation method was then applied to screen potential coatings and buffers for optimizing Exo1 aptamer selection. First, 5.1 μM of Exo1 was fluorescently labeled using Chromeo P503, and then pressure propagated in a bare silica capillary across both a 10 and 40 cm distance [**Figure 36**]. The electrolyte used for sample propagation was 50 mM Tris-acetate (pH 8.2) for the first 40 min of the experiment. A 100 mM NaOH rinse was then introduced in order to wash off the protein that remained adsorbed to the surface. The results shown in **Figure 36** confirm the adsorptive nature of Exo1 in an uncoated capillary surface.

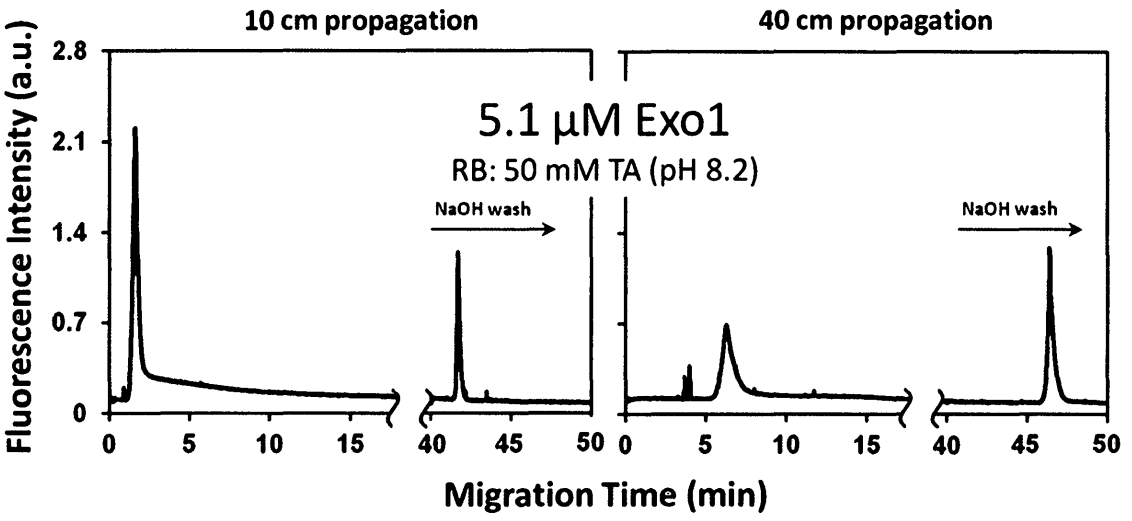

[**Figure 36**] Temporal propagation patterns of 5.1 μM Chromeo-labeled Exo1 after 10-cm and 40-cm pressure-driven propagations using an uncoated capillary and 50 mM Tris acetate (pH 8.2) as the run buffer for the first 40 min of the experiment. After the 40 min time point, 100 mM NaOH was introduced to strip off any adsorbed protein.

Several coatings and buffer additives were then tested to determine whether protein adsorption can be eliminated prior to aptamer selection. The pressure-driven propagation method was tested using (i) PVA coated capillary, (ii) Ultratrol semi-permanent coating, and (iii) an uncoated surface using a buffer of 50 mM Tris acetate (pH 8.2) supplemented with 0.015% Triton-X 100. All three of these attempts resulted in a reduced level of protein adsorption. However, in both the PVA and Ultratrol coated capillaries, the electrophoretic separation of free

inhibitor form Exo1-inhbitor complex was narrowed in comparison to untreated silica due to the highly reduced or absent EOF. In the case where 0.015% Triton X-100 was introduced into the run buffer, the EOF became rather unpredictable and this option was then abandoned.

4.5.1 Pressure-Propagation and Exo1-Inhibitor Complex Adsorption

When performing NECEEM experiments using an equilibrium mixture that contained Exo1 and the oligonucleotide inhibitor, the complex peak appeared to be well defined and demonstrated the characteristics of a typical NECEEM electropherogram (refer to panels **D,E** and **F** of **Figure 32**). These results imply that, although Exo1 on its own adsorbs to the fused-silica surface, the Exo1-inhibitor complex does not. In order to confirm this hypothesis, the pressure-driven propagation method was performed using the Exo1-inhibitor complex as a sample. First, an equilibrium mixture was prepared using 437 nM unlabeled Exo1 and 100 nM of the Alexa647-labeled 15 nucleotide inhibitor. Under these conditions, all of the inhibitor remains bound to the protein, and the rate of dissociation was found to be quite slow. The equilibrium mixture was then injected into the capillary outlet and pressure propagated well past the detection window using a reversed pressure of 0.5 psi. After 6 min of pressure propagation, an electric field of 400 V/cm was applied, in order to separate any unbound inhibitor from the Exo1-inhibitor complex (see black trace in **Figure 37**). The electrophoretic separation is necessary in order to verify that the peak obtained through the pressure propagation, is that of the complex rather than that of the unbound or dissociated inhibitor. The equilibrium mixture was then heated at 95°C for 20 min, in order to denature Exo1 and rupture the Exo1-inhibitor complex. The heat-denatured sample was then injected into the capillary and the experiment was then repeated (see red trace in **Figure 37**). By comparing these results to a control containing only the inhibitor without any Exo1 (blue trace in **Figure 37**), we can conclude that the pressure-

driven propagation peak is indeed that of the Exo1-inhibitor complex rather the unbound inhibitor.

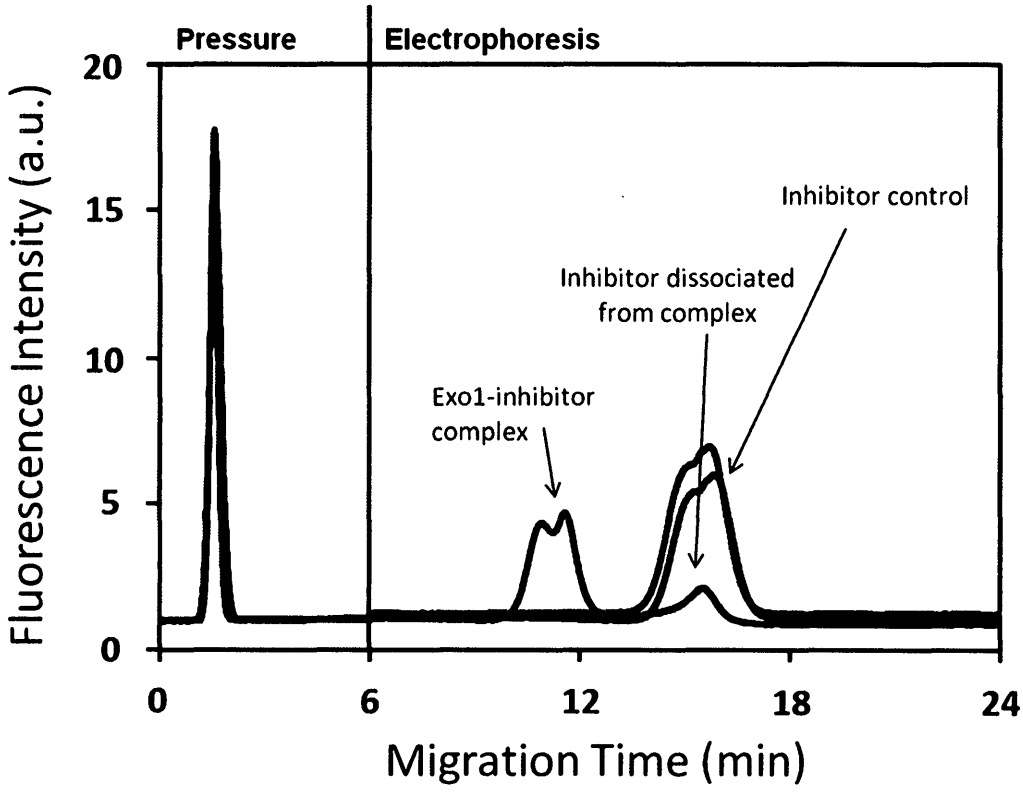

[**Figure 37**]: Pressure-induced propagation patterns are shown up until the 6 min migration time mark. An electric field of 400 V/cm was introduced after the 6 min pressure propagation and maintained throughout the remainder of the experiment. Black traces represent temporal propagation pattern/electropherograms of the equilibrium mixture containing 437 nM of Exo1 and 100 nM of the 15 nucleotide inhibitor. Blue traces illustrate the temporal propagation pattern/electropherogram of the inhibitor controls, and red traces depict pressure propagation/electropherogram of the heat denatured equilibrium mixture.

As a result, the pressure-based propagation analysis of analyte adsorption can be applied towards the protein-ligand complex as well as the free protein. It can be seen from **Figure 38**, that the Exo1-inhibitor complex expresses a negligible interaction with the fused-silica surface, and therefore, an uncoated capillary will be suffice when performing aptamer selection on this target.

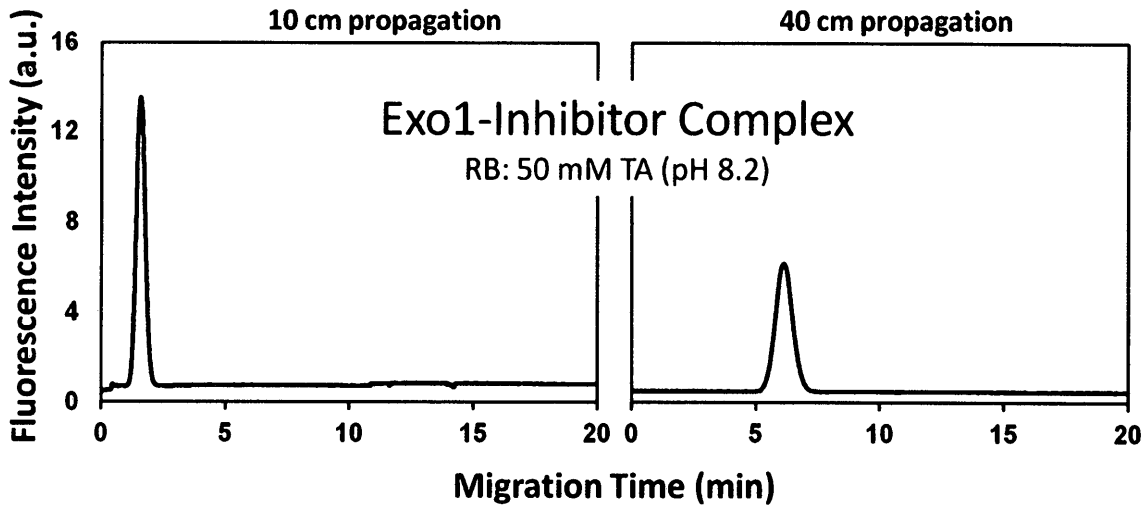

[**Figure 38**] Temporal propagation patterns of the Exo1-15 nucleotide inhibitor complex after 10-cm and 40-cm pressure-driven propagations using an uncoated capillary using a 50 mM Tris acetate (pH 8.2) run buffer. The equilibrium mixture containing 437 nM Exo1 and the 100 nM 15 nucleotide inhibitor was prepared to ensure complete binding and propagation of the pure complex peak.

The significant differences in adsorption between the Exo1-inhibitor complex and the free Exo1 agree with previously reported structural research on the protein.[144] The highly processive nuclease activity occurs after the enzyme experiences a conformational change, which allows it to completely enclose its substrate. The active site likely contains a number of positively charged amino acid residues in order to interact with the negative DNA substrate. Once the active site is blocked, the positive charges are masked and no longer capable of interacting with the capillary surface.

4.6 Separation Efficiency and Peak Resolution of the Exo1-Inhibitor Complex from the DNA Library

Prior to KCE-SELEX, and the first round of aptamer collection, the separation window between the target (Exo1-inhibitor complex) and N40 DNA library must be maximized. During selection, the capillary length should be 80 cm or larger, as this will maximize peak separation

and improve the resolution. Superior separation leads to greater collection efficiency and less contamination with undesirable DNA sequences.

To accurately assess the separation efficiency and resolution of the Exo1-inhibitor-library mixture, a competition assay was performed in a 102 cm capillary. First, Exo1 was incubated with the 15 nt inhibitor for 5 min in an incubation buffer of 50 mM Tris-acetate supplemented with 50 mM KCl and 5 mM EDTA. Due to its high affinity for the active site and relatively rapid rate of association, this short incubation time is enough to enable the maximal binding of the inhibitor. Then, the library was introduced to the Exo1-inhibitor EM, and an additional incubation was executed for 15 min. After reaching equilibrium, the mixture was separated in the 102 cm capillary and fluorescence was detected via simultaneous excitation with two laser sources at 488 nm and 637 nm, and the corresponding emission signals were detected using 520 nm and 655 nm band-pass filters in two distinct channels. The results of this competition assay are illustrated in **Figure 39.** Again, the green traces represent fluorescence emission at 520 nm and the black traces signify the signal recorded at 655 nm. **Figures 39A** and **B** portray the results of the competition assay with equimolar and a 3-fold excess of the inhibitor, respectively. Panels **C** and **D** are the magnified images of the overhead competition assays, highlighting the inefficient separation and resolution between the Exo1-inhibitor complex peak and the N40 DNA library.

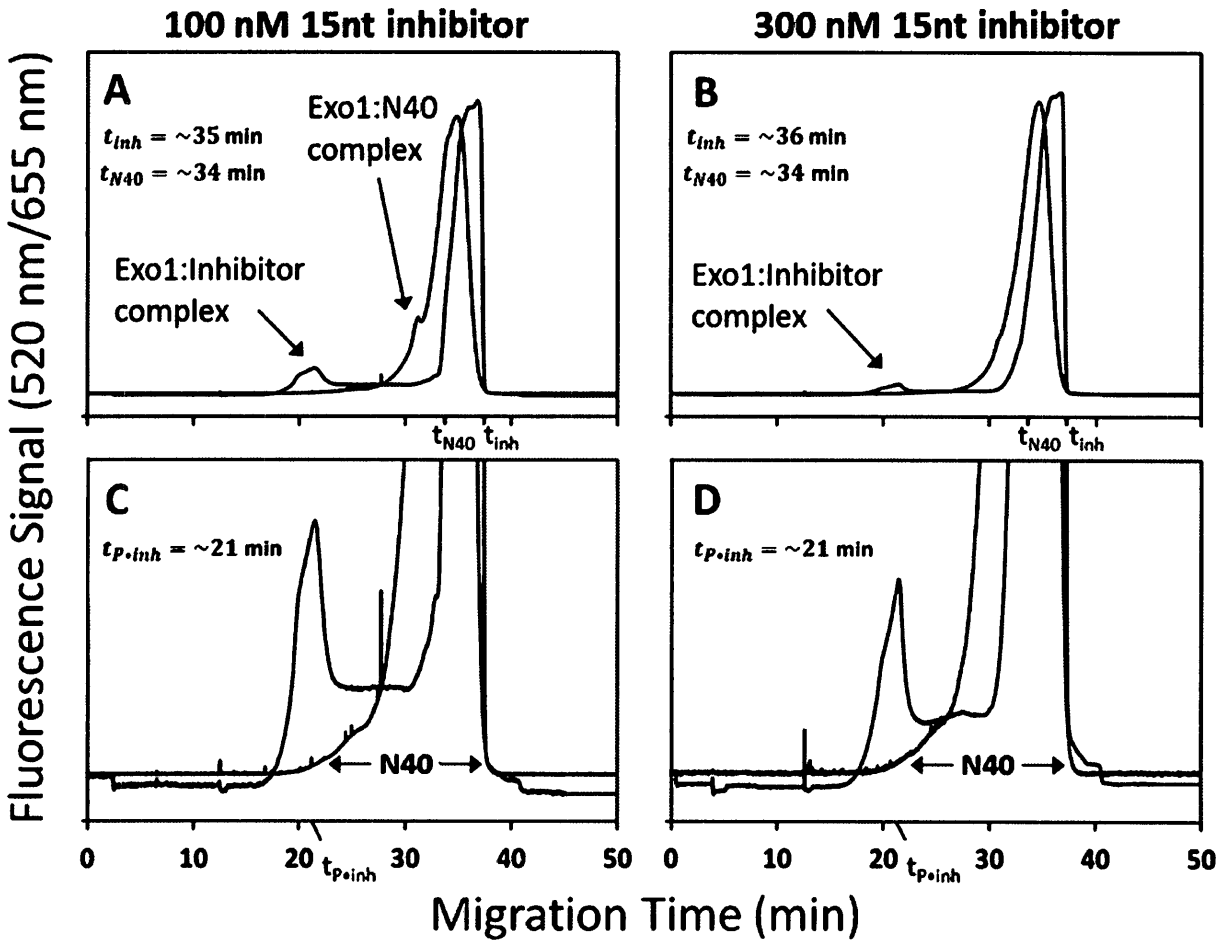

[Figure 39] Two substrate competition assays investigated in a 102 cm capillary. Exo1 was incubated with the Alexa-488 labeled N40 DNA library and the Alexa-647 labeled 15 nt inhibitor. Fluorescence emission at 520 nm and 655 nm were detected simultaneously using a two channel filtration system. Green traces correspond to Alexa-488 emission after separation through a 520 nm band-pass filter. Black traces correspond to Alexa-647 emission following the separation through a 655 nm band-pass filter. The top panels illustrate results of the competition assay after the 5 min incubation with the inhibitor followed by a subsequent 15 min incubation with both substrates. All experiments were performed in a 50 mM Tris-acetate (pH 8.2); 50 mM KCl; 5 mM EDTA incubation buffer and a 50 mM Tris-acetate (pH 8.2) run buffer. (A) 96.7 nM Exo1; 100 nM 15 nt inhibitor; 100 nM N40 library. (B) Magnified image of panel A illustrating poor peak resolution. (C) 96.7 nM Exo1; 300 nM 15 nt inhibitor; 100 nM N40 library. (B) Magnified image of panel B illustrating poor peak resolution.

Since the triple complex (Exo1-Inhibitor-N40 library) would have a migration intermediary to the Exo1-Inhibitor complex and the unbound DNA library, the separation distance between these peaks must be improved prior to selection. Since resolution is maximized through μ_{eo} (see **equation 18**), the designated separation buffer should produce a μ_{eo} value similar in magnitude but opposite in direction to the μ_{ep} of each analyte (i.e. the Exo1-inhibitor complex, N40 library and 15 nt polyT inhibitor).

Moreover, under these experimental conditions, the peak widths are broad due to differences in the ionic strengths of the incubation and run buffers. Since the incubation buffer contains significantly more salts than does the run buffer, anti-stacking effects tend to decrease the separation efficiency between peaks. This can easily be corrected in future work by implementing identical incubation and separation buffers

4.7 Experimental

4.7.1 Materials

Uncoated fused-silica capillaries with 75μm inner diameter (375 μm outer diameter) and 101.0 μm inner diameters (i.d.) (357 μm o.d.) were purchased from Polymicro (Phoenix, AZ). An Oligel ssDNA/ssRNA gel Package for ssDNA separation was purchased from Advanced Analytical (Orangeville, ON, Canada) and the Chromeo P503 pyrylium dye was purchased from Active Motif (Burlington, ON, Canada). Purified Exo1 was provided by collaborators from Oxford and the HPLC purified fluorescently labeled DNA library, N40,(5'-Alexa-488/CTC CTC TGA CTG TAA CCA CG$(N)_{40}$ GCA TAG GTA GTC CAG AAG CC-3'), 5 nucleotide Exo1 inhibitor (5'-Alexa647/TTT TT/PO_4-3'), 10 nucleotide Exo1 inhibitor (5'-Alexa647/TTT TTT TTT T/PO_4-3') and 15 nucleotide Exo1 inhibitor (5'-Alexa647/TTT TTT TTT TTT TTT/PO_4-3') were each purchased from Integrated DNA technologies Inc. (Coralville, IA). All DNA was dissolved in 10mM Tris-acetate buffer (pH 7.5) to obtain a high stock concentration which was then stored at -20°C. All other chemicals were purchased from Sigma Aldrich (Oakville, ON, Canada),

4.7.2 Instrumentation

All experiments were conducted using a P/ACE MDQ capillary electrophoresis instrument (Beckman-Coulter, Fullerton, CA) equipped an LIF detector. A 637 nm solid-state laser was used to excite all Alexa-647 labeled polyT inhibitors. A 488 nm argon-ion laser was used for fluorescence excitation in Gel CE experiments, while a 488 nm solid-state laser was used in all other experiments to excite Alexa-488 labeled DNA and Chromeo labeled proteins. A two-channel detection system was used to analyze both the protein and DNA library or DNA library and inhibitor simultaneously. A 520 nm filter was used to detect the fluorescently labeled DNA through one channel, while a 610 nm filter was used to detect the Chromeo-labeled proteins through the second channel. A 655 nm band pass filter was used to detect fluorescence emission of all Alexa-647 labeled DNA inhibitor sequences.

4.7.3 Gel CE for Exo1 Activity Analysis

All Gel CE experiments were performed using a 101 μm inner diameter capillary with a total length of 60 cm (50 cm to detection window) with the temperature controlled at 20°C. The capillary was first rinsed with the capillary conditioning solution placed at the inlet end for 15 min using a forward pressure of 60 psi. 0.1 mL of the Oligel ssDNA/ssRNA gel was transferred to a 0.2 mL PCR tube, placed at the outlet end and injected into the capillary using a reverse pressure of 100 psi for 60 min. Once the capillary was filled, a 40 min pre-run at -15 kV was performed using the ssDNA Oligel buffer in the inlet vial and Oligel ssDNA/ssRNA gel as the outlet vial. A DNA ladder was prepared in a 50 mM Tris-acetate (pH 8.2); 100 mM NaCl buffer using fluorescently labeled DNA of different lengths that were readily available in the lab. The composition of the DNA ladder is as follows: 100 nM of a 20 nucleotide (nt) sequence, 400 nM

of a 37 nt sequence, 300 nM of a 56 nt sequence, and 200 nM of an 80 nt sequence. The DNA ladder was injected electrokinetically using -5 kV for 13 seconds and CE separation was performed at -12 kV for 80 minutes. Three different incubation buffers were used to characterize Exo1 activity: (i) 50 mM Tris-acetate (pH 8.2); 100 mM NaCl (ii) 50 mM Tris-acetate (pH 8.2); 100 mM NaCl; 5mM $MgCl_2$ and (iii) 50 mM Tris-acetate (pH 8.2); 100 mM NaCl; 5 mM ethylenediaminetetraacetic acid (EDTA). Equilibrium mixtures containing 100 nM Exo1 and 5 μM N40 Library were prepared in one of the respective buffers. Mixtures were incubated for over 60 minutes in buffers (i) and (iii), while only 15 min incubation was tested for buffer (ii). The DNA ladder and the respective equilibrium mixture were co-injected into the capillary using -5 kV for 13 seconds with a water dip between each injection. Samples were then separated using -12 kV for 80 minutes.

4.7.4 Labeling of Exo1 with Chromeo P503

The Chromeo P503 working solution was prepared by dissolving 1 mg of the lyophilized product 100 μL of dimethylformamide as recommended by the manufacturer. A 100 fold dilution of the working solution was then produced in a 0.1 M $NaHCO_3$ (pH 8.3) buffer. 5.1 μM of Exo1 was reacted with the 100-fold diluted Chromeo P503 solution and left to incubate overnight at 4°C to allow complete conjugation of the active protein. Reaction completion was observed visually as a colour change from blue to a faint pink. All experiments involving the labeled Exo1 protein were performed within 3 days of the conjugation reaction as to preserve the proteins native structural state.

4.7.5 NECEEM-based Analysis of Protein-DNA Interactions

All protein-DNA equilibrium mixtures that were analyzed using NECEEM are indicated in **Table 3**. Uncoated fused-silica capillaries were first rinsed with (i) 0.1 M HCl, (ii) 0.1M NaOH,(iii) ddH_2O, and (iv) 50 mM Tris-acetate (pH 8.2) with a pressure of 20 psi for 5 minutes. The DNA library was annealed by heating at 95°C for 1 min in a thermal cycler (Eppendorf, Hamburg, Germany) with a calculated cooling of 0.5°C/s, until a temperature of 25°C was achieved. The EM was prepared in the respective incubation buffer at the concentrations indicated in **Table 3** of the **Appendix** and left to incubate as tabulated. For all capillaries with 50 cm total length, 50 nL of the EM was then introduced into the inlet using a 0.5 psi pressure injection for 7 seconds. For capillaries with a 102 cm total length, 150 nL was injected in the inlet by applying a pressure of 1 psi for 33 s. The sample was the separated using the voltages listed in **Table 3** with at controlled temperature of 15°C. For all experiments, the EM was heated to 95°C for 20 minutes in order to denature the protein and any complex that may have formed. This heat-denatured EM was re-run on the CE using the same method, and the resultant electropherogram was assessed for DNA degradation

4.7.6 Pressure Propagation Adsorption Analysis

A bare fused-silica capillary was rinsed sequentially with 0.1 M HCl, 0.1 M NaOH, ddH_2O and 50 mM Tris-acetate (pH 8.2) each at a pressure of 20 psi for 2 min. All pressure propagation experiments intended for Exo1 adsorption analysis were performed with the labeled protein as described in Chapter 3. To investigate adsorption of the Exo1-Inhibitor complex, an equilibrium mixture containing 435 nM of the unlabeled Exo1 and 100 nM of the Alexa-647 labeled 15 nt inhibitor was prepared in an incubation buffer consisting of 50 mM Tris-acetate

(pH 82), 50 mM KCl and 5 mM EDTA. After a 15 min incubation, all of the inhibitor is bound to the excess protein (see **Figure 34**). The EM was then injected into the uncoated capillary outlet using a reverse pressure of 0.5 psi for 7 s, and propagated past the detector using a pressure of the same magnitude and direction for 6 min. At this point, the pressure was immediately stopped and a potential difference of 20 kV was the applied across the 50 cm capillary to induce separation in the EM. This procedure was repeated for the control as well as the heat-denatured sample, which consisted of the EM after a 20 min exposure at a temperature of 95°C. Once the pressure peak had been accurately identified as the complex, the pressure-driven propagation of the EM was repeated from the capillary inlet.

4.8 Conclusions

Four main conclusions can be made from this work (i) 5 mM EDTA suppresses DNA degradation and (ii) a 15 nucleotide polyT inhibitor with a 3' PO_4^{2-} can be utilized as a powerful competitive inhibitor in order to suppress non-specific binding (iii) the Exo1-Inhibitor complex does not adsorb to the uncoated capillary surface and (iv) the separation efficiency and peak resolution must be improved prior to the commencement of KCE-SELEX. Although a number of target-specific complications have been resolved, separation between the target and DNA library must be maximized in order to determine an appropriate collection window. This can be done through slight alterations of the composition of the run buffer, incubation buffer or both. Moreover, the anti-stacking effect should be eliminated to generate more narrow and distinct peaks. This can be done by reducing the salt concentration in the incubation buffer, or increasing the ionic strength of the background electrolyte, provided that the extent of Joule heating is controlled.

Appendix

[Table 3] NECEEM experiments performed throughout chapter 4 of this report. Target concentration, ligand concentration, incubation time, incubation buffer, capillary and applied voltage are indicated for each experiment.

Target concentration	Ligand concentration	Incubation time	Incubation buffer	Capillary	Voltage
435 nM unlabeled Exo1	100 nM Alexa-488 labeled N40 Library	15 min	50 mM Tris-acetate (pH 8.2); 100 mM KCl	Uncoated 50 cm (75 µm id)	10 kV/5 min then increased to 20kV
435 nM unlabeled Exo1	100 nM Alexa-488 labeled N40 Library	15 min	50 mM Tris-acetate (pH 8.2); 100 mM KCl; 5 mM EDTA	Uncoated 50 cm (75 µm id)	10 kV/5 min then increased to 20kV
510 nM Chromeo-labeled Exo1	100 nM Alexa-488 labeled N40 Library	15 min	50 mM Tris-acetate (pH 8.2); 50 mM KCl; 5 mM EDTA	Uncoated 50 cm (75 µm id)	10 kV for 5 min then increased to 20 kV
435 nM unlabeled Exo1	100 nM Alexa-647 labeled 5nt inhibitor	15 min	50 mM Tris-acetate (pH 8.2); 100 mM KCl	Uncoated 50 cm (75 µm id)	10 kV for 5 min then increased to 20 kV
435 nM unlabeled Exo1	100 nM Alexa-647 labeled 5nt inhibitor	15 min	50 mM Tris-acetate (pH 8.2); 50 mM KCl; 5 mM EDTA	Uncoated 50 cm (75 µm id)	10 kV for 5 min then increased to 20 kV
435 nM unlabeled Exo1	100 nM Alexa-647 labeled 10nt inhibitor	15 min	50 mM Tris-acetate (pH 8.2); 100 mM KCl	Uncoated 50 cm (75 µm id)	10 kV for 5 min then increased to 20 kV
435 nM unlabeled Exo1	100 nM Alexa-647 labeled 10nt inhibitor	15 min	50 mM Tris-acetate (pH 8.2); 100 mM KCl; 5 mM EDTA	Uncoated 50 cm (75 µm id)	10 kV for 5 min then increased to 20 kV
435 nM unlabeled Exo1	100 nM Alexa-647 labeled 15nt inhibitor	15 min	50 mM Tris-acetate (pH 8.2); 100 mM KCl	Uncoated 50 cm (75 µm id)	10 kV for 5 min then increased to 20 kV
435 nM unlabeled Exo1	100 nM Alexa-647 labeled 15nt inhibitor	15 min	50 mM Tris-acetate (pH 8.2); 100 mM KCl; 5 mM EDTA	Uncoated 50 cm (75 µm id)	10 kV for 5 min then increased to 20 kV

Target concentration	Ligand concentration	Incubation time	Incubation buffer	Capillary	Voltage
435 nM unlabeled Exo1	100 nM Alexa-647 labeled 15nt inhibitor	5 min	50 mM Tris-acetate (pH 8.2); 100 mM KCl	Uncoated 50 cm (75 μm id)	10 kV for 5 min then increased to 20 kV
96.7 nM unlabeled Exo1	**1.** 100 nM Alexa-647 labeled 5nt inhibitor **2.** 100 nM Alexa-488 labeled N40 library	15 min	50 mM Tris-acetate (pH 8.2); 100 mM KCl; 5 mM EDTA	Uncoated 50 cm (75 μm id)	10 kV for 5 min then increased to 20 kV
96.7 nM unlabeled Exo1	**1.** 100 nM Alexa-647 labeled 10nt inhibitor **2.** 100 nM Alexa-488 labeled N40 library	15 min	50 mM Tris-acetate (pH 8.2); 100 mM KCl; 5 mM EDTA	Uncoated 50 cm (75 μm id)	10 kV for 5 min then increased to 20 kV
96.7 nM unlabeled Exo1	**1.** 100 nM Alexa-647 labeled 15nt inhibitor **2.** 100 nM Alexa-488 labeled N40 library	15 min	50 mM Tris-acetate (pH 8.2); 100 mM KCl; 5 mM EDTA	Uncoated 50 cm (75 μm id)	10 kV for 5 min then increased to 20 kV
96.7 nM unlabeled Exo1	**1.** 300 nM Alexa-647 labeled 15nt inhibitor **2.** 100 nM Alexa-488 labeled N40 library	15 min	50 mM Tris-acetate (pH 8.2); 100 mM KCl; 5 mM EDTA	Uncoated 50 cm (75 μm id)	10 kV for 5 min then increased to 20 kV
131 nM unlabeled Exo1	50 nM Alexa-647 labeled 15 nt inhibitor	15 min	50 mM Tris-acetate (pH 8.2); 100 mM KCl; 5 mM EDTA	Uncoated 50 cm (75 μm id)	10 kV for 5 min then increased to 20 kV

Target concentration	**Ligand concentration**	**Incubation time**	**Incubation buffer**	**Capillary**	**Voltage**
96.7 nM unlabeled Exo1	**1.** 100 nM Alexa-647 labeled 15nt inhibitor **2.** 100 nM Alexa-488 labeled N40 library	**1.** 5 min with inhibitor **2.** 15 min with inhibitor + library	50 mM Tris-acetate (pH 8.2); 100 mM KCl; 5 mM EDTA	Uncoated 102 cm (75 μm id)	30 kV
96.7 nM unlabeled Exo1	**1.** 300 nM Alexa-647 labeled 15nt inhibitor **2.** 100 nM Alexa-488 labeled N40 library	**1.** 5 min with inhibitor **2.** 15 min with inhibitor + library	50 mM Tris-acetate (pH 8.2); 100 mM KCl; 5 mM EDTA	Uncoated 102 cm (75 μm id)	30 kV

Mathematical Relationship between K_d and $[L]$

The equilibrium association constant, K_a, is the mathematical inverse of the equilibrium dissociation constant (explained fully on page 6 of main text) and can be defined through equation (ii). The fractional amount of ligand-bound target can be easily expressed though the fractional occupancy equation (ii).

$$K_a = \frac{1}{K_d} = \frac{[TL]}{[T][L]} \qquad (i)$$

$$r = \frac{[TL]}{[T] + [TL]} \qquad (ii)$$

$$[TL] = K_a[T][L] \qquad (iii)$$

Here r is the fractional concentration ratio of bound target to total target at equilibrium. Rearranging equation (i) allows for $[TL]$ to be solved for in terms of $[T]$, $[L]$, and K_a (equation (iii)) which can then be substituted into equation (ii) to yield the following expression (iv):

$$r = \frac{K_a[T][L]}{[T] + K_a[T][L]} = \frac{K_a[L]}{1 + K_a[L]} \qquad (iv)$$

Dividing both the numerator and denominator by K_a leads to a simplified equation (v), which describes the fractional saturation of target in terms of initial ligand concentration and K_d value.

$$r = \frac{[L]}{K_d + [L]} \qquad (v)$$

When the fractional occupancy is plotted graphically against ligand concentration, equation (v) conforms to a rectangular hyperbola where the horizontal asymptote corresponds to the complete saturation of target. When the fractional occupancy is equal to 0.5, the ligand concentration is equal to the K_d value as illustrated in equations (vi) through $(viii)$

$$\frac{1}{2} = \frac{[L]_{1/2}}{K_d + [L]_{1/2}} \qquad (vi)$$

$$K_d + [L]_{1/2} = 2[L]_{1/2} \qquad (vii)$$

$$K_d = [L]_{1/2} \qquad (viii)$$

Separation Efficiency in CE

In analytical separations, it is useful to quantify the efficiency of an individual separation numerically. In CE, this can be achieved experimentally by evaluating a few basic parameters associated with the time-dependent molecular diffusion acquired during a separation. The apparent velocity, v_{ap}, for a given analyte refers to the speed at which the sample travels from the capillary inlet to the detector and can be measured experimentally using equation (ix), where L_d is the capillary length to the detection point. Since v_{ap} is a function of the electric field strength, E, and thus the applied voltage, V, a parameter termed apparent mobility, μ_{ap}, (equation (x)) is introduced to express the intrinsic analyte mobility

$$v_{ap} = \frac{L_d}{t_m} \qquad (ix)$$

$$\mu_{ap} = \frac{v_{ap}}{E} = \frac{v_{ap} L_t}{V} \qquad (x)$$

The efficiency of any system is defined numerically through the maximal number of theoretical plates achieved across the column. Giddings applied this principle to CE, where the number of theoretical plates, N, is expressed as a function of two parameters (i) the capillary length from inlet to detector, L_d, and (ii) the spatial variance of the sample zone, σ (see equation (xi) for relationship).

$$N = \frac{{L_d}^2}{\sigma^2} \qquad (xi)$$

$$\sigma^2 = 2Dt_m \frac{2DL_d}{v_{ap}} = \frac{2DL_d L_t}{\mu_{ap} V} \qquad (xii)$$

$$N = \frac{\mu_{ap} V L_d}{2 D L_t} \qquad (xiii)$$

Ideally, the only source of zone dispersion is the time-dependent longitudinal diffusion experienced by a given analyte upon detection. As a result, σ^2, can be defined through the Einstein equation (equation (xii)) where D, is the analyte diffusion coefficient in the given separation buffer. Through the appropriate substitutions, equation $(xiii)$ is produced which then defines N, in terms of measurable parameters.

Peak Resolution in CE

In CE, the resolution between two peaks, as derived by Giddings, can be quantified using equation (xiv), where R_s is the resolution and $\Delta v/\bar{v}$ is the relative velocity difference between the two zones being separated. In the presence of an electroosmotic flow, $\Delta v/\bar{v}$ can be related to relative motilities through equation (xv), where μ_1, μ_2, and represent the mobility of species 1 and 2 that are being separated, $\bar{\mu}$ refers to the average mobility of each species $\left(\bar{\mu} = 1/2\ (\mu_1 + \mu_2)\right)$ and μ_{eo} is the electroosmotic mobility. Then by substituting equation (xv) into equation (xiv), the final expression relating the peak resolution to the systems efficiency $\left(\sqrt{N}/4\right)$ and relative mobility between analyes is produced (equation (xvi)).

$$R_s = \frac{1}{4}\sqrt{N}\frac{\Delta v}{\bar{v}} \qquad (xiv)$$

$$\frac{\Delta v}{\bar{v}} = \frac{\mu_1 - \mu_2}{\bar{\mu} + \mu_{eo}} \qquad (xv)$$

$$R_s = \frac{1}{4}\sqrt{N}\frac{\mu_1 - \mu_2}{\bar{\mu} + \mu_{eo}} \qquad (xvi)$$

As indicated through equation (xvi), the maximal resolution occurs when $\bar{\mu} + \mu_{eo}$ approaches zero. Hence, it is desirable for μ_{eo} and $\bar{\mu}$ to be similar in magnitude but opposite in direction.

Derivation of K_d Expression through Quantifiable Parameters determined with NECEEM.

The equilibrium dissociation constant is mathematically defined through equation $(xvii)$, where $[T]_{eq}$, $[L]_{eq}$, and $[TL]_{eq}$ refer to the equilibrium concentrations of target, ligand and complex, respectively.

$$K_d = \frac{[T]_{eq}[L]_{eq}}{[TL]_{eq}} \qquad (xvii)$$

Since the ligand is experimentally detectable in typical CE-based aptamer selection, a NECEEM electropherogram can provide information pertaining to the ratio of unbound to free ligand which exists at equilibrium. This information along with the initial concentrations of target and ligand makes it possible to determine the equilibrium concentration of each species, and thus, K_d.

The area denoted as $A_1$is directly proportional to $[L]_{eq}$, and $[TL]_{eq}$ corresponds to the sum of areas A_2 and A_3. When fluorescence emission is used as the detection method, variations in the quantum yield of each detectable species must be accounted for. This adjustment is presented in equations $(xviii)$ and (xix) through the parameters φ_L and φ_{TL}, which refers to the fluorescence quantum yield of the ligand and target-ligand complex, respectively.

$$[L]_{eq} \propto \frac{A_1}{\varphi_L} \qquad (xviii)$$

$$[TL]_{eq} \propto \frac{A_2}{\varphi_{TL}} + \frac{A_3}{\varphi_L} \qquad (xix)$$

An additional parameter, R, is defined in equation (xx) as fractional amount of unbound ligand at equilibrium to the total ligand which is measured through the detectable areas of the electropherogram.

$$R = \frac{[L]_{eq}}{[L]_0} = \frac{\frac{A_1}{\varphi_L}}{\frac{A_1}{\varphi_L} + \frac{A_2}{\varphi_{TL}} + \frac{A_3}{\varphi_L}} = \frac{A_1}{A_1 + A_2\frac{\varphi_L}{\varphi_{TL}} + A_3} \qquad (xx)$$

Rearranging equation (xx) produces equation (xxi), which can be subsitutued into :

$$[L]_{eq} = R[L]_0 \qquad (xxi)$$

The total amount of ligand within the equilibrium mixture does not change, and so according to the law of mass balance, the complex concentration at equilibrium is defined

$$[TL]_{eq} = [L]_0 - [L]_{eq} \qquad (xxii)$$

$$[TL]_{eq} = [L]_0 - R[L]_0 = [L]_0(1 - R) \qquad (xxiii)$$

Similarly, the equilibrium concentrations of the target can be established through the simple mass balance law with the appropriate substitutions. Conceptually, the amount of unbound target present during equilibrium is equivalent to the total amount of target in the sample subtracted by the equilibrium amount target-ligand complex ligand.

$$[T]_{eq} = [T]_0 - [TL]_{eq} \qquad (xxiv)$$

$$[T]_{eq} = [T]_0 - [L]_0(1 - R) \qquad (xxv)$$

The equations (xxi), $(xxiii)$, and (xxv) express the required equilibrium concentration of each species in through measurable variables. By substituting the equations (xxi), $(xxiii)$, and (xxv), into the generalized K_d expression equation $(xvii)$, equation $(xxvi)$ is produced.

$$K_d = \frac{([T]_0 - [L]_0(1 - R))R[L]_0}{[L]_0(1 - R)} = \frac{([T]_0 - [L]_0(1 - R))R}{1 - R} \qquad (xxvi)$$

By dividing the numerator and denominator by R, and substituting R through equation (xx), equations $(xxvii)$ and $(xxviii)$ are formed.

$$K_d = \frac{[T]_0 - [L]_0(1-R)}{1/R - 1} \qquad (xxvii)$$

$$K_d = \frac{[T]_0 - [L]_0\left(1 - A_1/\left(A_1 + A_2\frac{\varphi_L}{\varphi_{TL}} + A_3\right)\right)}{\left(A_1 + A_2\frac{\varphi_L}{\varphi_{TL}} + A_3\right)/A_1 - 1} \qquad (xxviii)$$

Assuming that the fluorescence quantum yield values of the pure ligand and complex are comparable, the ratio can be approximated to 1, and equation $(xxviii)$ simplifies to equation $(xxix)$.

$$K_d = \frac{[T]_0 - [L]_0(1 - A_1/(A_1 + A_2 + A_3))}{(A_1 + A_2 + A_3)/A_1 - 1} \qquad (xxix)$$

Derivation of the Intrinsic Rate of Dissociation, k_{off} using NECEEM

The unimolecular rate constant of complex dissociation, k_{off} can be easily derived using classical reaction kinetics and rate laws (equation (xxx)). When the re-association of target and ligand is not possible, the rate of complex dissociation can be derived as the change in complex concentration over time (equation $(xxxi)$). By integrating both sides (equation $(xxxii)$), equation $(xxxiii)$ is produced where $\ln[TL]_0$ describes the initial equilibrium conditions, and $\ln[TL]_t$ refers to the detection conditions at a time, t, after initiating complex dissociation. After rearranging and solving for k_{off} equation $(xxxv)$ is produced which relates the rate constant to the initial and final complex concentrations ($[TL]_0$and $[TL]_t$, respectively) at time, t.

$$Reaction\ rate = k_{off}[TL] \qquad (xxx)$$

$$-\frac{d[TL]}{dt} = k_{off}[TL] \qquad (xxxi)$$

$$\int_0^t \frac{1}{[TL]} d[TL] = -\int_0^t k_{off} dt \qquad (xxxii)$$

$$\ln[TL]_t - \ln[TL]_0 = -k_{off}t \qquad (xxxiii)$$

$$k_{off} = \frac{1}{t}\ln\frac{[TL]_0}{[TL]_t} \qquad (xxxv)$$

The relative complex concentration, at time = 0 and time = t, can determined be from the relative areas under the NECEEM electropherogram as shown in equation $(xxxvi)$. Here, $[TL]_0$ refers to the equilibrium concentration of the complex and corresponds to the sum of area A_2 and A_3 of the electropherogram. The complex concentration upon detection, $[TL]_t$ corresponds exclusively to the area of intact complex, A_2 at $t_{P \bullet DNA}$.

$$k_{off} = \frac{1}{t_{P \bullet DNA}} \ln\left(\frac{A_2 + A_3}{A_2}\right) \qquad (xxxvi)$$

References

1. de Jong S, Krylov SN. Pressure-based approach for the analysis of protein adsorption in capillary electrophoresis. *Anal Chem.* 2011;84(1):453-458.

2. de Jong S, Epelbaum N, Liyanage R, Krylov SN. A semi-permanent coating for preventing protein adsorption at physiological pH in kinetic capillary electrophoresis. *Electrophoresis.* 2012;33(16):2584-2590.

3. de Jong S, Krylov SN. Protein labeling enhances aptamer selection by methods of kinetic capillary electrophoresis. *Anal Chem.* 2011;83(16):6330-6335.

4. Leckband D, Israelachvili J. Intermolecular forces in biology. *Q Rev Biophys.* 2001;34(02):105-267.

5. Lewis GN. The atom and the molecule. *J Am Chem Soc.* 1916;38(4):762-785.

6. Gillespie R. The electron-pair repulsion model for molecular geometry. *J Chem Educ.* 1970;47(1):18.

7. Frieden E. Non-covalent interactions: Key to biological flexibility and specificity. *J Chem Educ.* 1975;52(12):754.

8. Černý J, Hobza P. Non-covalent interactions in biomacromolecules. *Phys.Chem.Chem.Phys.* 2007;9(39):5291-5303.

9. Sharp KA, Honig B. Electrostatic interactions in macromolecules: Theory and applications. *Annu Rev Biophys Biophys Chem.* 1990;19(1):301-332.

10. Dzyaloshinskii I, Lifshitz E, Pitaevskii LP. General theory of van der Waals' forces. *Physics-Uspekhi.* 1961;4(2):153-176.

11. Hamaker H. The London—van der Waals attraction between spherical particles. *physica.* 1937;4(10):1058-1072.

12. London F. The general theory of molecular forces. *Transactions of the Faraday Society.* 1937;33:8b-26.

13. Jeffrey GA, Jeffrey GA. *An introduction to hydrogen bonding.* Vol 12. Oxford University Press New York; 1997.

14. Howard JAK, Hoy VJ, O'Hagan D, Smith GT. How good is fluorine as a hydrogen bond acceptor? *Tetrahedron.* 1996;52(38):12613-12622.

15. Emsley J. Very strong hydrogen bonding. *Chem Soc Rev.* 1980;9(1):91-124.

16. Hubbard RE, Kamran Haider M. Hydrogen bonds in proteins: Role and strength. *eLS.*

17. Sharp KA. The hydrophobic effect. *Curr Opin Struct Biol.* 1991;1(2):171-174.

18. Connors KA. *Chemical kinetics: The study of reaction rates in solution.* John Wiley & Sons; 1990.

19. Steinfeld JI, Francisco JS, Hase WL. *Chemical kinetics and dynamics.* Vol 3. Prentice Hall Englewood Cliffs (New Jersey); 1989.

20. Nelson DL, Cox MM. *Lehninger principles of biochemistry.* Wh Freeman; 2010.

21. Cornish-Bowden A, Cornish-Bowden A. *Fundamentals of enzyme kinetics.* Vol 3. Portland Press London; 1995.

22. Krylov SN. Kinetic CE: Foundation for homogeneous kinetic affinity methods. *Electrophoresis.* 2007;28(1-2):69-88.

23. Mitchell P. A perspective on protein microarrays. *Nat Biotechnol.* 2002;20(3):225-229.

24. Wilson DS, Szostak JW. In vitro selection of functional nucleic acids. *Annu Rev Biochem.* 1999;68(1):611-647.

25. Famulok M, Mayer G, Blind M. Nucleic acid aptamers from selection in vitro to applications in vivo. *Acc Chem Res.* 2000;33(9):591-599.

26. Jayasena SD. Aptamers: An emerging class of molecules that rival antibodies in diagnostics. *Clin Chem.* 1999;45(9):1628-1650.

27. Brody EN, Gold L. Aptamers as therapeutic and diagnostic agents. *Reviews in Molecular Biotechnology.* 2000;74(1):5-13.

28. German I, Buchanan DD, Kennedy RT. Aptamers as ligands in affinity probe capillary electrophoresis. *Anal Chem.* 1998;70(21):4540-4545.

29. Ng EW, Shima DT, Calias P, Cunningham ET, Guyer DR, Adamis AP. Pegaptanib, a targeted anti-VEGF aptamer for ocular vascular disease. *Nature reviews drug discovery.* 2006;5(2):123-132.

30. Farokhzad OC, Jon S, Khademhosseini A, Tran TT, LaVan DA, Langer R. Nanoparticle-aptamer bioconjugates a new approach for targeting prostate cancer cells. *Cancer Res.* 2004;64(21):7668-7672.

31. Tuerk C, Gold L. Systematic evolution of ligands by exponential enrichment: RNA ligands to bacteriophage T4 DNA polymerase. *Science.* 1990;249(4968):505-510.

32. Ellington AD, Szostak JW. In vitro selection of RNA molecules that bind specific ligands. *Nature*. 1990;346(6287):818-822.

33. Nimjee SM, Rusconi CP, Sullenger BA. Aptamers: An emerging class of therapeutics. *Annu Rev Med*. 2005;56:555-583.

34. Hamula CLA, Guthrie JW, Zhang H, Li X, Le XC. Selection and analytical applications of aptamers. *TrAC Trends in Analytical Chemistry*. 2006;25(7):681-691.

35. Ciesiolka J, Yarus M. Small RNA-divalent domains. *RNA*. 1996;2(8):785.

36. Hofmann H, Limmer S, Hornung V, Sprinzl M. Ni2 -binding RNA motifs with an asymmetric purine-rich internal loop and a GA base pair. *RNA*. 1997;3(11):1289.

37. Connell GJ, Illangesekare M, Yarus M. Three small ribooligonucleotides with specific arginine sites. *Biochemistry (N Y)*. 1993;32(21):5497-5502.

38. Famulok M. Molecular recognition of amino acids by RNA-aptamers: An L-citrulline binding RNA motif and its evolution into an L-arginine binder. *J Am Chem Soc*. 1994;116(5):1698-1706.

39. Wallace ST, Schroeder R. In vitro selection and characterization of streptomycin-binding RNAs: Recognition discrimination between antibiotics. *RNA*. 1998;4(1):112-123.

40. Wallis M, Streicher B, Wank H, et al. In vitro selection of a viomycin-binding RNA pseudoknot. *Chem Biol*. 1997;4(5):357-366.

41. Nieuwlandt D, Wecker M, Gold L. In vitro selection of RNA ligands to substance P. *Biochemistry (N Y)*. 1995;34(16):5651-5659.

42. Williams KP, Liu X, Schumacher TN, et al. Bioactive and nuclease-resistant L-DNA ligand of vasopressin. *Proceedings of the National Academy of Sciences*. 1997;94(21):11285-11290.

43. Tuerk C, MacDougal S, Gold L. RNA pseudoknots that inhibit human immunodeficiency virus type 1 reverse transcriptase. *Proceedings of the National Academy of Sciences*. 1992;89(15):6988-6992.

44. Dang C, Jayasena S. Oligonucleotide inhibitors of taq DNA polymerase facilitate detection of low copy number targets by PCR. *J Mol Biol*. 1996;264(2):268-278.

45. Kubik MF, Stephens AW, Schneider D, Marlar RA, Tasset D. High-affinity RNA ligands to human α-thrombin. *Nucleic Acids Res*. 1994;22(13):2619-2626.

46. Wiegand TW, Williams PB, Dreskin SC, Jouvin M, Kinet J, Tasset D. High-affinity oligonucleotide ligands to human IgE inhibit binding to fc epsilon receptor I. *The Journal of Immunology*. 1996;157(1):221-230.

47. Smith D, Kirschenheuter G, Charlton J, Guidot D, Repine J. In vitro selection of RNA-based irreversible inhibitors of human neutrophil elastase. *Chem Biol.* 1995;2(11):741-750.

48. Mallikaratchy P, Stahelin RV, Cao Z, Cho W, Tan W. Selection of DNA ligands for protein kinase C-δ. *Chem.Commun.* 2006(30):3229-3231.

49. Huizenga DE, Szostak JW. A DNA aptamer that binds adenosine and ATP. *Biochemistry (N Y).* 1995;34(2):656-665.

50. Pan W, Craven RC, Qiu Q, et al. Isolation of virus-neutralizing RNAs from a large pool of random sequences. *Proceedings of the National Academy of Sciences.* 1995;92(25):11509-11513.

51. Misono TS, Kumar PK. Selection of RNA aptamers against human influenza virus hemagglutinin using surface plasmon resonance. *Anal Biochem.* 2005;342(2):312-317.

52. Kumar P, Machida K, Urvil PT, et al. Isolation of RNA aptamers specific to the NS3 protein of hepatitis C virus from a pool of completely random RNA. *Virology.* 1997;237(2):270-282.

53. Shangguan D, Li Y, Tang Z, et al. Aptamers evolved from live cells as effective molecular probes for cancer study. *Proceedings of the National Academy of Sciences.* 2006;103(32):11838-11843.

54. Chen HW, Medley CD, Sefah K, et al. Molecular recognition of Small-Cell lung cancer cells using aptamers. *ChemMedChem.* 2008;3(6):991-1001.

55. Sefah K, Tang Z, Shangguan D, et al. Molecular recognition of acute myeloid leukemia using aptamers. *Leukemia.* 2009;23(2):235-244.

56. Wang C, Zhang M, Yang G, et al. Single-stranded DNA aptamers that bind differentiated but not parental cells: Subtractive systematic evolution of ligands by exponential enrichment. *J Biotechnol.* 2003;102(1):15-22.

57. Masliyah JH, Bhattacharjee S. *Electrokinetic and colloid transport phenomena.* Wiley-Interscience; 2006.

58. Whatley H. 1. Basic principles of capillar electrophoresis. *Clinical and Forensic Applications of Capillary Electrophoresis.* 2001;4:21.

59. Xu Y. Tutorial: Capillary electrophoresis. *The Chemical Educator.* 1996;1(2):1-14.

60. Crew H. *General physics: An elementary text-book for colleges.* The Macmillan company; 1908.

61. Grossman PD, Colburn JC. *Capillary electrophoresis: Theory and practice.* Academic Press; 1992.

62. Weinberger R. *Practical capillary electrophoresis.* Academic Press San Diego, CA; 1993.

63. Cohen A, Paulus A, Karger B. High-performance capillary electrophoresis using open tubes and gels. *Chromatographia.* 1987;24(1):15-24.

64. Ewing AG, Wallingford RA, Olefirowicz TM. Capillary electrophoresis. *Anal Chem.* 1989;61(4):292A-303A.

65. Li SFY. *Capillary electrophoresis: Principles, practice and applications.* Vol 52. Elsevier Science; 1992.

66. Swinney K, Bornhop DJ. Detection in capillary electrophoresis. *Electrophoresis.* 2000;21(7):1239-1250.

67. Schwer C, Kenndler E. Electrophoresis in fused-silica capillaries: The influence of organic solvents on the electroosmotic velocity and the. zeta. potential. *Anal Chem.* 1991;63(17):1801-1807.

68. Grahame DC. The electrical double layer and the theory of electrocapillarity. *Chem Rev.* 1947;41(3):441-501.

69. Kirby BJ, Hasselbrink EF. Zeta potential of microfluidic substrates: 1. theory, experimental techniques, and effects on separations. *Electrophoresis.* 2004;25(2):187-202.

70. Fairhurst D, Lee RW. ZETA. .

71. Smoluchowski MV. Zur theorie der elektrischen kataphorese und der oberflchenleitung. *Phys.Z.* 1905;6:529

72. Ghosal, S. Fluid mechanics of electroosmotic flow and its effect on band broadening in capillary electrophoresis. *Electrophoresis.* 2004;25(2):214-228

73. Qiao R. Control of electroosmotic flow by polymer coating: Effects of the electrical double layer. *Langmuir.* 2006;22(16):7096-7100.

74. Giddings JC. Generation of variance, "theoretical plates," resolution, and peak capacity in electrophoresis and sedimentation. *Sep Sci Technol.* 1969;4(3):181-189.

75. Jorgenson JW, Lukacs KD. Zone electrophoresis in open-tubular glass capillaries. *Anal Chem.* 1981;53(8):1298-1302.

76. Musheev MU, Krylov SN. Selection of aptamers by systematic evolution of ligands by exponential enrichment: Addressing the polymerase chain reaction issue. *Anal Chim Acta.* 2006;564(1):91-96.

77. Mendonsa SD, Bowser MT. In vitro evolution of functional DNA using capillary electrophoresis. *J Am Chem Soc*. 2004;126(1):20-21.

78. Mendonsa SD, Bowser MT. In vitro selection of high-affinity DNA ligands for human IgE using capillary electrophoresis. *Anal Chem*. 2004;76(18):5387-5392.

79. Mendonsa SD, Bowser MT. In vitro selection of aptamers with affinity for neuropeptide Y using capillary electrophoresis. *J Am Chem Soc*. 2005;127(26):9382-9383.

80. Mosing RK, Mendonsa SD, Bowser MT. Capillary electrophoresis-SELEX selection of aptamers with affinity for HIV-1 reverse transcriptase. *Anal Chem*. 2005;77(19):6107-6112.

81. Petrov A, Okhonin V, Berezovski M, Krylov SN. Kinetic capillary electrophoresis (KCE): A conceptual platform for kinetic homogeneous affinity methods. *J Am Chem Soc*. 2005;127(48):17104-17110.

82. Javaherian S, Musheev MU, Kanoatov M, Berezovski MV, Krylov SN. Selection of aptamers for a protein target in cell lysate and their application to protein purification. *Nucleic Acids Res*. 2009;37(8):e62-e62.

83. Kanoatov M, Javaherian S, Krylov SN. Selection of aptamers for a non-DNA binding protein in the context of cell lysate. *Anal Chim Acta*. 2010;681(1):92-97.

84. Tran DT, Janssen KP, Pollet J, et al. Selection and characterization of DNA aptamers for egg white lysozyme. *Molecules*. 2010;15(3):1127-1140.

85. Turner DJ, Tuytten R, Janssen KP, et al. Toward clinical proteomics on a next-generation sequencing platform. *Anal Chem*. 2010;83(3):666-670.

86. Berezovski MV, Musheev MU, Drabovich AP, Jitkova JV, Krylov SN. Non-SELEX: Selection of aptamers without intermediate amplification of candidate oligonucleotides. *Nature protocols*. 2006;1(3):1359-1369.

87. Berezovski M, Musheev M, Drabovich A, Krylov SN. Non-SELEX selection of aptamers. *J Am Chem Soc*. 2006;128(5):1410-1411.

88. Tok J, Lai J, Leung T, Li SFY. Selection of aptamers for signal transduction proteins by capillary electrophoresis. *Electrophoresis*. 2010;31(12):2055-2062.

89. Drabovich AP, Berezovski M, Okhonin V, Sergey N. Selection of smart aptamers by methods of kinetic capillary electrophoresis. *Anal Chem*. 2006;78(9):3171-3178.

90. Drabovich AP, Berezovski MV, Musheev MU, Krylov SN. Selection of smart small-molecule ligands: The proof of principle. *Anal Chem*. 2008;81(1):490-494.

91. Berezovski M, Drabovich A, Krylova SM, et al. Nonequilibrium capillary electrophoresis of equilibrium mixtures: A universal tool for development of aptamers. *J Am Chem Soc.* 2005;127(9):3165-3171.

92. Berezovski M, Sergey N. Nonequilibrium capillary electrophoresis of equilibrium mixtures-A single experiment reveals equilibrium and kinetic parameters of protein-DNA interactions. *J Am Chem Soc.* 2002;124(46):13674-13675.

93. Krylov SN. Nonequilibrium capillary electrophoresis of equilibrium mixtures (NECEEM): A novel method for biomolecular screening. *Journal of biomolecular screening.* 2006;11(2):115-122.

94. Acinas SG, Sarma-Rupavtarm R, Klepac-Ceraj V, Polz MF. PCR-induced sequence artifacts and bias: Insights from comparison of two 16S rRNA clone libraries constructed from the same sample. *Appl Environ Microbiol.* 2005;71(12):8966-8969.

95. Dohm JC, Lottaz C, Borodina T, Himmelbauer H. Substantial biases in ultra-short read data sets from high-throughput DNA sequencing. *Nucleic Acids Res.* 2008;36(16):e105-e105.

96. Howorka S, Siwy Z. Nanopore analytics: Sensing of single molecules. *Chem Soc Rev.* 2009;38(8):2360-2384.

97. Stoddart D, Heron AJ, Mikhailova E, Maglia G, Bayley H. Single-nucleotide discrimination in immobilized DNA oligonucleotides with a biological nanopore. *Proceedings of the National Academy of Sciences.* 2009;106(19):7702-7707.

98. Lehman I, Nussbaum A. The deoxyribonucleases of Escherichia coli. *J Biol Chem.* 1964;239:2628-2636.

99. Lehman I. The deoxyribonucleases of Escherichia coli I. Purification and properties of a phosphodiesterase. *J Biol Chem.* 1960;235(5):1479-1487.

100. Deamer D. Nanopore analysis of nucleic acids bound to exonucleases and polymerases. *Annual review of biophysics.* 2010;39:79-90.

101. Stoyanov AV, Ahmadzadeh H, Krylov SN. Heterogeneity of protein labeling with a fluorogenic reagent, 3-(2-furoyl) quinoline-2-carboxaldehyde. *Journal of Chromatography B.* 2002;780(2):283-287.

102. Wetzl BK, Yarmoluk SM, Craig DB, Wolfbeis OS. Chameleon labels for staining and quantifying proteins. *Angewandte Chemie International Edition.* 2004;43(40):5400-5402.

103. Ramsay LM, Dickerson JA, Dada O, Dovichi NJ. Femtomolar concentration detection limit and zeptomole mass detection limit for protein separation by capillary isoelectric focusing and laser-induced fluorescence detection. *Anal Chem.* 2009;81(5):1741-1746.

104. Ramsay LM, Dickerson JA, Dovichi NJ. Attomole protein analysis by CIEF with LIF detection. *Electrophoresis*. 2009;30(2):297-302.

105. Bock LC, Griffin LC, Latham JA, Vermaas EH, Toole JJ. Selection of single-stranded DNA molecules that bind and inhibit human thrombin. . 1992.

106. Krylova SM, Karkhanina AA, Musheev MU, Bagg EA, Schofield CJ, Krylov SN. DNA aptamers for as analytical tools for the quantitative analysis of DNA-dealkylating enzymes. *Anal Biochem*. 2011;414(2):261-265.

107. Carrasco-Correa EJ, Beneito-Cambra M, Herrero-Martínez JM, Ramis-Ramos G. Evaluation of molecular mass and tacticity of polyvinyl alcohol by non-equilibrium capillary electrophoresis of equilibrium mixtures of a polymer and a dye. *Journal of Chromatography A*. 2011;1218(16):2334-2341.

108. Yang P, Mao Y, Lee AW, Kennedy RT. Measurement of dissociation rate of biomolecular complexes using CE. *Electrophoresis*. 2009;30(3):457-464.

109. Sloat AL, Roper MG, Lin X, Ferrance JP, Landers JP, Colyer CL. Protein determination by microchip capillary electrophoresis using an asymmetric squarylium dye: Noncovalent labeling and nonequilibrium measurement of association constants. *Electrophoresis*. 2008;29(16):3446-3455.

110. Evenhuis CJ, Musheev MU, Krylov SN. Heat-associated field distortion in electro-migration techniques. *Anal. Chem*. 2010;80(20):8398-8401

111. Evenhuis CJ, Musheev MU, Krylov SN. Universal method for determining electrolyte temperatures in capillary electrophoresis. *Anal Chem*. 2011;83(5):1808-1814

112. Towns JK, Regnier FE. Impact of polycation adsorption on efficiency and electroosmotically driven transport in capillary electrophoresis. *Anal Chem*. 1992;64(21):2473-2478.

113. Gaš B, Štědrý M, Kenndler E. Peak broadening in capillary zone electrophoresis. *Electrophoresis*. 1997;18(12-13):2123-2133

114. Schure MR, Lenhoff, AM. Consequences of wall adsorption in capillary electrophoresis: Theory and simulation. *Anal Chem*. 1993;65(21):3024-3037

115. McCormick RM. Capillary zone electrophoretic separation of peptides and proteins using low pH buffers in modified silica capillaries. *Anal Chem.* 1988;60(21):2322-2328

116. Lauer HH, McManigill D. Capillary zone electrophoresis in untreated fused silica tubing. *Anal Chem.* 1986;58(1):166-170

117. Towns JK, Regnier FE. Capillary electrophoretic separations of proteins using non-ionic surfactant coatings. *Anal Chem.* 1991;63(11):1126-1132

118. Regnier FE. The role of protein structure in chromatographic behaviour. *Science.* 1987;238(4825):319-323

119.Yao Y, Khoo K, Chung M, Li S. Determination of isoelectric points of acidic and basic proteins by capillary electrophoresis. *Journal of Chromatography A.* 1994;680(2):431-435

120. Witorowicz JE, Colburn JC. Separation of cationic proteins via charge reversal in capillary electrophoresis. *Electrophoresis.* 1990;11(9):769-773

121. Dong M, Oda RP, Strausbauch MA, Wettstein PJ, Landers JP, Miller LJ. Hydrophobic peptide mapping of clinically relevant heptathelical membrane proteins by capillary electrophoresis. *Electrophoresis.* 1997;18(10):1767-1774

122. Legaz ME, Pedrosa MM. Effect of polyamines on the separation of ovalbumin glycoforms by capillary electrophoresis *Journal of Chromatography A.* 1996;719(1):159-170

123. Córdova E, Gao J, Whitesides GM. Noncovalent polycationic coatings for capillaries in capillary electrophoresis of proteins. *Anal Chem.* 1997;69(7):1370-1379.

124. Lucy CA, MacDonald AM, Gulcev MD. Non-covalent capillary coatings for protein separations in capillary electrophoresis. *Journal of Chromatography A.* 2008;1184(1):81-105

125. Verzola B, Gelfi C, Righetti PG. Protein adsorption to the bare silica wall in capillary electrophoresis: Quantitative study on the chemical composition of the background electrolyte for minimizing the phenomenon. *Journal of Chromatography A.* 2000;868(1):85-99

126. Verzola B, Gelfi C, Righetti PG. Quantitative studies on the adsorption of proteins to the bare silica wall in capillary electrophoresis: II: Effects of adsorbed, neutral polymers on quenching the interaction. *Journal of Chromatography A.* 2000;874(2):293-303

127. Castelletti L, Verzola B, Gelfi C, Stoyanov A, Righetti PG. Quantitative studies on the adsorption of proteins to the bare silica wall in capillary electrophoresis: III: Effects of adsorbed surfactants on quenching the interaction. *Journal of Chromatography A.* 2000;894(1):281-289

128. Tran DT, Taverna M, Miccoli L, Angulo JF. Poly (ethylene oxide) facilitates the characterization of an affinity between strongly basic proteins with DNA by affinity capillary electrophoresis. *Electrophoresis.* 2005;26(16):3105-3112

129. Okhonin V, Liu X, Krylov SN. Transverse diffusion of laminar flow profiles to produce capillary nanoreactors. *Anal Chem.* 2005;77(18):5925-5929

130. Righetti PG, Gelfi C, Verzola B, Castelletti L. The state of the art of dynamic coatings. *Electrophoresis.* 2001;22(4):603-611

131. Janssens J, Chevigne R, Louis P. Capillary electrophoresis method using initialized capillary and polyanion-containing buffer and chemical kit therefor. *US Patent 5 611 903.*1997

132. Boone C, Jonkers E, Franke J, De Zeeuw R, Ensing K. Dynamically coated capillaries improve the identification power of capillary zone electrophoresis for basic drugs in toxicological analysis. *Journal of Chromatography A.* 2001;927(1):203-210

133. Nakatani M, Shibukawa A, Nakagawa T. Chemical stability of polyacrylamide-coating on fused silica capillary. *Electrophoresis.* 1995;16(1):1451-1456

134. Berezovski M, Nutiu R, Li Y, Krylov SN. Affinity analysis of protein-aptamer complex using nonequilibrium capillary electrophoresis of equilibrium mixtures. *Anal Chem.* 2003;75(6):1382-1386

135. MacDonald AM, Lucy CA. Highly efficient separations in capillary electrophoresis using a supported bilayer/diblock copolymer coating. *Journal of Chromatography A.*2006;1130(2):265-271

136. MacDonald AM, Bahnasy MF, Lucy CA. A modified supported bilayer/diblock polymer-Working towards a tunable coating for capillary electrophoresis. *Journal of Chromatography A.* 2011;1218(1):178-184

137. Belder D, Deege A, Husmann H, Kohler F, Ludwig M. Cross-linked poly (vinyl alcohol) as a permanent hydrophilic column coating for capillary electrophoresis. *Electrophoresis.* 2001;22(17):3813-3818

138. Thomas KR, Olivera BM. Processivity of DNA exonucleases. *J. Biol Chem.* 1978;253(2):424-429

139. Brody R, Doherty K, Zimmerman P. Processivity and kinetics of the reaction of exonuclease I from Escherichia coli with polydeoxyribonucleotides. *J. Biol Chem.* 1986;261(16):7136-7143

140. Brody, RS. Nucleotide positions responsible for the processivity of the reaction of exonuclease I with oligodeoxyribonucleotides. *Biochemistry.* 1991;30(29):7072-7080.

141. Towns JK, Bao J, Regnier FE. Synthesis and evaluation of epoxy polymer coatings for the analysis of proteins by capillary zone electrophoresis. *Journal of Chromatography A.* 1992;599(1):227-237

142. Liu Y, Fu R, Gu J. Capillary zone electrophoretic separations of proteins using a column coated with epoxy polymer. *Journal of Chromatography A.* 1995;694(2):498-506

143. Liu Y, Fu R, Gu J. Epoxy resin coatings for capillary zone electrophoretic separation of basic proteins. *Journal of Chromatography A.* 1996; 723(1):157-167

144. Breyer WA, Matthews BW. Structure of Escherichia coli exonuclease I suggests how processivity is achieved. *Nature Structural & Molecular Biology*. 2000;7(12):1125-1128